

**EXPLORING BROWN CARBON ANALYSIS:
RIGOROUS CHARACTERIZATION AND SOURCE APPORTIONMENT**

by

© Robert Anthony Di Lorenzo

A Thesis submitted to the

School of Graduate Studies

in partial fulfillment of the requirements for the degree of

Doctor of Philosophy

Department of Chemistry

Memorial University of Newfoundland

December 2016

St. John's, Newfoundland and Labrador

Abstract

Atmospheric particulate matter (PM) represents the greatest factor underlying the total uncertainty of anthropogenically derived radiative forcing. It has been shown that particles containing a large fraction of water soluble carbon have organic species with the ability to absorb solar radiation, referred to as brown carbon (BrC). Preliminary work has shown that BrC is strongly correlated to biomass burning (BB) events, is predominantly composed of extremely low volatility organic compounds (ELVOCs) and is of large molecular weight character.

Particle characterization of multiple real-world forest fires and regional background aerosol has been achieved using multiple analytical techniques including size exclusion chromatography, reverse-phase liquid chromatography, ion chromatography, molecular absorption spectroscopy, and multiple combinations of mass spectrometric ionization and detection techniques. Particles were collected both in bulk and by cascade impaction, which size fractionated particles into 13 size bins between 18 μm and 10 nm.

This work shows that biomass burning particulate matter composition is highly complex and cannot be characterized mass spectrally using one ionization technique alone. Although comparisons in the literature are often made to the composition of humic acid, the organic aerosol fraction, particularly derived from BB, differs greatly. Further, absorbing species comprising BrC are not accurately represented when commonly employed electrospray ionization is used.

These BrC absorbing species have been found to be of large molecular weight character, with a large proportion greater than 500 Da. The molecular weight profile

distribution is consistent across multiple forest fire samples, as well as in background aerosol. BB was confirmed to be the dominant source of large molecular weight BrC in the background aerosol samples. The absorbing species were found not to be internally mixed with common BB markers, but the absorbance distribution across particle diameters coincided with the observance of ammonium and dialkyl ammonium species, potentially representing new tracers. The molecular characteristics of these large absorbing molecules would be consistent with the ELVOC-BrC species previously identified in the literature. Large molecular weight BrC absorbers represent a recalcitrant source of absorbing organic molecules to the atmosphere. These large, long-lived absorbing molecules may have important climate impacts and are worthy of further study.

Acknowledgements

I was eleven or twelve years old, out for dinner with my parents, waiting for our food to arrive. I was scribbling on a napkin, doodling, writing out my signature. In front of one of the signatures I hastily wrote ‘Dr.’. “Wouldn’t that be cool?”, I said to my parents. They agreed with a smile. After the same signature, I then wrote ‘PhD’, looked up again at my parents and said, “Nah, that will never happen...”. I never thought I would see the day I would be thanking people for helping me to finish a PhD, but here I am, and I could not be more grateful to each and every one of you for your help along the way.

I first and foremost have to thank my supervisor, Cora Young. Your continuous guidance, honesty, inspiration, periodic stern looks of “get your *stuff* together” and wake-up calls from my desk-naps could not be more appreciated. Thank you for giving me independence, but also for always having your door open and a comfy chair in your office. Thank you for trusting me to be your first student. Thank you for always having my back. I would not be half the scientist I am today without your support. Also, I’m sorry for all the meat I cooked in your house.

I also have to thank Trevor VandenBoer, because, without you and a few beers at the GSU, I might not have made my way to St. John’s. Thank you for the continual encouragement, always thorough scientific discussion, the not-so-subtle “get your *stuff* together”, the copious amounts of food, beer and whiskey we shared, and, along with Cora of course, moving me out of an apartment and into your home on an hour’s notice. I consider you both a part of my family.

Speaking of which, being away from my parents was probably (definitely) harder on them than it was on me. Thank you for always believing me, especially at times when I didn't think I had it in me. Thank you for your patience and encouragement. Thank you for your lessons of respect and honour, because they made me who I am today.

I would also like to thank my fellow CJY group members: Joseph, John, Bryan, Teles, Kat, Li, Heidi and the rest of the Young-sters, the Young-Gunz, Research is not done in a vacuum. We are shaped by the opinions, reassurance and skepticism of those around us. Thank you for talking with me through problems, supporting me through doubts, challenging my conclusions and helping me grow as a scientist and a person. And of course, all the beers at Bitters. In a similar fashion, I would like to thank my collaborators for allowing me to expand my scientific horizon, specifically Rebecca Washenfelder, Karl Jobst and Eric Reiner. Because of you, I've gained a considerable amount of technical and theoretical knowledge and made many more connections than I ever thought I would.

Last, and most certainly not least, I would like to thank my person, Melanie. Thank you for knowing me better than I know myself. For knowing when to buckle down and when to pull me out of the bat-cave for lunch. For your patience. For making me laugh and for calming my stress. For the adventures, big and small. For listening to me ramble on about mass spectrometry without a single complaint. Thank you for simultaneously being the perfect distraction and the ultimate motivation. Without your continual and unconditional love and support, I would not have made it through with any semblance of sanity.

Table of Contents

Abstract	ii
Acknowledgements	iv
List of Tables	xi
List of Figures.....	xii
List of Symbols, Nomenclature, or Abbreviations	xxii
List of Appendices.....	xxiv
Preface	xxv
1 Introduction.....	1
1.1 Atmospheric Particulate Matter	2
1.1.1 Size Distribution	2
1.1.2 Sources and Composition	3
1.2 Radiative Forcing by Atmospheric Particulate Matter.....	9
1.2.1 Indirect Climate Effects.....	10
1.2.2 Direct Climate Effects	10
1.3 Aerosol Sampling and Analysis	13
1.3.1 Online Methods	13
1.3.2 Offline Methods.....	16
1.4 Organic Aerosol Speciation	22

1.4.1	Ultra-High Resolution Mass Spectrometry	22
1.4.2	Humic-Like Species.....	25
1.4.3	Size Exclusion Chromatography	26
1.5	Thesis Objectives	27
1.6	References	28
2	Comprehensive mass spectral analysis of an aged biomass burning aerosol sample	46
2.1	Abstract	47
2.2	Introduction	47
2.3	Methods.....	50
2.3.1	Sample Collection.....	50
2.3.2	Sample Preparation.....	50
2.3.3	Mass Spectrometric Analysis	51
2.3.4	Data Handling.....	53
2.4	Results and Discussion.....	53
2.4.1	ESI.....	53
2.4.2	APPI.....	63
2.4.3	EL.....	65
2.5	Conclusions	68

2.6	References	70
3	Size separation method for absorption characterization in brown carbon: Application to an aged biomass burning sample	77
3.1	Abstract	78
3.2	Introduction	78
3.3	Methods.....	81
3.3.1	Sample Collection.....	81
3.3.2	Sample Preparation.....	81
3.3.3	Sample Analysis	82
3.4	Results and Discussion.....	83
3.5	Acknowledgements	92
3.6	References	93
4	Size-resolved composition of aged biomass burning aerosols derived from a real-world boreal wildfire.....	102
4.1	Abstract	103
4.2	Introduction	103
4.3	Methods.....	106
4.3.1	Sample Collection and Extraction.....	106
4.3.2	Sample Analysis	107

4.4	Results and Discussion.....	110
4.4.1	Size Distribution of Measured Species.....	110
4.4.2	Size Distribution of BrC Absorption.....	114
4.4.3	Comparison between BrC Absorption and Measured Species.....	117
4.5	Conclusions.....	123
4.6	References.....	125
5	Molecular size separated brown carbon absorption for fresh and aged biomass burning plumes at multiple field sites.....	134
5.1	Abstract.....	135
5.2	Introduction.....	135
5.3	Methods.....	138
5.3.1	Sampling Sites.....	138
5.3.2	Fire Identification and Transport Time.....	141
5.3.3	Sample Extraction and Analysis by Size Exclusion Chromatography Absorption Spectrophotometry (SEC-UV).....	141
5.4	Results and Discussion.....	142
5.4.1	Calculated Ages for Biomass Burning Aerosol.....	142
5.4.2	BrC Absorbance as a Function of Molecular Weight.....	144
5.4.3	Comparison of Absorbance for SEC-UV Filter Samples and Online PiLS-LWCC.....	148

5.4.4	Sources of BrC in background aerosol at the SOAS site.....	150
5.5	Conclusions	153
5.6	References	155
6	Conclusions.....	163
Appendix A Supporting Information for Chapter 2		167
Appendix B Supporting Information for Chapter 3		169
B.1	Size Exclusion Chromatography Molecular Weight Calibration.....	169
B.2	Total Organic Carbon Analysis.....	170
B.3	MOUDI Analysis	170
Appendix C Supporting Information for Chapter 4		178
C.1	Conversion of peak areas to absorption coefficients.....	178
Appendix D Supporting Information for Chapter 5		183

List of Tables

Table C-1: Summary of measured particle-bound species concentrations reported as
d mass/d log D_p concentrations in units of $\mu\text{g}/\text{m}^3$. MMA – monomethyl ammonium, DMA
– dimethyl ammonium, TMA – trimethyl ammonium, MEA – monoethyl ammonium, DEA
– diethyl ammonium, TEA – triethyl ammonium.....182

List of Figures

Figure 1-1: Simulated mass weighted size distribution of atmospheric particles. The red region denotes ultrafine particles, the green region denotes fine mode particles, the blue region denotes coarse mode particles and the black line is the sum of all three modes	3
Figure 1-2: Summary of particle formation mechanisms. Not included is the direct formation of fine mode particles produced via combustion.	4
Figure 1-3: Summary of particle emission magnitudes. Bars represent literature reported minimum to maximum emissions. Red bars represent natural emissions, and blue bars represent anthropogenic emissions. Hashed bars denote primarily coarse mode emissions, while solid bars represent precursors to fine mode particles. PBAPs – primary biological aerosol particles, SOA – secondary organic aerosol, BVOCs – non-monoterpene and isoprene biogenic volatile organic compounds, NMVOCs – non-methane volatile organic compounds, POA – primary organic aerosol. Data from the 2013 Intergovernmental Panel on Climate Change report ¹²	5
Figure 1-4: Structure of biopolymers as fuel during biomass burning: A) Cellulose and B) lignin.	7
Figure 1-5: Anhydrosugar combustion products of incomplete biomass combustion: A) Levoglucosan, B) mannosan, C) galactosan.	8
Figure 1-6: Total radiative forcing effects dominant species relative to the year 1750 ⁴⁸ . Total gas-phase contributions include the greenhouse gas effect of atmospheric CO ₂ , CH ₄ , N ₂ O and halocarbons. Direct aerosol effects include particle scattering and absorption. Indirect aerosol effects are due to changes in cloud albedo.	9

Figure 1-7: Particle collection via elutriation	17
Figure 1-8: Particle collection via centrifugation	18
Figure 1-9: Particle collection via inertial impaction	18
Figure 1-10: Example Kendrick mass defect plot. Note how species only differing by a CH ₂ unit fall on the same horizontal line, while species with the same nominal mass, but different chemical formula, can be easily distinguished in the vertical direction	24
Figure 2-1: Kendrick mass defect plots for molecularly assigned peaks of (top) aqueous BB extract and (bottom) humic acid ionized using electrospray ionization in negative mode, coloured by the number of oxygens contained in the assigned molecular formula. Left panels correspond to peaks with assigned formulas containing C, H and O. Middle panels correspond to peaks with assigned formulas containing C, H, N and O. Right panels correspond to peaks with assigned formulas containing C, H, S and O. Black points correspond to formulas with no oxygen.....	55
Figure 2-2: Summed relative intensity of each compound class of assigned peaks as ionized by electrospray ionization in negative mode. Top panel corresponds to HA. Bottom panel corresponds to HULIS, methanolic and aqueous BB extracts in shaded, hashed and filled bars respectively.	56
Figure 2-3: Distribution of double bond equivalents of assigned molecular formula for (top) an aqueous biomass burning extract and (bottom) humic acid. Points are coloured by degree of oxygenation as measured by number of oxygens in the assigned molecular formula.....	57
Figure 2-4: Van Krevelen diagrams for the assigned peaks from (top) an aqueous BB extract and (bottom) HA. Red dots correspond to formulas including C, H and O; blue dots	

correspond to formulas including C, H, O and S; green dots correspond to formulas including C, H, O and N.59

Figure 2-5: Kendrick mass defect plots for molecularly assigned peaks of (top) aqueous and (bottom) HULIS BB extract ionized using electrospray ionization in positive mode, coloured by heteroatom inclusion. Blue dots correspond to peaks with assigned formulas containing C, H and O. Green dots correspond to peaks with assigned formulas containing C, H, N and O. Green dots correspond to peaks with assigned formulas containing C, H, S and O.61

Figure 2-6: Summed relative intensity of each compound class of assigned peaks as ionized by electrospray ionization in positive mode. Shaded, hashed and filled bars correspond to aqueous, methanolic and HULIS extracts, respectively.62

Figure 2-7: Top: Overlaid chromatograms from a size exclusion chromatography separation of an aqueous BB extract measured by APPI-MS in positive mode (solid black line) and by UV-vis absorbance spectrophotometry (dashed black line). Bottom: Summed and background subtracted APPI-MS spectra for each chromatographic region. Spectrum colour corresponds to the region in the above chromatogram: red – summed spectra from 9-10 min, green – from 10-12 min, blue – from 12-14 min. Black spectra corresponds to the background signal.64

Figure 2-8: Top - Kendrick Mass Defect plot for BB aerosol as analyzed using EI-UHRMS introduced using a direct insertion probe. Bottom - Summed relative intensity of each compound class of assigned peaks.67

Figure 2-9: Total ion current (TIC) for EI-UHRMS analysis as a function of desorption time overlaid with the time dependent desorption temperature in red.....68

Figure 3-1: Absorption density plots for (a) an aqueous extract of biomass burning PM_{2.5} and (b) an aqueous extract of Suwannee River Humic Acid. The chromatogram extracted from absorption at 300 nm is overlaid to highlight the molecular weight distribution of absorbing species in each sample.....85

Figure 3-2: a) Comparison of the TIC as measured by ESI(-)-MS (green) and absorption profile at 300 nm (black) as separated by SEC showing a mismatch between molecules responsible for absorption and those detected by ESI(-)-MS. b) Overlaid Kendrick Mass Defect Plots (CH₂-normalized) of the individual TIC peaks A (red) and B (blue) highlighting spectral similarity across the range of species separated by SEC.....90

Figure 4-1: Particle size distributions of (top) potassium, (middle) levoglucosan, and (bottom) acetate.....111

Figure 4-2: Particle size distributions of (red) sulfate, (green) chloride, (blue) nitrate and (black) sodium ions. Traces are offset for clarity.112

Figure 4-3: Particle size distributions of the most abundant ammonium species: (red) diethyl ammonium, (black) ammonium and (green) dimethyl ammonium.113

Figure 4-4: Particle size distributions of BrC absorption by (blue) molecules larger than 500 Da and (red) molecules less than 500 Da. Traces are stacked to reflect total absorption at each size fraction.....114

Figure 4-5: BrC molecular size distribution across particle stages as measured using SEC-UV115

Figure 4-6: Relative contribution of different sized molecules to the total absorption as a function of particle diameter.....116

Figure 4-7: Correlation between various (left) biomass burning markers (top - potassium, middle - levoglucosan, bottom - acetate) and (right) ammonium species (top - ammonium, middle - monoethyl ammonium, bottom - diethyl ammonium). Blue markers and lines correspond to correlations made with molecular absorption greater than 500 Da, where red markers and lines correspond to correlations made with molecular absorption < 500 Da.118

Figure 4-8: Reaction scheme outlining potential atmospheric imine formation and hydrolysis during sonication. Ammonia potentially reacts with carbonyl species to form an imine, and is hydrolysed back during extraction. Primary amines can undergo the same Schiff base reaction as ammonia, but may not be hydrolysed during extraction, leading to negatively biased primary amine concentrations. Secondary amines cannot undergo Schiff base reactions with carbonyls, and are thus not hydrolysed122

Figure 5-1: A) Locations of three sampling sites highlighted in yellow diamonds. Red circles denote locations of forest fires relevant to respective sampling periods with sizes of circles denoting size of forest fire from the Canadian National Fire Database. B) 48 h airmass back trajectories from the Vancouver sampling sites from 6 July 2015 as computed using the Hybrid Single Particle Lagrangian Trajectory (HYSPLIT) model. C) 72 h airmass back trajectories from the St. John’s sampling site from 6 July 2013 as computed using the HYSPLIT mode. Trace color denotes airmass transport time.143

Figure 5-2: Absorption density of BrC as a function of molecular weight across different sampling regions. Image color corresponds to normalized absorbance intensity. White trace denotes absorption profile at 300 nm. Plume age increases moving from figures A to C. A) Freshly emitted BB aerosol (~10-15 h) at the BKP site. B) Aged BB-aerosol

(~48 h) collected at the St. John's, NL site. C) Background emissions as collected at the SOAS site.....144

Figure 5-3: Absorbance distribution as a function of molecular weight for filters collected from 11 June 2013 – 13 July 2013 during the SOAS campaign. Each blue line represents a single analysis. The anomalous molecular weight profile from 11 June 2013 is shown in light grey.....145

Figure 5-4: A) BrC absorbance at 365 nm relative to CO as a function of plume age. Black squares denote average $\Delta\text{BrC}/\Delta\text{CO}$ for both Vancouver sites, black triangle denotes the St. John's site, red circles denote values obtained from Rim 1 fire in Forrister et al.²¹ B) Absorbance ratio for large molecules (>500 Da) to small molecules (<500 Da) as a function of plume age. Transport times for the Vancouver and St. John's sites are estimated from back trajectories calculated using the HYSPLIT model.146

Figure 5-5: A) Absorbance as measured by SEC-UV for samples acquired from the SOAS campaign. Blue bars represent the absorbance by molecules greater than 500 Da, red bars represent the absorbance by molecules less than 500 Da. B) In-situ measured absorption at the SOAS campaign. Green bars show OA absorption, the black line represents absorption by BC, the red dotted line represents calculated k values, including OA absorption. C) Correlation between BrC absorption as measured by SEC-UV offline and by PiLS-LWCC online. Points colored by sampling date. D) Correlation between BrC absorption as measured by SEC-UV and BC absorbance as measured by MAAP. Points also colored by sampling date.....149

Figure 5-6: Correlation of BrC absorption as measured by SEC-UV to A) CO, B) SO ₂ , and organic aerosol fractions determined by PMF from AMS data in panels C-F. All points are colored by date.	151
Figure 5-7: 2D Volatility Basis Set space based on Donahue et al. ⁴⁹ , highlighting in red the region likely occupied by the large molecular weight BrC species characterized in this study based on molecular weight and probable O:C ratios. Red arrows indicate that the lower end log ₁₀ (C°) for the largest molecules is likely lower than -14, based on the molecular weights calculated.	154
Figure A-1: Kendrick Mass Defect plot comparison between aqueous extracts, in blue dots and (top) methanolic and (bottom) HULIS extracts, in red dots as analyzed using electrospray ionization in negative mode. Common peaks between extracts are represented in black dots.	167
Figure A-2: Kendrick Mass Defect plot of humic acids as analyzed using electrospray ionization in positive mode.	168
Figure B-1: Calibration of size exclusion chromatography molecular weight distributions using Polysep GFC P-2000 column.	172
Figure B-2: Real-time PM _{2.5} and CO measurements from St. John's monitoring site. Measurements were averaged to an hourly time base. The average PM _{2.5} concentration during the sampling period was 78.6 µg/m ³ , where background PM _{2.5} concentrations were 5.7 µg/m ³ from June 1 to August 31, 2013.	172
Figure B-3: 48h air mass back-trajectories from July 6, 2013 in St. John's, NL as computed using the Hybrid Single Particle Lagrangian Integrated Trajectory Model (HYSPLIT).	173

Figure B-4: Absorption density plot of an aqueous extract of BMB aerosols collected on stage 6 ($0.56 < D_p < 1 \mu\text{m}$) of the nanoMOUDI. Overlaid is the absorption at 300 nm to highlight the molecular weight distribution of absorbing species. 173

Figure B-5: SEC-UV chromatograms at 300, 365 and 405 nm of water and methanol PM2.5 extracts highlighting their similarity in the quantity of light absorption and molecular weight distribution. No statistical difference in the integrated quantity of light absorption at 300, 365, and 405 nm was found ($P < 0.46$). 174

Figure B-6: Absorption density of an aqueous extract of BMB aerosols as measured by RP-HPLC-UV. Overlaid is the absorption at 365 nm to highlight the unresolved absorption feature. The absorption at 23 minutes is an instrumental artifact. 174

Figure B-7: Total absorption comparison as measured by total integrated area between SEC-UV and RP-HPLC-UV analyses. Error bars indicate the standard deviation of multiple integrations. Red bars represent absorption measured by RP-HPLC. Blue bars represent absorption measured by SEC. 175

Figure B-8: Top Panel – RP-HPLC chromatogram of a 1ppm 4-nitrocatechol standard measured at 365 nm. Middle Panel – RP-HPLC chromatogram of an aqueous extract of a BMB aerosol sample measured at 365 nm with no evidence of absorption from 4-nitrocatechol. Bottom Panel – Extracted ion chromatogram at $m/z = 154.01$ (representing the $[M-H]^-$ ion for 4-nitrocatechol) as measured by RP-HPLC with ESI- detection. Although there is an increase in signal near the expected elution time of 4-nitrocatechol, the peak shape is not representative and the intensity is very low. 175

Figure B-9: Range of k values as a function of wavelength for total OA (ELVOCs, LVOCs and SVOCs) and ELVOCs only, assuming ELVOCs are 10% of total particle mass.....176

Figure B-10: Summed mass spectra under peaks A and B from SEC-MS TICs. Inset spectra show ion clusters and ^{13}C isotope peaks are separated by 1 m/z, thus it can be assumed that the majority of ions are singly charged.176

Figure B-11: SEC-MS chromatograms at cone voltages ranging from 125 to 325 V. As cone voltage is increased, the absolute intensity decreases resulting in negative peaks during the elution of absorbing species from the column.....177

Figure C-1: Real-time $\text{PM}_{2.5}$ and CO measurements from St. John’s monitoring site. Measurements were averaged to an hourly time base. The average $\text{PM}_{2.5}$ concentration during the sampling period was $78.6 \mu\text{g}/\text{m}^3$, where background $\text{PM}_{2.5}$ concentrations were $5.7 \mu\text{g}/\text{m}^3$ from June 1 to August 31, 2013.180

Figure C-2: 72 h air mass back-trajectories from July 6, 2013 in St. John’s, NL as computed using the Hybrid Single Particle Lagrangian Integrated Trajectory Model (HYSPLIT).180

Figure C-3: Correlations between absorbance by (blue) molecules greater than 500 Da and (red) molecules less than 500 Da with potassium in A) all particle diameters, B) ultrafine particles and C) accumulation mode particles.....181

Figure D-1: CO and $\text{PM}_{2.5}$ loading in Vancouver during wildfire collection. Data acquired from British Columbia Air Data Archive, as part of the British Columbia Ministry of Environment, available at <http://envistaweb.env.gov.bc.ca/>183

Figure D-2: Directionality of signals arising from A) BBOA from AMS, B) absorbance by SEC-UV, and C) organic aerosol absorption by PiLS-LWCC184

Figure D-3: Ratio of large to small molecular weight absorbers throughout the SOAS campaign. Species greater than 500 Da consistently contributed roughly three times greater absorption than species less than 500 Da.....184

Figure D-4: Correlations between absorbance determined by SEC-UV with (A) NO₂, (B) O₃, (C) PM_{2.5} mass, (D) particulate NH₄⁺, (E) particulate SO₄²⁻, and (F) particulate NO₃⁻.....185

List of Symbols, Nomenclature, or Abbreviations

°	degrees
λ	wavelength
μg	micrograms
μL	microlitre
μm	microns
AIM	Ambient Ion Monitor
AMS	aerosol mass spectrometer
APPI	atmospheric pressure photo ionization
BB	biomass burning
BBCEAS	broadband cavity enhanced spectrometer
BC	black carbon
BKP	Burnaby/Kensington Park
BrC	brown carbon
CCN	cloud condensation nuclei
CI	chemical ionization
DBE	double bond equivalents
DEA	diethyl ammonium
DIP	direct insertion probe
DMA	dimethyl ammonium
EI	electron ionization
ELVOC	extremely low volatility organic compound
ESI	electrospray ionization
FTICR	Fourier transform ion cyclotron resonance
FWHM	full width half max
GC	gas chromatograph
GDAS1	Global Data Assimilation System
HA	humic acid
HILIC	hydrophilic interaction chromatography
HPLC	high performance liquid chromatography
HR-TOF	high resolution time of flight
HULIS	humic like substances
HYSPLIT	Hybrid Single Particle Lagrangian Integrated Trajectory
IC	ion chromatograph
IPCC	Intergovernmental Panel on Climate Change
IUPAC	International Union of Pure and Applied Chemistry

KMD	Kendrick Mass Defect
LOOOA	less oxidized oxygenated organic aerosol
LWCC	liquid waveguide capillary cell
m	meters
MAAP	multi-angle absorption photometer
MARGA	Monitor for Aerosols and Gases in Ambient Air
MEA	monoethyl ammonium
MMA	monomethyl ammonium
MOOOA	more oxidized oxygenated organic aerosol
MOUDI	Micro Orifice Uniform Deposit Impactor
MS	mass spectrometer
NDIR	non-dispersive infrared detection
NOM	natural organic matter
NVSN	North Vancouver/Second Narrows
OA	organic aerosol
PAH	polycyclic aromatic hydrocarbon
PiLS	Particle into Liquid Sampler
PM	particulate matter
POA	primary organic aerosol
PTOF	particle time of flight
RF	radiative forcing
RP	resolving power
RP	reverse phase
RSD	relative standard deviation
SEARCH	Southeastern Aerosol Research and Characterization Network
SEC	size exclusion chromatography
SOA	secondary organic aerosol
SPE	solid phase extraction
SRHA	Suwannee River humic acid
SRM	standard reference material
TEA	triethyl ammonium
TIC	total ion current
TMA	trimethyl ammonium
TOF	time of flight
UHRMS	ultra-high resolution mass spectrometry
VOC	volatile organic compound

List of Appendices

Appendix A – Supporting Information for Chapter 2

Appendix B – Supporting Information for Chapter 3

Appendix C – Supporting Information for Chapter 4

Appendix D – Supporting Information for Chapter 5

Preface

This thesis is comprised of a series of manuscripts that have been published or are in preparation for submission to be published in peer-reviewed scientific journals. Consequently, repetition of introductory and experimental details was inevitable. All manuscripts were written by Robert A. Di Lorenzo with critical comments provided by Cora J. Young. All research and manuscript preparation was conducted under the guidance of Cora J. Young. The contributions of co-authors are detailed below:

Chapter One: Introduction

Contributions – Prepared by Robert A. Di Lorenzo with editorial comments provided by Cora J. Young

Chapter Two: Comprehensive mass spectral analysis of an aged biomass burning aerosol sample

Author List – Robert A. Di Lorenzo, Stefanie Maedler, Karl J. Jobst, Xavier Ortiz, Vasile I. Furdui, Eric, J. Reiner, Cora J. Young

Contributions – Sample collection, preparation and APPI experiments were performed by Robert A. Di Lorenzo. ESI experiments were performed by Robert A. Di Lorenzo and Stefanie Maedler. DIP-EI experiments were performed by Robert A. Di Lorenzo and Xavier Ortiz. Data analysis was performed by Robert A. Di Lorenzo with critical contributions from Karl J. Jobst.

Chapter Three: Size separation method for absorption characterization in brown carbon:
Application to an aged biomass burning sample

Published in: Geophys. Res. Lett. 43(1), 458–465, doi:10.1002/2015GL066954, 2016.

Author List – Robert A. Di Lorenzo, Cora J. Young

Contributions – Sample collection, preparation and analysis was performed by Robert A. Di Lorenzo.

Chapter Four: Size-resolved composition of aged biomass burning aerosols derived from a real-world boreal wildfire

Author List – Robert A. Di Lorenzo, Bryan K. Place, Trevor C. VandenBoer, Cora J. Young

Contributions – Sample collection, preparation and SEC analysis was performed by Robert A. Di Lorenzo. IC experiments were performed by Bryan K. Place. Data interpretation and manuscript preparation was performed by Robert A. Di Lorenzo with critical comments provided by Trevor C. VandenBoer and Bryan K. Place.

Chapter Five: Molecular size separated brown carbon absorption for fresh and aged biomass burning plumes at multiple field sites

Author List – Robert A. Di Lorenzo, Rebecca A. Washenfelder, Alexis R. Attwood, Hongyu Guo, Lu Xu, Nga L. Ng, Rodney J. Weber, Karsten Baumann, Eric Edgerton, Cora J. Young

Contributions – Sample collection at the SOAS site was performed by Rebecca A. Washenfelder and Alexis R. Attwood. Sample preparation and SEC analysis was

performed by Robert A. Di Lorenzo. PiLS-LWCC data was acquired by Hongyu Guo under the supervision of Rodney J. Weber. AMS data was acquired by Lu Xu under the supervision of Nga L. Ng. Carbon monoxide data was provided by Karsten Baumann and Eric Edgerton. Data interpretation and manuscript preparation was performed by Robert A. Di Lorenzo with assistance from Rebecca A. Washenfelder. Critical manuscript comments were provided by Lu Xu, Nga L. Ng, and Rodney J. Weber.

Chapter Six: Conclusions

Contributions – Prepared by Robert A. Di Lorenzo with editorial comments provided by Cora J. Young

1 Introduction

1.1 Atmospheric Particulate Matter

Atmospheric particles are microscopic solid or liquid droplets suspended in the atmosphere. They are also referred to as atmospheric particulate matter (PM) or atmospheric aerosols. PM can be formed directly through mechanical processes, such as wind¹ and wave action²⁻⁴, as a by-product of incomplete combustion in biomass burning (BB)⁵, diesel fuel burning⁶ and volcanic eruption⁷, from the release of biological particles such as spores and pollen⁸, and from the condensation of precursor gases via atmospheric oxidation⁹.

1.1.1 Size Distribution

The mechanism by which particles are formed generally determines their size distribution. Particles are grouped into two different modes, or regions of local maxima in the number weighted size distribution. Coarse mode particles, or those with a diameter between 1 and 100 μm , tend to be derived from tribological and mechanical processes or are of biological origin¹⁰. Fine mode particles, those below 1 μm in diameter, tend to be derived from gas condensation mechanisms and atmospheric oxidation¹¹. It is important to distinguish between these two populations because they differ not only in their formation mechanism, but also in chemical composition, optical properties and removal mechanisms¹⁰. The fine mode can be further divided into two fractions: the ultrafine mode containing particles up to 100 nm in diameter, and the accumulation mode containing particles between 100 nm and 1 μm ¹⁰. A typical mass-weighted size distribution of atmospheric particles can be seen in Figure 1-1. Accumulation and coarse mode particles encompass the bulk of particle mass. Although the ultrafine mode contains a significant

number of particles, their mass contribution is negligible because of their small size. Particles below 2.5 μm in diameter, or $\text{PM}_{2.5}$, are of particular importance due to their correlation with negative health effects; particles in this size range have the ability to pass through the alveolar membrane in the human lung and be deposited directly into the blood stream, giving rise to an exposure route for environmental contaminants that is rarely studied and poorly understood¹¹. A summary of particle formation mechanisms can be found in Figure 1-2.

1.1.2 Sources and Composition

Particle concentrations can range from about 1 $\mu\text{g}/\text{m}^3$ (particle mass per volume of air) in remote environments to 100 $\mu\text{g}/\text{m}^3$ or more in polluted regions¹¹. The impacts of PM cannot be understood solely by the quantity in the atmosphere. It is imperative to understand their composition in order to assess the toxicity of PM, the role in direct and indirect radiative effects, etc. Since aerosols have atmospheric lifetimes up to one week,

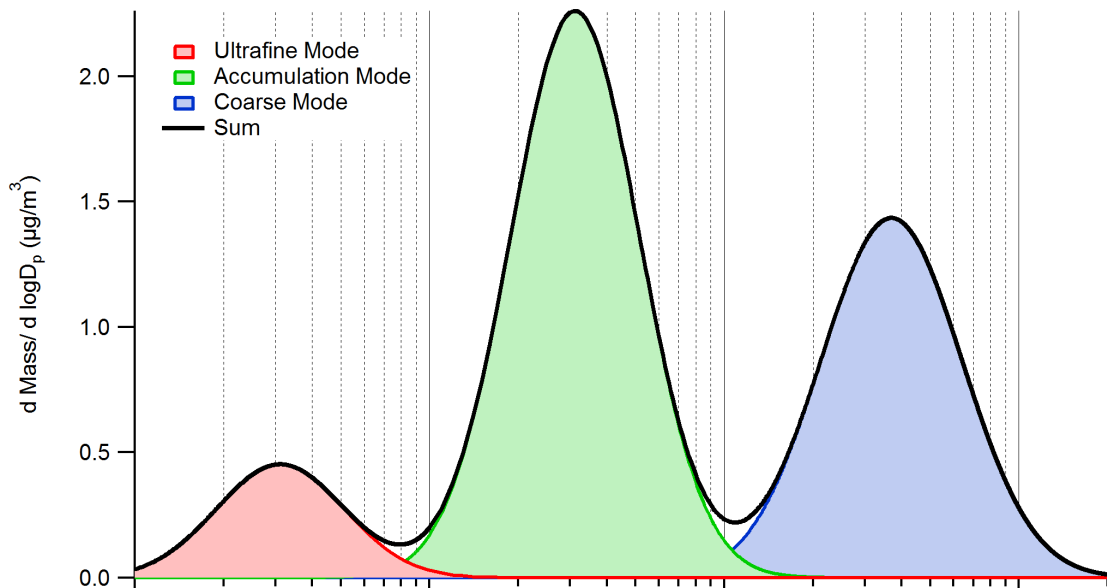


Figure 1-1: Simulated mass weighted size distribution of atmospheric particles. The red region denotes ultrafine particles, the green region denotes fine mode particles, the blue region denotes coarse mode particles and the black line is the sum of all three modes

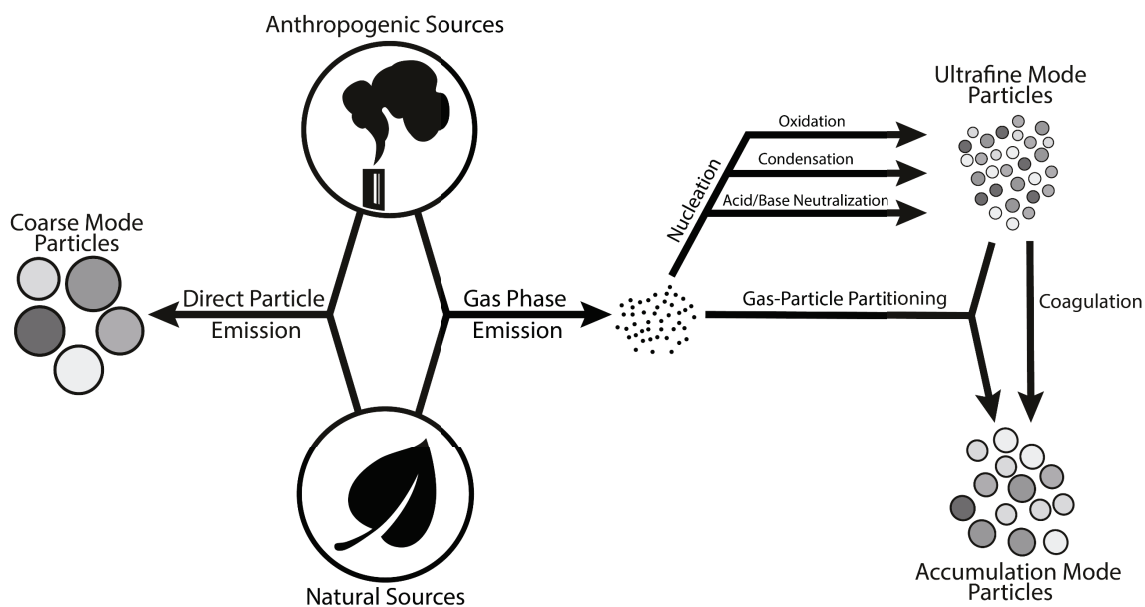


Figure 1-2: Summary of particle formation mechanisms. Not included is the direct formation of fine mode particles produced via combustion.

they have the potential to be globally transported. This highlights the importance of anthropogenic aerosol regulations, as local particle pollution has the potential to influence remote regions¹².

Atmospheric PM can be derived from a multitude of global sources as previously mentioned. A summary of their emission magnitudes can be seen in Figure 1-3¹². It is observed that natural, coarse mode emissions dominate the total aerosol mass in the atmosphere, specifically from wind- and wave-generated marine aerosols and wind-mediated uplifting of mineral dust. Precursors to fine mode aerosols of both anthropogenic and natural sources contribute roughly one order of magnitude less mass than coarse mode emissions to global particle loadings. Dimethylsulfide derived from biological ocean activity and biogenic volatile organic compounds (VOC), such as monoterpenes and isoprene, represent the dominant natural gas-phase precursors to fine mode aerosols in the

atmosphere¹⁰. Anthropogenic precursor emissions are primarily derived from combustion, specifically from the burning of biomass, coal and hydrocarbon fuels¹².

The inorganic mass fraction of fine particles primarily consists of SO_4^{2-} , NH_4^+ , NO_3^- and Cl^- ions, while the inorganic fraction of coarse particles is dominated by various sea salt, mineral dust and soil components such as carbonates and metal oxides¹⁰. Although the carbonate fraction of coarse particles tends to be a minor contributor by mass, it is an important species due to its reactivity with HNO_3 and N_2O_5 to form the corresponding nitrates, representing a sink for these nitrogenous gas phase species^{13,14}. This inorganic

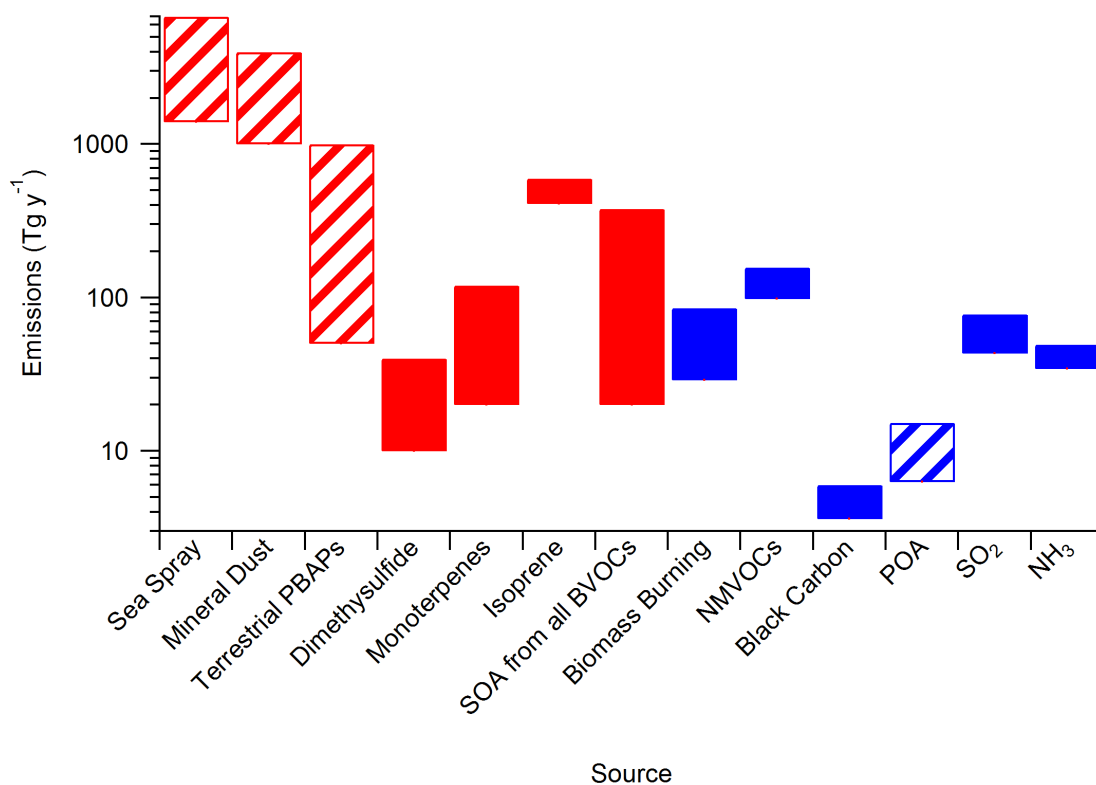


Figure 1-3: Summary of particle emission magnitudes. Bars represent literature reported minimum to maximum emissions. Red bars represent natural emissions, and blue bars represent anthropogenic emissions. Hashed bars denote primarily coarse mode emissions, while solid bars represent precursors to fine mode particles. PBAPs – primary biological aerosol particles, SOA – secondary organic aerosol, BVOCs – non-monoterpene and isoprene biogenic volatile organic compounds, NMVOCs – non-methane volatile organic compounds, POA – primary organic aerosol. Data from the 2013 Intergovernmental Panel on Climate Change report¹².

fraction can range between 25-75% of any given particle's composition⁹. SO_4^{2-} and NO_3^- in particles are derived from the photochemical oxidation of gas phase SO_2 , NO and NO_2 , which are products of anthropogenic combustion, such as coal burning and vehicle exhaust¹⁰. Particulate Cl^- is more prominent in coastal regions, due to the influence of marine-based aerosols, in regions prone to BB or regions that partake in waste incineration where particulate Cl^- is a direct result of the combustion of polyvinyl chloride¹¹. NH_4^+ in atmospheric aerosols is a result of acid-base neutralization reactions of NH_3 , most commonly derived from agricultural livestock waste, with atmospheric H_2SO_4 and HNO_3 ¹⁵.

While work on the inorganic speciation has been widely undertaken due to the low number of analytes and relatively high concentration of each species, speciation of the complex organic fraction of particles is still in its infancy. Organics are generally lumped into one category, or separated into three or four categories based on their degree of oxidation determined from their oxygen to carbon ratio (O:C ratio)⁹. It is expected that the number of organic species is in the thousands, as determined with ultra high resolution mass spectrometry (UHRMS) experiments¹⁶⁻¹⁹. The mixture of organics is often likened to other complex natural organic mixtures such as soil and aqueous-dissolved organic matter²⁰⁻²². Organic aerosols derived from the nucleation, condensation, oxidation or partitioning of gas-phase VOCs are defined as secondary organic aerosol (SOA), whereas directly emitted organic particles are defined as primary organic aerosol (POA)¹⁰. SOA represents the dominant form of organic aerosol^{9,23-25}. As such, SOA production mechanisms are widely studied throughout the atmospheric community²⁶⁻²⁸, but will not be discussed here in the interest of brevity.

1.1.2.1 Biomass Burning Aerosol

Second to only those derived from the processing of biogenic VOCs, combustion represents a large source of organic aerosol to the atmosphere, specifically the combustion of biomass¹². The burning of biomass fuels is a long recorded natural process, but has accelerated in recent years due to anthropogenic intervention and the anthropogenic effect on climate²⁹. During the heating process, biopolymers in woods and grasses, such as cellulose and lignin (Figure 1-4), begin to dehydrate, hydrolyze, oxidize and pyrolyze to release combustible VOCs, which are the main species responsible for the combustion process³⁰⁻³². Combustion products include many forms of reduced and oxidized carbonaceous species including n-alkanes, n-alkenes, n-alkanoic acids, n-alkanols,

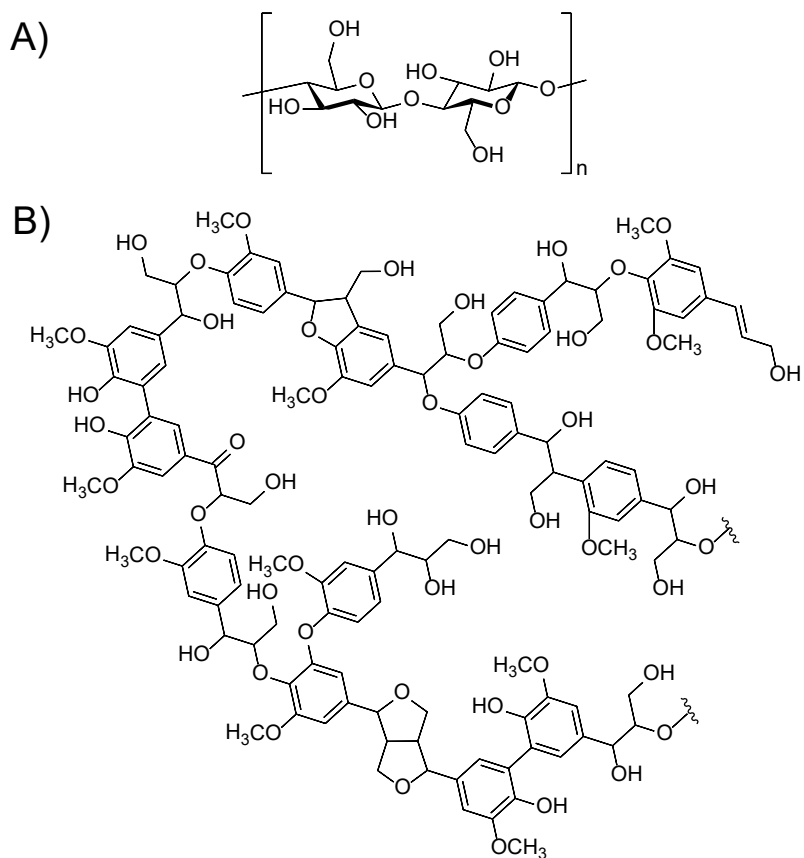


Figure 1-4: Structure of biopolymers as fuel during biomass burning: A) Cellulose and B) lignin.

methoxyphenolics, monosaccharide derivatives, steroids, terpenoids, and polycyclic aromatic hydrocarbons (PAHs)³³⁻³⁵. Two factors contribute to the formation of particles, both of which are a result of incomplete combustion: first, when moisture content is above 20-30% in the wood fibres, a large portion of energy is used to vaporize entrained water which leads to decreased burning efficiency and the formation of primary aerosol³⁶; second, in the case of wildfires, where woods are of low moisture content, fast burning leads to an oxygen deficiency which in turns leads to incomplete combustion and the formation of primary aerosol²⁹.

Many different molecular markers are used to identify the influence of BB in the atmosphere, the most common of which are potassium and the stereoisomeric anhydrosugars levoglucosan, mannosan and galactosan (Figure 1-5)²⁹. It has also been shown that nitrogenous species contribute a significant portion of emitted compounds, as nitrogen comprises roughly 3.5% of the total product mass³⁷. In this way, ammonia and alkyl amines also represent potential BB molecular markers in regions where alternative sources of amines are negligible^{5,38-44}.

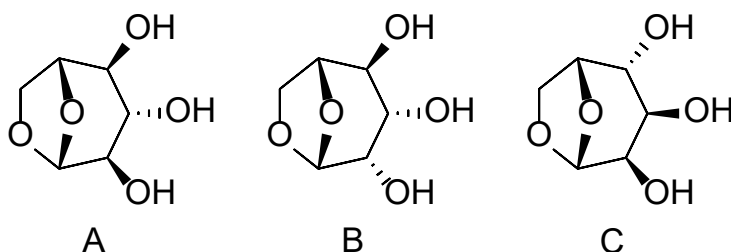


Figure 1-5: Anhydrosugar combustion products of incomplete biomass combustion: A) Levoglucosan, B) mannosan, C) galactosan.

1.2 Radiative Forcing by Atmospheric Particulate Matter

Atmospheric particles are of growing concern not only due to their public health effects, but due to their contribution to global radiative forcing (RF) and climate change⁴⁵⁻⁴⁷. RF is defined as the capacity for a particular species to change the radiative flux of the earth-atmosphere relative to the year 1750, measured in W/m^2 . Species with a positive RF have a net warming effect, whereas species with a negative RF have a net cooling effect. Continued work by the Intergovernmental Panel on Climate Change (IPCC) has shown that although atmospheric PM has a net negative contribution to radiative forcing, the uncertainty in PM measurements continue to be the greatest factor in the uncertainty of total anthropogenic radiative forcing (Figure 1-6)⁴⁸. Much uncertainty in PM measurements arises due to the heterogeneity of particle samples. Aerosols are an extremely complex and diverse matrix, where the composition of particles can differ greatly between populations

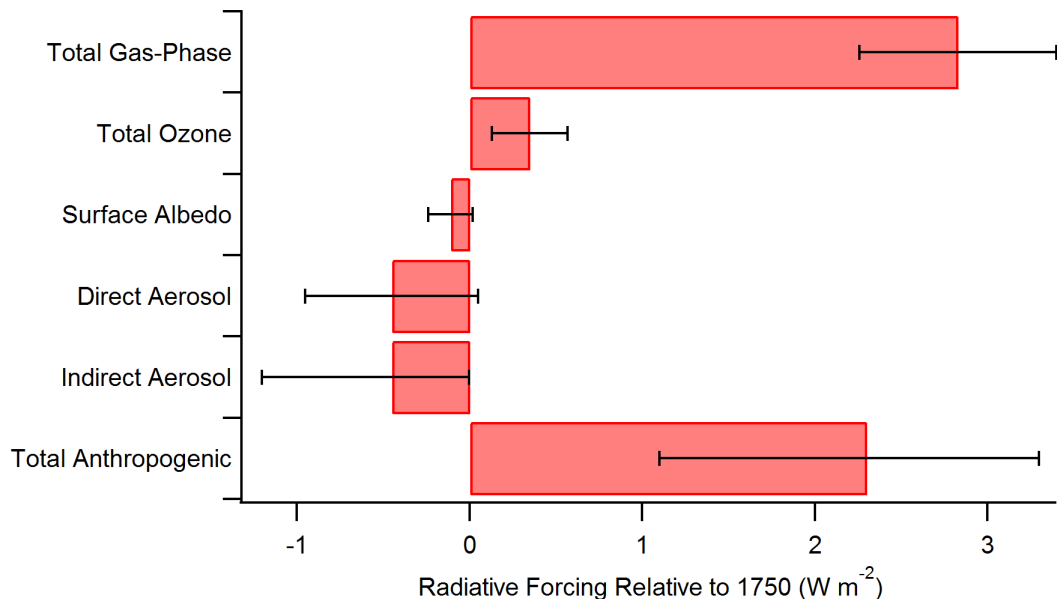


Figure 1-6: Total radiative forcing effects dominant species relative to the year 1750⁴⁸. Total gas-phase contributions include the greenhouse gas effect of atmospheric CO₂, CH₄, N₂O and halocarbons. Direct aerosol effects include particle scattering and absorption. Indirect aerosol effects are due to changes in cloud albedo.

and within a given population; their composition will determine their propensity to directly interact with incoming solar radiation or indirectly through their influence on cloud formation.

1.2.1 Indirect Climate Effects

Atmospheric PM has the unique ability to affect the formation and structure of clouds in the atmosphere. In this way, it can enhance total cloud albedo and increase their net cooling effect on the globe¹². Certain particles have the ability to seed the formation of clouds in the atmosphere; these are referred to as cloud condensation nuclei (CCN). The efficacy of particles as CCN depends on their composition, size as well as mixing state in the atmosphere⁴⁹. This increase in cloud droplet number concentration for a constant liquid water content is referred to as the first indirect effect⁵⁰. CCN also influence the properties of existing clouds; they have the ability to increase cloud density, extend cloud lifetime, increase cloud height and suppress rain events⁵⁰. These secondary indirect phenomena also effectively increase cloud albedo and the overall negative RF signature of aerosols.

1.2.2 Direct Climate Effects

Particles can interact with incoming solar radiation in two contrasting fashions: light scattering and light absorption. All aerosol particles have the ability to scatter light with their effectiveness being a function of their diameter⁵¹. Since particle scattering transforms directional, incoming solar radiation and directs a portion of that radiation away from the surface of the earth, particle scattering has a net negative RF¹². Certain particles, depending on their composition, have the ability to absorb light and affect the atmosphere in a similar way as greenhouse gases¹¹. The ratio of scattering to total extinction, which is the sum of

scattering and absorption, is described by the single scattering albedo, which can be calculated for particles of known composition by Mie theory⁵². A particle with a single scattering albedo value of one is purely scattering, and a value of zero denotes a purely absorbing particle.

Aerosol absorption is dominated by the occurrence of black carbon (BC), or carbonaceous soot, in the particle⁵³; it is still the only aerosol-bound species recognized to have a net-positive RF⁴⁸. BC is optically characterized by its wavelength independent absorption, following a λ^{-1} dependence⁵⁴. It is chemically characterized by its extended aromaticity, lack of chemical functionality and aqueous insolubility⁵⁵. It is emitted in primary aerosol as a product of incomplete combustion from both hydrocarbon and biomass fuels⁵⁵.

1.2.2.1 Brown Carbon

Although BC is the dominant carbonaceous particle absorber, particles often contain other organic species that have the ability to absorb light. These particular absorbing species have been named brown carbon (BrC) due to their brown appearance when collected⁵⁵. This colour arises from the wavelength dependent absorption properties of the absorbing organic species. Where BC generally shows little dependence in absorption as a function of wavelength (λ^{-1}), BrC is operationally defined by its enhanced absorption moving from the visible region to the ultraviolet, following a λ^{-2} to λ^{-6} dependence, which is attributed to the summed absorption of many individual organic molecules^{55,56}. In the field, direct measurements of BrC are often inferred from small spectral remainders after BC and mineral dust components have been subtracted^{54,57-60}; thus, there is large

uncertainty in the contribution of BrC to total particle absorption. There have been recent advances in the in-situ measurement of BrC^{61,62}, but confirmation of their accuracy is still needed as the chemical composition of BrC is unknown and only operationally defined. Only recently has BrC begun to be recognized to impact particle RF and included in climate models. BrC potentially represents the difference between previously calculated negative RF, or cooling-effect, of total particle contribution, and the measured positive RF, or net-warming effect⁶³. BrC could contribute up to +0.5 W/m², or about a third of the contribution of CO₂⁶³.

1.2.2.2 Secondary Organic Aerosol-Derived Brown Carbon

Two general sources have been described for BrC, the first of which is through the production of light absorbing SOA, which comprises the bulk of mechanistic laboratory studies. Many different SOA-BrC formation mechanisms have been proposed, where the inclusion of nitrogen is central to most⁶⁴. There are three dominant SOA-derived BrC formation mechanisms proposed. First, it has been proposed that when particles rich in glyoxal, a major degradation product of the dominant biogenic VOC isoprene and known particle nucleator^{65,66}, undergo dehydration in the presence of ammonium salts, Schiff-base reactions promote the formation of polyimine species that show appreciable light absorption in the visible region^{67,68}. A second proposed formation mechanism is the oxidation of toluene-rich particles in high NO_x environments, which leads to the production of organo-nitrate absorbing species⁶⁹. A third mechanism involves the polymerization of catechol and guaiacol in the presence of iron rich particles to form light-absorbing oligomers that resemble humic acids⁷⁰. Although SOA-derived BrC has dominated

laboratory mechanistic studies, it has been found to be only a minor contributor to field measured BrC⁷¹.

1.2.2.3 Biomass Burning-Derived Brown Carbon

BB has been shown to be the dominant source of BrC in multiple field samples⁷²⁻⁷⁴, although the formation mechanism and specific species responsible for absorption are unknown. Although certain individual small molecule absorbers (e.g. methyl nitrocatechols) have been proposed to dominate BrC absorption, this has been refuted by other studies^{57,71,74,75}. Laboratory studies have shown that BrC derived from BB is primarily composed of extremely low volatility organic compounds (ELVOCs): large, very oxidized and potentially oligomeric species that have been proposed to form rapidly in the highly oxidizing radical environment of a fire⁷⁶. Other studies have observed similar large molecular weight organic species resembling humic acid, which are sometimes referred to as humic like species, or HULIS^{16,20-22,77,78}. Half-lives of BrC with respect to oxidation in the atmosphere have been shown to be on the order of 9 to 15 h^{79,80}. Although the BrC atmospheric lifetime is rather short, there contains a recalcitrant fraction that is seemingly resistant to oxidation that leads to reduced light absorption^{79,80}. It is potentially the SOA-derived BrC fraction that is most susceptible to this degradation, where these large, already oxidized ELVOCs may represent background, long-lived BrC.

1.3 Aerosol Sampling and Analysis

1.3.1 Online Methods

With on-line methods, particles are sampled in real-time and measurements are made *in situ*. These methods eliminate the need for sample preparation and are usually automated

in their analysis and quantification. This poses a significant advantage over offline methods since a significant portion of aerosols can contain reactive species that will no longer be present after any degree of sample storage or preparation. In the case of aerosol mass spectrometers and single-particle mass spectrometers, these real-time instruments have the unique task of promoting mobilized condensed phase analytes into gas-phase ions. Offline mass spectral methods for the analysis of condensed phase compounds involve some sort of immobilization on a substrate or analysis from a surface. Traditionally, in-situ measurements are much less comprehensive in terms of their speciation, but allow for highly time resolved data sets and have the ability to give information about single particles. Real-time analysis is necessary for performing eddy covariance flux measurements⁸¹, the observation of new particle formation⁸², monitoring the concentrations of short lived atmospheric species, measuring the diurnal variation of important atmospheric constituents, detecting point sources of atmospheric contaminants and understanding atmospheric reaction mechanisms among many other applications. For this reason, the field of atmospheric chemistry has shown many recent and unique advances in technology relating to real-time, in situ mass spectrometric measurements. Instruments not only make rapid, highly sensitive measurements, but they are, for the most part, field deployable and relatively easily transportable.

1.3.1.1 Aerosol Mass Spectrometers (AMS)

These instruments have the capability to give size-resolved compositional information at rates faster than 1 Hz⁸³. Particles are sampled through an inlet held at atmospheric pressure, where they are guided through a series of aerodynamic lenses under

slight vacuum to yield a tight particle beam. From here, the instruments can be operated in one of two modes: mass spectrum (MS) mode and particle time of flight (PTOF) mode⁸⁴. In MS mode, an inlet chopper is left open such that all particles sampled will arrive at the high-temperature flash vaporization and ionization chamber of a mass spectrometer. Alternative desorption and ionization mechanisms based on laser ablation have also been applied⁸⁵. In this mode, a quadrupole mass analyzer is operated in scan-mode to obtain an averaged signal of all particle sizes. Signal interferences from gas phase components are removed by performing a background scan with the chopper in the closed position, such that only gas phase species would be sampled. In PTOF mode, the chopper modulates the incoming particle beam such that the particles in the range of 50-1000 nm can be aerodynamically sized in the particle drift region. Unfortunately, only single m/z data can be obtained for single particles with a quadrupole AMS, but more recent advances have added time of flight (TOF),⁸⁶ high resolution time of flight (HR-TOF)⁸⁷ and dual time of flight (dual TOF)^{88,89} mass analyzers to scan the positive and negative ion spectra simultaneously to give full spectral information for single particles.

1.3.1.2 Particle into Liquid Sampler-Ion Chromatograph (PiLS-IC) and Ambient Ion Monitor-Ion Chromatograph (AIM-IC)

The Particle into Liquid Sampler-Ion Chromatograph (PiLS-IC) and Ambient Ion Monitor-Ion Chromatograph (AIM-IC) obtain similar data sets through comparable sampling mechanisms and analysis methods, with minor differences attributed to variations in manufacturer design. Ambient aerosols are introduced through a size-selective cyclone head, discussed below, into the instrument via a slight vacuum at a rate of 1-5 L/min⁹⁰.

Particles then drift through a region of supersaturated water vapour to promote particle growth, which enhances sample collection efficiency⁹¹. At the end of the growth chamber, particles either impact a quartz stage and are collected with a slow stream of water for a PiLS system⁹⁰, or are collected via a second cyclone in the case of an AIM system⁹². For both samplers, the collected particles are automatically subjected to ion chromatography on an hourly basis^{91,93}. In the case of the AIM-IC, two ICs are present, such that both cations and anions can be quantified simultaneously⁹⁴. Water soluble gas phase compounds are removed prior to the growth tube using a wet-plate denuder⁹¹. Unfortunately, the detection of organics is generally limited with both the PiLS and AIM systems because they are restricted to highly water soluble analytes amenable to IC analysis.

1.3.2 Offline Methods

In order to truly gain insight into the composition of the organic fraction of aerosols, analysis methods other than mass spectrometry with hard ionization, as employed with AMS systems, must be explored. In order to use alternatives, particles must first be collected or immobilized and analyzed offline, based on the requirements of the desired analytical method. Aerosol particles can be collected on filter packs or other similar collection media, subjected to extraction and analysis via a wide range of instrumentation. These methods can be extremely effective for determining complex speciation and identification through the use of selective and rigorous extraction methods, long chromatography separations and mass spectrometric analysis. Unfortunately, these methods yield ensemble averaged data over time and over different particles.

1.3.2.1 Particle Size Selection

The most important feature for particle samplers is their size-selective inlet, which gives an upper size limit of collected particles. This is generally achieved in three different ways: elutriation, centrifugation and inertial impaction. Figure 1-7 shows the elutriation mechanism. Here, airflow is sampled in an upward direction to counteract the gravitational settling force acting on the particles. Particles of size greater than the cut-off diameter, as determined by various instrumental parameters such as flow rate and tube diameters, will settle out of the sampling head and will not be collected⁹⁵. With a cyclone inlet as shown in Figure 1-8, all suspended particles will enter the cyclone head, but only particles small enough to achieve a centripetal velocity great enough to counteract the gravitational settling force will enter upwards into the collection region.

The inertial impaction mechanism for size selection can be seen in Figure 1-9. Size selection occurs at each stage as a function of distance between the stage inlet and

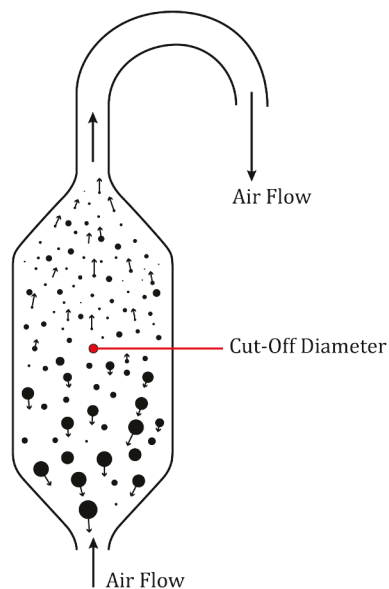


Figure 1-7: Particle collection via elutriation

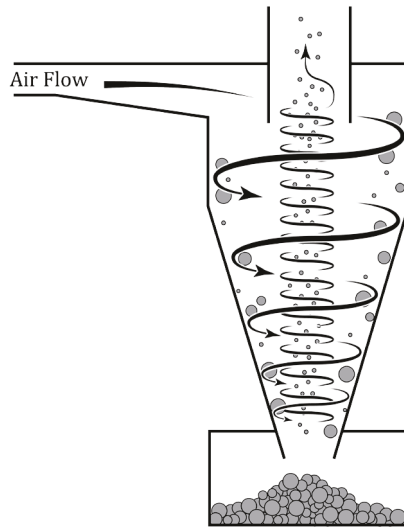


Figure 1-8: Particle collection via centrifugation

impaction plate as well as inlet flow rate⁹⁶. Particles that are small enough to follow the gas flow around the impaction plate are sent into the sampling apparatus or analyzer, but particles with larger vertical inertia will impact the plate and be immobilized⁹⁷. The smaller the distance between the stage inlet and plate, the smaller the particles that will bypass. To minimize impaction substrate overload and particle bounce, physical inertial impactors can

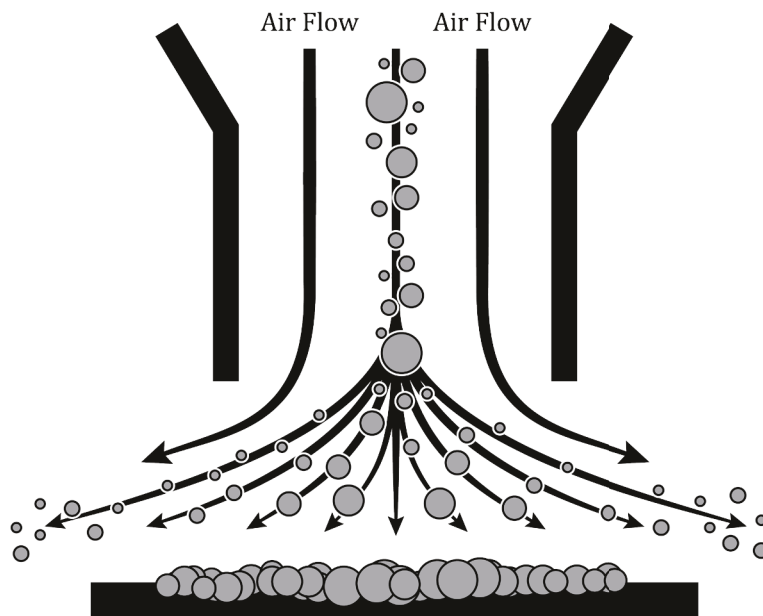


Figure 1-9: Particle collection via inertial impaction

be made into virtual impactors by replacing the impaction stage with a stagnant air layer where large particles can be then collected in sampling cup or high capacity filter. The majority of the flow will be directed around the stagnant air layer, where small particles will follow. Size selection then becomes a function of the ratio between the major flow horizontally around, and the minor flow vertically through the stagnant air layer⁹⁸.

1.3.2.2 Filtration-based High and Medium Volume Air Samplers

These samplers are the simplest, least expensive and most common for collecting atmospheric particles. They operate on the same basic principle as a commercial vacuum with an attached filter. Air is drawn in via a vacuum pump at a rate of tens (medium volume)⁹⁹ to hundreds (high volume)¹⁰⁰⁻¹⁰² of litres per minute, where particles are collected on quartz or Teflon filters placed in-line ahead of the vacuum pump.

High-volume samplers tend to suffer two major drawbacks in their simplicity. The first is sampling replicates, where high-volume samplers only collect one sample at a time. Filters can be split after analysis, but this can lead to sample loss, sample contamination, and the inability to determine the exact mass of particle collected in each sample fraction. Furthermore, multiple samplers placed adjacent to one another have shown high variability in their final extracted analyte concentrations. The lack of replicates also leads to difficulty in performing alternate analysis, such as simultaneously analyzing particulate organics and inorganics to determine a whole particle mass balance. The second drawback to high-volume samplers is the blow-on and blow-off sampling artifacts that lead to increased uncertainty in quantification. Since a very large volume of air is being passed over collected particles, gas phase compounds have the potential to sorb to filters creating a positive

sampling bias (blow-on effect) or semi-volatile analytes, such as ammonium nitrate, have the ability to re-enter the gas phase and be removed from collected particles (blow-off effect)^{103,104}. These blow-on and blow-off effects are greater at higher flow rates¹⁰⁵.

Both of these drawbacks are reduced with the advent of medium-volume samplers. URG Corp. has developed medium-volume samplers with multiple sampling inlets each with multiple sampling heads, leading to potential n=4 or n=6 sample replicates. Since this is achieved through the splitting of flow from one vacuum pump to multiple sampling heads and filter packs, differences in flow should be minimal. Furthermore, the same air sample is being identically sent to multiple filter packs, leading to significantly less variability than placing multiple different samplers, all with separate pumps, at the same site. Blow-on and blow-off effects are also reduced with medium-volume samplers due to their reduced flow rate. Additionally, there is the potential to place annular denuders ahead of the filter packs to scrub active gas phase compounds to essentially eliminate blow-on effects¹⁰⁵.

1.3.2.3 Inertial Impaction-based Micro-Orifice Uniform-Deposit Impactor (MOUDI)

Separating particle measurements into coarse and fine modes, as achievable with elutriation and centrifugation based sampling, is important for determining health-related air quality, but if further insight is necessary into understanding particle formation mechanisms, origin and lifetime, more highly resolved size information is necessary.¹⁰⁶⁻¹⁰⁸ This is particularly true for diameters approaching the ultrafine mode. This can be achieved with a MOUDI sampler¹⁰⁹. Just as in high-volume and medium volume samplers, air is drawn at a rate of tens of litres per minute via a vacuum pump through a size-selective head.

In this case, the particles are not collected on a filter, but are size separated by a series of inertial impaction stages with subsequently smaller cut-off diameters⁹⁶. These samplers have the ability to separate particles into thirteen different size bins between 18 μm and 10 nm^{110,111}. This is another sampling technique that requires creativity for obtaining sampling replicates. Although there are thirteen different stages for each sampler, each stage only accepts one sampling substrate. Particle compositions will differ throughout the size range, so averaging between stages becomes difficult.

1.3.2.4 Analytical Challenges to Offline Analysis

The more thorough analysis as achieved by offline methods allows for the identification of individual species present in particles, potentially elucidating markers for different atmospheric processes. Targeted analysis can be much more easily calibrated with established analytical methods and significantly more analytical rigor can be applied through the use of replicates, blanks, spike and recovery experiments and standard reference material (SRM) analysis. These are unavailable or very challenging to perform for online analysis. Unfortunately, aerosol matrix heterogeneity greatly increases the difficulty in defining blank and spike and recovery experiments for offline analysis in comparison to bulk phase measurements. Artificially representing the complexity of a particle for use as an analytical, method or sampling blank is nearly impossible. Furthermore, because compounds in particles are not necessarily on the surface of atmospheric particles, it is extremely difficult to representatively spike particles to quantify recoveries. Simply spiking a solution of analyte to a particle matrix does not reproduce the difficulty of extracting compounds from the core of particles. This leads to the potential for

significant negative systematic bias in quantification if SRMs are not available. Furthermore, most particle sampling instrumentation only has the potential to collect one sample at a time. Sampling and extraction replicates are a necessity for any method, especially for such a heterogeneous matrix as atmospheric particles. Splitting and fractionating single samples, which usually comprise filters and solid substrates, makes quantification difficult because the collected sample is not necessarily uniform over the collected surface. During splitting, the analyte could also be lost, or contamination could be introduced. Sample handling with aerosol samples is extremely important due to the inherent reactivity and semi-volatility of many of the sorbed compounds. Improper handling at elevated or decreased temperatures could lead to the reactivity, volatilization or sorption of various species, altering the composition of the collected sample. It is very difficult to assume that collected samples are identical at the time of analysis and during sampling. This highlights the importance of developing complementary *in situ*, on-line methods for analytical confirmation.

1.4 Organic Aerosol Speciation

1.4.1 Ultra-High Resolution Mass Spectrometry

The most common and powerful method for molecular-level offline characterization of organic aerosol samples is the use of ultra-high resolution mass spectrometry (UHRMS)¹¹², defined as having a resolving power (RP) greater than 100,000¹¹³. Resolving power is calculated using the following formula:

$$RP = \frac{m/z}{\Delta m/z_{FWHM}} \quad (1.1)$$

Where m/z is the mass to charge ratio of a detected ion and $\Delta m/z_{FWHM}$ is the peak width at 50% maximum intensity. An RP of this magnitude allows for the resolution of peaks differing by less than 5 mDa. For scale, an electron has a mass of approximately 0.5 mDa. This can be accomplished with the use of Fourier transform ion cyclotron resonance (FTICR) or Orbitrap mass analysers. These mass analysers are generally coupled to electrospray ionization sources due to their soft nature and propensity to generate molecular ions^{114,115}. They are generally operated in negative mode due to the acidic nature of most atmospheric organics^{27,116,117}. In this way, the thousands of molecules comprising the organic fraction of aerosols can be simultaneously analyzed in a relatively short, single experiment.

1.4.1.1 Data Handling

It is common to observe tens of thousands of individual peaks in a UHRMS spectrum of a complex material, like an organic aerosol sample¹¹⁸. Manually analyzing the data peak-by-peak becomes impossible. For this reason, creativity must be employed to visualize the data set for direct analysis and spectral comparison.

Although the International Union of Pure and Applied Chemistry (IUPAC) convention defines a mass scale based on the carbon exact mass ($^{12}\text{C} = 12.000\dots \text{Da}$), homologous series of organic species, those that only differ by a CH_2 , can be more easily identified if the mass scale is redefined for that unit ($^{12}\text{CH}_2 = 14.000\dots \text{Da}$): the Kendrick mass scale¹¹⁹. To fully utilize the power of the Kendrick mass scale, all masses must be first converted from the carbon scale in the following way:

$$\begin{aligned} \text{Kendrick Exact Mass} &= \text{Observed Mass} \times \frac{\text{Kendrick Mass}_{\text{CH}_2}}{\text{Exact Mass}_{\text{CH}_2}} \\ &= \text{Observed Mass} \times \frac{14.00000 \text{ Da}}{14.01565 \text{ Da}} \end{aligned} \quad (1.2)$$

Then, the Kendrick mass defect, the difference between the Kendrick exact mass and nominal mass, can be calculated. This is important because CH₂-based homologous series of compounds will have the same mass defect on this scale.

$$\text{Kendrick Mass Defect} = \text{Nominal Mass} - \text{Kendrick Exact Mass} \quad (1.3)$$

When plotting the Kendrick mass defect against the observed exact mass of each peak, homologous series of compounds differing by a CH₂ unit will fall on a horizontal line, as in the example Kendrick mass defect plot shown in Figure 1-10. This enhances the ability to assign molecular formulae, since if the molecular formula of one peak can be assigned, all peaks falling on the same horizontal line can be also be assigned. The different mass

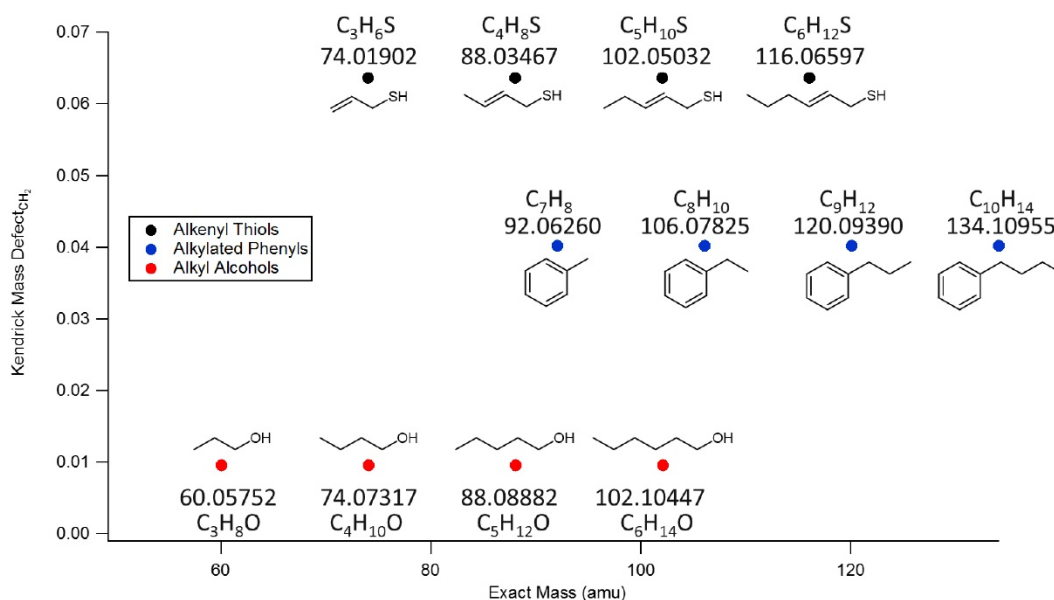


Figure 1-10: Example Kendrick mass defect plot. Note how species only differing by a CH₂ unit fall on the same horizontal line, while species with the same nominal mass, but different chemical formula, can be easily distinguished in the vertical direction

defects of common heteroatoms, especially the negative mass defect of halogens, allows them to be identified easily within a single spectrum and between spectra¹²⁰.

The enhanced ability to assign molecular formula can also be used in conjunction with van Krevelen diagrams, where H:C ratio is plotted against the O:C ratio for all assigned molecular formulae. A third dimension for the N:C ratio or intensity can be added for additional selectivity. With these visualization methods, complex spectra can be analysed to determine compound classes within the mixture, reaction and formation pathways, relative significance of structurally related compounds and compositional differentiation between samples¹²¹.

1.4.2 Humic-Like Species

Many of the mass spectral analysis methods for organic aerosol complex mixtures have been adapted from work done in the soil community on the analysis of natural organic matter (NOM), in particular the speciation of humic acid (HA)^{16,20–22,75,77,78}. HA comprises the bulk of soil organic matter and is composed of oligomeric species derived from the microbial degradation of plant matter¹²². HA is an operationally defined subset of NOM, determined from the extraction method from soil and water used in their preparation, but is poorly characterized at the molecular level¹²³. Similar methods are used in the extraction of organic aerosol for two reasons: (1) it is thought that HA is compositionally similar to that of organic aerosol^{27,116,124}; and (2) HA is commonly used as a spectral proxy for BrC absorbing species, especially those generated from BB^{21,55}. Aerosol organic matter extracted using these methods has thus been named HULIS. This seems to be a reasonable approximation due to the observation of highly oxidized, potentially oligomeric ELVOCs

observed to be generated during BB⁷⁶. However, it has been found that besides the acidic nature of the extract, HULIS differs greatly from HA. It is of lower average molecular weight, contains less aromaticity and higher surface activity among other differences²². Despite these observations, the term HULIS is still prevalent in the BrC literature.

1.4.3 Size Exclusion Chromatography

The potentially oligomeric nature of organic aerosol, specifically BB-generated ELVOCs, leads one to explore characterization methods employed in the polymer community. Paramount is the use of size exclusion chromatography (SEC) to determine the molecular weight distribution of the polymers of interest. SEC separates compounds solely on the basis of their hydrodynamic diameter, where chemical interactions and partitioning between the analyte and stationary phase are optimized to be negligible¹²⁵. Proper calibration using polymers with similar aggregation properties allows for highly accurate molecular weight distributions to be calculated. Due to the oligomeric nature of HA, SEC has been commonly used for analysis. It has been shown that due to its highly complex nature, HA has a large propensity to interact with the stationary phase. As a result, proper column choice and the use of solvent modifiers is important for proper molecular weight estimates^{126,127}. Further, common polymer standards, such as poly(ethylene glycol) are not sufficient for molecular weight calibration, since their structure and aggregation properties differ greatly from HA; poly(styrene sulfonate) displays similar hydrodynamic diameters and viscosities to HA¹²⁸.

1.5 Thesis Objectives

This work aims to accomplish two main goals: (1) to determine chemical composition of the soluble fraction of BB aerosol; and (2) determine the species responsible for BrC absorption in primarily BB-influenced aerosol particles. This will be accomplished in four parts: (1) the chemical composition of a BB-derived aerosol sample will be analyzed using UHRMS coupled to multiple ionization techniques (Goal 1, Chapter 2); (2) the BrC absorption profile will be analyzed using multiple chromatographic techniques coupled to molecular absorption and mass spectrometric detectors to determine the species responsible for absorption (Goals 1 and 2, Chapter 3); (3) the distribution of BB-derived BrC along with multiple BB markers and other atmospheric species will be determined across a wide range of particle diameters to determine its source, formation and mixing state (Goals 1 and 2, Chapter 4); and (4) the origin of BrC will be determined in background aerosol samples from a field campaign using co-located measurements of multiple gas- and particle-phase species to determine its origin and similarity to BB-derived BrC (Goal 2, Chapter 5).

1.6 References

- (1) Loye-Pilot, M. D.; Martin, J. M.; Morelli, J. Influence of Saharan dust on the rain acidity and atmospheric input to the Mediterranean. *Nature* **1986**, *321* (6068), 427–428.
- (2) Blanchard, D. C.; Woodcock, A. H. Bubble Formation and Modification in the Sea and its Meteorological Significance. *Tellus IX* **1957**, *9* (2), 145–158.
- (3) Blanchard, D. C.; Syzdek, L. D. Film drop production as a function of bubble size. *J. Geophys. Res.* **1988**, *93* (C4), 3649–3654.
- (4) Spiel, D. E. On the births of film drops from bubbles bursting on seawater surfaces. *J. Geophys. Res. Ocean.* **1998**, *103* (C11), 24907–24918.
- (5) Andreae, M. O.; Merlet, P. Emission of trace gases and aerosols from biomass burning. *Global Biogeochem. Cycles* **2001**, *15* (4), 955–966.
- (6) Kittelson, D. B. Engines and nanoparticles: A review. *J. Aerosol Sci.* **1998**, *29* (5–6), 575–588.
- (7) Mather, T. A.; Pyle, D. M.; Oppenheimer, C. Tropospheric volcanic aerosol. In *Volcanism and the Earth's Atmosphere*; **2003**; pp 189–212.
- (8) Bernstein, J. A.; Alexis, N.; Barnes, C.; Bernstein, I. L.; Bernstein, J. A.; Nel, A.; Peden, D.; Diaz-Sanchez, D.; Tarlo, S. M.; Williams, P. B. Health effects of air pollution. *J. Allergy Clin. Immunol.* **2004**, *114* (5), 1116–1123.
- (9) Jimenez, J. L.; Canagaratna, M. R.; Donahue, N. M.; Prevot, a S. H.; Zhang, Q.; Kroll, J. H.; DeCarlo, P. F.; Allan, J. D.; Coe, H.; Ng, N. L.; et al. Evolution of organic aerosols in the atmosphere. *Science* **2009**, *326* (5959), 1525–1529.
- (10) Seinfeld, J. H.; Pandis, S. N. *Atmospheric Chemistry and Physics: From air*

- Pollution to Climate Change*, 2nd ed.; John Wiley & Sons: Hoboken, NJ, **2006**.
- (11) Finlayson-Pitts, B. J.; Pitts, J. N. *Chemistry of the Upper and Lower Atmosphere: Theory, Experiments, and Applications*; Academic Press: San Diego, CA, **2000**.
- (12) Boucher, O.; Randall, D.; Artaxo, P.; Bretherton, C.; Feingold, G.; Forster, P. M.; Kerminen, V.-M.; Kondo, Y.; Liao, H.; Lohmann, U.; et al. Clouds and Aerosols. In *Climate Change 2013: The Physical Science Basis. Contribution of Working Group I to the Fifth Assessment Report of the Intergovernmental Panel on Climate Change*; Stocker, T. F., Qin, D., Plattner, G.-K., Tignor, M., Allen, S. K., Boschung, J., Nauels, A., Xia, Y., Bex, V., Midgley, P. M., Eds.; Cambridge University Press: Cambridge, United Kingdom and New York, NY, USA, **2013**.
- (13) Matsuki, A.; Iwasaka, Y.; Shi, G.; Zhang, D.; Trochkin, D.; Yamada, M.; Kim, Y.-S.; Chen, B.; Nagatani, T.; Miyazawa, T.; et al. Morphological and chemical modification of mineral dust: Observational insight into the heterogeneous uptake of acidic gases. *Geophys. Res. Lett.* **2005**, *32* (22), L22806.
- (14) Laskin, A.; Iedema, M. J.; Ichkovich, A.; Graber, E. R.; Taraniuk, I.; Rudich, Y. Direct observation of completely processed calcium carbonate dust particles. *Faraday Discuss.* **2005**, *130*, 453.
- (15) Andreae, M. O.; Crutzen, P. J. Atmospheric Aerosols: Biogeochemical Sources and Role in Atmospheric Chemistry. *Science* (80-.). **1997**, *276* (5315), 1052–1058.
- (16) Lin, P.; Rincon, A. G.; Kalberer, M.; Yu, J. Z. Elemental composition of HULIS in the Pearl River Delta Region, China: results inferred from positive and negative electrospray high resolution mass spectrometric data. *Environ. Sci. Technol.* **2012**, *46* (14), 7454–7462.

- (17) Rincón, A. G.; Calvo, A. I.; Dietzel, M.; Kalberer, M. Seasonal differences of urban organic aerosol composition - an ultra-high resolution mass spectrometry study. *Environ. Chem.* **2012**, *9* (3), 298.
- (18) Wozniak, A. S.; Bauer, J. E.; Sleighter, R. L.; Dickhut, R. M.; Hatcher, P. G. Technical Note: Molecular characterization of aerosol-derived water soluble organic carbon using ultrahigh resolution electrospray ionization Fourier transform ion cyclotron resonance mass spectrometry. *Atmos. Chem. Phys.* **2008**, *8* (17), 5099–5111.
- (19) Ikeya, K.; Sleighter, R. L.; Hatcher, P. G.; Watanabe, A. Fourier transform ion cyclotron resonance mass spectrometric analysis of the green fraction of soil humic acids. *Rapid Commun. Mass Spectrom.* **2013**, *27* (22), 2559–2568.
- (20) Paglione, M.; Kiendler-Scharr, A.; Mensah, A. A.; Finessi, E.; Giulianelli, L.; Sandrini, S.; Facchini, M. C.; Fuzzi, S.; Schlag, P.; Piazzalunga, A.; et al. Identification of humic-like substances (HULIS) in oxygenated organic aerosols using NMR and AMS factor analyses and liquid chromatographic techniques. *Atmos. Chem. Phys.* **2014**, *14* (1), 25–45.
- (21) Hoffer, A.; Gelencsér, A.; Guyon, P.; Kiss, G.; Schmid, O.; Frank, G.; Artaxo, P.; Andreae, M. O. Optical properties of humic-like substances (HULIS) in biomass-burning aerosols. *Atmospheric Chemistry and Physics Discussions*. 2005, pp 7341–7360.
- (22) Graber, E. R.; Rudich, Y. Atmospheric HULIS: how humic-like are they? A comprehensive and critical review. *Atmos. Chem. Phys. Discuss.* **2005**, *5*, 9801–9860.

- (23) Kroll, J. H.; Seinfeld, J. H. Chemistry of secondary organic aerosol: Formation and evolution of low-volatility organics in the atmosphere. *Atmos. Environ.* **2008**, *42* (16), 3593–3624.
- (24) Volkamer, R.; San Martini, F.; Molina, L. T.; Salcedo, D.; Jimenez, J. L.; Molina, M. J. A missing sink for gas-phase glyoxal in Mexico City: Formation of secondary organic aerosol. *Geophys. Res. Lett.* **2007**, *34* (19), L19807.
- (25) de Gouw, J.; Warneke, C. Measurements of volatile organic compounds in the earth's atmosphere using proton-transfer-reaction mass spectrometry. *Mass Spectrom. Rev.* **2007**, *26* (2), 223–257.
- (26) Hallquist, M.; Wenger, J. C.; Baltensperger, U.; Rudich, Y.; Simpson, D.; Claeys, M.; Dommen, J.; Donahue, N. M.; George, C.; Goldstein, a. H.; et al. The formation, properties and impact of secondary organic aerosol: current and emerging issues. *Atmos. Chem. Phys.* **2009**, *9* (14), 5155–5236.
- (27) Kanakidou, M.; Seinfeld, J. H.; Pandis, S. N.; Barnes, I.; Dentener, F. J.; Facchini, M. C.; Van Dingenen, R.; Ervens, B.; Nenes, A.; Nielsen, C. J.; et al. Organic aerosol and global climate modelling: a review. *Atmos. Chem. Phys.* **2005**, *5*, 1053–1123.
- (28) Atkinson, R. Atmospheric chemistry of VOCs and NO(x). *Atmos. Environ.* **2000**, *34* (12–14), 2063–2101.
- (29) Simoneit, B. R. T. *Biomass burning - A review of organic tracers for smoke from incomplete combustion*; **2002**; Vol. 17.
- (30) Roberts, A. F. A review of kinetics data for the pyrolysis of wood and related substances. *Combust. Flame* **1970**, *14* (2), 261–272.
- (31) Alger, R. Pyrolysis and Combustion of Cellulosic Materials. In *The Mechanisms of*

- Pyrolysis, Oxidation, and Burning of Organic Materials*; Wall, L. A., Ed.; National Bureau of Standards Special Publication, **1972**; pp 171–184.
- (32) Shafizadeh, F. The Chemistry of Pyrolysis and Combustion. In *The Chemistry of Solid Wood*; **1984**; pp 489–529.
- (33) Simoneit, B. R. T. Biomarker PAHs in the Environment. In *PAHs and Related Compounds*; Neilson, A. H., Ed.; Springer Berlin Heidelberg: Berlin, Heidelberg, **1998**; Vol. 3, pp 175–221.
- (34) Oros, D. R.; Simoneit, B. R. T. Identification and emission factors of molecular tracers in organic aerosols from biomass burning Part 2 . Deciduous trees. *Appl. Geochemistry* **2001**, *16*, 1513–1544.
- (35) Oros, D. R.; Simoneit, B. R. T. Identification of molecular tracers in organic aerosols from temperate climate vegetation subjected to biomass burning. *Aerosol Sci. Technol.* **1999**, *31* (6), 433–445.
- (36) Core, J.; Cooper, J.; Neulicht, R. Current and projected impacts of residential wood combustion on Pacific Northwest air quality. *J Air Pollut Control Assoc* **1983**, *Feb*;34 (2article available), 138–143.
- (37) Levine, J. S. Global biomass burning: Atmospheric, climatic and biospheric implications. *Eos, Trans. Am. Geophys. Union* **1991**, *71* (37), 3–22.
- (38) Cape, J. N.; Cornell, S. E.; Jickells, T. D.; Nemitz, E. Organic nitrogen in the atmosphere — Where does it come from? A review of sources and methods. *Atmos. Res.* **2011**, *102* (1–2), 30–48.
- (39) Youn, J.-S.; Crosbie, E.; Maudlin, L. C.; Wang, Z.; Sorooshian, A. Dimethylamine as a major alkyl amine species in particles and cloud water: Observations in semi-

- arid and coastal regions. *Atmos. Environ.* **2015**, *122*, 250–258.
- (40) Laskin, A.; Smith, J. S.; Laskin, J. Molecular characterization of nitrogen-containing organic compounds in biomass burning aerosols using high-resolution mass spectrometry. *Environ. Sci. Technol.* **2009**, *43* (10), 3764–3771.
- (41) Mace, K. A.; Artaxo, P.; Duce, R. A. Water-soluble organic nitrogen in Amazon Basin aerosols during the dry (biomass burning) and wet seasons. *Journal of Geophysical Research.* 2003, p 4512.
- (42) Maudlin, L. C.; Wang, Z.; Jonsson, H. H.; Sorooshian, A. Impact of wildfires on size-resolved aerosol composition at a coastal California site. *Atmos. Environ.* **2015**, *119*, 59–68.
- (43) Li, J.; Wang, G.; Aggarwal, S. G.; Huang, Y.; Ren, Y.; Zhou, B.; Singh, K.; Gupta, P. K.; Cao, J.; Zhang, R. Comparison of abundances, compositions and sources of elements, inorganic ions and organic compounds in atmospheric aerosols from Xi'an and New Delhi, two megacities in China and India. *Sci. Total Environ.* **2014**, *476–477*, 485–495.
- (44) Popovicheva, O.; Kistler, M.; Kireeva, E.; Persiantseva, N.; Timofeev, M.; Kopeikin, V.; Kasper-Giebl, a. Physicochemical characterization of smoke aerosol during large-scale wildfires: Extreme event of August 2010 in Moscow. *Atmos. Environ.* **2014**, No. August 2010.
- (45) Anderson, T. L.; Charlson, R. J.; Schwartz, S. E.; Knutti, R.; Boucher, O.; Rodhe, H.; Heintzenberg, J. Atmospheric science. Climate forcing by aerosol--a hazy picture. *Science (80-.).* **2003**, *300* (5622), 1103–1104.
- (46) Buseck, P. R.; Posfai, M. Airborne minerals and related aerosol particles: Effects on

- climate and the environment. *Proc. Natl. Acad. Sci.* **1999**, 96 (7), 3372–3379.
- (47) Pope, C. A.; Ezzati, M.; Dockery, D. W. Fine-particulate air pollution and life expectancy in the United States. *N. Engl. J. Med.* **2009**, 360 (4), 376–386.
- (48) Myhre, G.; Shindell, D.; Bréon, F.-M.; Collins, W.; Fuglestvedt, J.; Huang, J.; Koch, D.; Lamarque, J.-F.; Lee, D.; Mendoza, B.; et al. Anthropogenic and Natural Radiative Forcing. In *Climate Change 2013: The Physical Science Basis. Contribution of Working Group I to the Fifth Assessment Report of the Intergovernmental Panel on Climate Change*; Stocker, T. F., Qin, D., Plattner, G.-K., Tignor, M., Allen, S. K., Boschung, J., Nauels, A., Xia, Y., Bex, V., Midgley, P. M., Eds.; Cambridge University Press: Cambridge, United Kingdom and New York, NY, USA, **2013**; Vol. AR5.
- (49) Penner, J. E.; Andreae, M.; Annegarn, H.; Barrie, L.; Feichter, J.; Hegg, D.; Jayaraman, A.; Leaitch, R.; Murphy, D.; Nganga, J.; et al. Aerosols, their Direct and Indirect Effects. In *Climate change 2001: The scientific basis*; **2001**; pp 289–348.
- (50) Ramaswamy, V.; Boucher, O.; Haigh, J.; Hauglustaine, D.; Haywood, J.; Myhre, G.; Nakajima, T.; Shi, G.; Solomon, S.; Betts, R. E.; et al. *Radiative Forcing of Climate Change*; **2001**.
- (51) van de Hulst, H. C. *Light scattering by small particles*; Dover: New York, NY, **1981**.
- (52) Bohren, C. F.; Huffmann, D. R. *Absorption and scattering of light by small particles*; Wiley-Interscience: New York, NY, **1983**.
- (53) Ramanathan, V.; Carmichael, G. Global and regional climate changes due to black carbon. *Nat. Geosci.* **2008**, 1 (4), 221–227.
- (54) Kirchstetter, T. W.; Novakov, T.; Hobbs, P. V. Evidence that the spectral

- dependence of light absorption by aerosols is affected by organic carbon. *J. Geophys. Res. D Atmos.* **2004**, *109* (21), D21208.
- (55) Andreae, M. O.; Gelencsér, A. Black carbon or brown carbon? The nature of light-absorbing carbonaceous aerosols. *Atmos. Chem. Phys.* **2006**, *6* (10), 3131–3148.
- (56) Eck, T. F.; Holben, B. N.; Reid, J. S.; Dubovik, O.; Smirnov, A.; O'Neill, N. T.; Slutsker, I.; Kinne, S. Wavelength dependence of the optical depth of biomass burning, urban, and desert dust aerosols. *Journal of Geophysical Research.* 1999, p 31333.
- (57) Zhang, X.; Lin, Y. H.; Surratt, J. D.; Weber, R. J. Sources, composition and absorption Ångström exponent of light-absorbing organic components in aerosol extracts from the Los Angeles basin. *Environ. Sci. Technol.* **2013**, *47* (8), 3685–3693.
- (58) Bond, T. C.; Bergstrom, R. W. Light Absorption by Carbonaceous Particles: An Investigative Review. *Aerosol Sci. Technol.* **2006**, *40* (1), 27–67.
- (59) Yang, M.; Howell, S. G.; Zhuang, J.; Huebert, B. J. Attribution of aerosol light absorption to black carbon, brown carbon, and dust in China – interpretations of atmospheric measurements during EAST-AIRE. *Atmos. Chem. Phys. Discuss.* **2008**, *8* (3), 10913–10954.
- (60) Favez, O.; Alfaro, S. C.; Sciare, J.; Cachier, H.; Abdelwahab, M. M. Ambient measurements of light-absorption by agricultural waste burning organic aerosols. *J. Aerosol Sci.* **2009**, *40* (7), 613–620.
- (61) Hecobian, A.; Zhang, X.; Zheng, M.; Frank, N.; Edgerton, E. S.; Weber, R. J. Water-Soluble Organic Aerosol material and the light-absorption characteristics of aqueous

- extracts measured over the Southeastern United States. *Atmos. Chem. Phys.* **2010**, *10* (13), 5965–5977.
- (62) Washenfelder, R. A.; Flores, J. M.; Brock, C. A.; Brown, S. S.; Rudich, Y. Broadband measurements of aerosol extinction in the ultraviolet spectral region. *Atmos. Meas. Tech.* **2013**, *6* (4), 861–877.
- (63) Saleh, R.; Marks, M.; Heo, J.; Adams, P. J.; Donahue, N. M.; Robinson, A. L. Contribution of brown carbon and lensing to the direct radiative effect of carbonaceous aerosols from biomass and biofuel burning emissions. *J. Geophys. Res. Atmos.* **2015**, *120* (19), 10,285–10,296.
- (64) Laskin, A.; Laskin, J.; Nizkorodov, S. A. Chemistry of atmospheric brown carbon. *Chem. Rev.* **2015**, *115* (10), 4335–4382.
- (65) Volkamer, R.; Platt, U.; Wirtz, K. Primary and secondary glyoxal formation from aromatics: experimental evidence for the bicycloalkyl–radical pathway from benzene, toluene, and p -xylene. *J. Phys. Chem. A* **2001**, *105* (33), 7865–7874.
- (66) Volkamer, R.; Jimenez, J. L.; San Martini, F.; Dzepina, K.; Zhang, Q.; Salcedo, D.; Molina, L. T.; Worsnop, D. R.; Molina, M. J. Secondary organic aerosol formation from anthropogenic air pollution: Rapid and higher than expected. *Geophys. Res. Lett.* **2006**, *33* (17), 7–10.
- (67) Shapiro, E. L.; Szprengiel, J.; Sareen, N.; Jen, C. N.; Giordano, M. R.; McNeill, V. F. Light-absorbing secondary organic material formed by glyoxal in aqueous aerosol mimics. *Atmos. Chem. Phys.* **2009**, *9* (7), 2289–2300.
- (68) Lee, A. K. Y.; Zhao, R.; Li, R.; Liggió, J.; Li, S. M.; Abbatt, J. P. D. Formation of light absorbing organo-nitrogen species from evaporation of droplets containing

- glyoxal and ammonium sulfate. *Environ. Sci. Technol.* **2013**, *47* (22), 12819–12826.
- (69) Lin, P.; Liu, J.; Shilling, J. E.; Kathmann, S. M.; Laskin, J.; Laskin, A. Molecular characterization of brown carbon (BrC) chromophores in secondary organic aerosol generated from photo-oxidation of toluene. *Phys. Chem. Chem. Phys.* **2015**, *17* (36), 23312–23325.
- (70) Slikboer, S.; Grandy, L.; Blair, S. L.; Nizkorodov, S. a.; Smith, R. W.; Al-Abadleh, H. a. Formation of light absorbing soluble secondary organics and insoluble polymeric particles from the dark reaction of catechol and guaiacol with Fe(III). *Environ. Sci. Technol.* **2015**, No. Iii, 150615070810007.
- (71) Laskin, A.; Laskin, J.; Nizkorodov, S. A. Chemistry of atmospheric brown carbon. *Chem. Rev.* **2015**, *115* (10), 4335–4382.
- (72) Washenfelder, R. A.; Attwood, A. R.; Brock, C. A.; Guo, H.; Xu, L.; Weber, R. J.; Ng, N. L.; Allen, H. M.; Ayres, B. R.; Baumann, K.; et al. Biomass burning dominates brown carbon absorption in the rural southeastern United States. *Geophys. Res. Lett.* **2015**, *42*, 653–664.
- (73) Lack, D. A.; Langridge, J. M.; Bahreini, R.; Cappa, C. D.; Middlebrook, A. M.; Schwarz, J. P. Brown carbon and internal mixing in biomass burning particles. *Proc. Natl. Acad. Sci.* **2012**, *109* (37), 14802–14807.
- (74) Iinuma, Y.; Böge, O.; Gräfe, R.; Herrmann, H. Methyl-nitrocatechols: atmospheric tracer compounds for biomass burning secondary organic aerosols. *Environ. Sci. Technol.* **2010**, *44* (22), 8453–8459.
- (75) Claeys, M.; Vermeylen, R.; Yasmineen, F.; Gómez-González, Y.; Chi, X.; Maenhaut, W.; Mészáros, T.; Salma, I. Chemical characterisation of humic-like substances

- from urban, rural and tropical biomass burning environments using liquid chromatography with UV/vis photodiode array detection and electrospray ionisation mass spectrometry. *Environ. Chem.* **2012**, *9* (3), 273.
- (76) Saleh, R.; Robinson, E. S.; Tkacik, D. S.; Ahern, A. T.; Liu, S.; Aiken, A. C.; Sullivan, R. C.; Presto, A. a.; Dubey, M. K.; Yokelson, R. J.; et al. Brownness of organics in aerosols from biomass burning linked to their black carbon content. *Nat. Geosci.* **2014**, *7* (9), 647–650.
- (77) Lin, Y.; Budisulistiorini, S. H.; Chu, K.; Siejack, R. A.; Zhang, H.; Riva, M.; Zhang, Z.; Gold, A.; Kautzman, K. E.; Surratt, J. D. Light-absorbing oligomer formation in secondary organic aerosol from reactive uptake of isoprene epoxydiols. *Environ. Sci. Technol.* **2014**, *48* (20), 12012–12021.
- (78) Gaffney, J. S.; Marley, N. A.; Smith, K. J. Characterization of Fine Mode Atmospheric Aerosols by Raman Microscopy and Diffuse Reflectance FTIR. *J. Phys. Chem. A* **2015**, 150203151218000.
- (79) Vakkari, V.; Kerminen, V. M.; Beukes, J. P.; Tiitta, P.; Van Zyl, P. G.; Josipovic, M.; Venter, A. D.; Jaars, K.; Worsnop, D. R.; Kulmala, M.; et al. Rapid changes in biomass burning aerosols by atmospheric oxidation. *Geophys. Res. Lett.* **2014**, *41*, 2644–2651.
- (80) Forrister, H.; Liu, J.; Scheuer, E.; Dibb, J.; Ziemba, L.; Thornhill, K. L.; Anderson, B.; Diskin, G.; Perring, A. E.; Schwarz, J. P.; et al. Evolution of brown carbon in wildfire plumes. *Geophys. Res. Lett.* **2015**, *42* (11), 4623–4630.
- (81) Farmer, D. K.; Kimmel, J. R.; Phillips, G.; Docherty, K. S.; Worsnop, D. R.; Sueper, D.; Nemitz, E.; Jimenez, J. L. Eddy covariance measurements with high-resolution

- time-of-flight aerosol mass spectrometry: a new approach to chemically resolved aerosol fluxes. *Atmos. Meas. Tech.* **2011**, *4* (6), 1275–1289.
- (82) Junninen, H.; Ehn, M.; Petäjä, T.; Luosujärvi, L.; Kotiaho, T.; Kostianen, R.; Rohner, U.; Gonin, M.; Fuhrer, K.; Kulmala, M.; et al. A high-resolution mass spectrometer to measure atmospheric ion composition. *Atmospheric Measurement Techniques Discussions*. 2010, pp 599–636.
- (83) Jayne, J. T.; Leard, D. C.; Zhang, X.; Davidovits, P.; Smith, K. A.; Kolb, C. E.; Worsnop, D. R. Development of an aerosol mass spectrometer for size and composition analysis of submicron particles. *Aerosol Sci. Technol.* **2000**, *33* (1–2), 49–70.
- (84) Jimenez, J. L. Ambient aerosol sampling using the Aerodyne Aerosol Mass Spectrometer. *J. Geophys. Res.* **2003**, *108* (D7), 8425.
- (85) Bente, M.; Adam, T.; Ferge, T.; Gallavardin, S.; Sklorz, M.; Streibel, T.; Zimmermann, R. An on-line aerosol laser mass spectrometer with three, easily interchangeable laser based ionisation methods for characterisation of inorganic and aromatic compounds on particles. *Int. J. Mass Spectrom.* **2006**, *258* (1–3), 86–94.
- (86) Drewnick, F.; Hings, S. S.; DeCarlo, P.; Jayne, J. T.; Gonin, M.; Fuhrer, K.; Weimer, S.; Jimenez, J. L.; Demerjian, K. L.; Borrmann, S.; et al. A new time-of-flight aerosol mass spectrometer (TOF-AMS)—instrument description and first field deployment. *Aerosol Sci. Technol.* **2005**, *39* (7), 637–658.
- (87) DeCarlo, P. F.; Kimmel, J. R.; Trimborn, A.; Northway, M. J.; Jayne, J. T.; Aiken, A. C.; Gonin, M.; Fuhrer, K.; Horvath, T.; Docherty, K. S.; et al. Field-deployable, high-resolution, time-of-flight aerosol mass spectrometer. *Anal. Chem.* **2006**, *78*

- (24), 8281–8289.
- (88) Brands, M.; Kamphus, M.; Böttger, T.; Schneider, J.; Drewnick, F.; Roth, A.; Curtius, J.; Voigt, C.; Borbon, A.; Beekmann, M.; et al. Characterization of a newly developed aircraft-based laser ablation aerosol mass spectrometer (ALABAMA) and first field deployment in urban pollution plumes over Paris during MEGAPOLI 2009. *Aerosol Sci. Technol.* **2011**, *45* (1), 46–64.
- (89) Li, L.; Huang, Z.; Dong, J.; Li, M.; Gao, W.; Nian, H.; Fu, Z.; Zhang, G.; Bi, X.; Cheng, P.; et al. Real time bipolar time-of-flight mass spectrometer for analyzing single aerosol particles. *Int. J. Mass Spectrom.* **2011**, *303* (2–3), 118–124.
- (90) Weber, R. J.; Orsini, D.; Daun, Y.; Lee, Y.-N.; Klotz, P. J.; Brechtel, F. A Particle-into-Liquid Collector for Rapid Measurement of Aerosol Bulk Chemical Composition. *Aerosol Sci. Technol.* **2001**, *35* (3), 718–727.
- (91) Orsini, D. a.; Ma, Y.; Sullivan, A.; Sierau, B.; Baumann, K.; Weber, R. J. Refinements to the particle-into-liquid sampler (PILS) for ground and airborne measurements of water soluble aerosol composition. *Atmos. Environ.* **2003**, *37* (9–10), 1243–1259.
- (92) Khlystov, A. The steam-jet aerosol collector. *Atmos. Environ.* **1995**, *29* (17), 2229–2234.
- (93) Markovic, M. Z.; VandenBoer, T. C.; Murphy, J. G. Characterization and optimization of an online system for the simultaneous measurement of atmospheric water-soluble constituents in the gas and particle phases. *J. Environ. Monit.* **2012**, *14* (7), 1872–1884.
- (94) Wu, W. S.; Wang, T. On the performance of a semi-continuous PM_{2.5} sulphate and

- nitrate instrument under high loadings of particulate and sulphur dioxide. *Atmos. Environ.* **2007**, *41* (26), 5442–5451.
- (95) Kaye, B. H. *Characterization of Powders and Aerosols*; Wiley-VCH: Weinheim; New York; Chichester; Brisbane; Singapore; Toronto, **1999**.
- (96) Marple, V. A.; Rubow, K. L.; Behm, S. M. A microorifice uniform deposit impactor (MOUDI): description, calibration, and use. *Aerosol Sci. Technol.* **1991**, *14* (4), 434–446.
- (97) Marple, V. A.; Willeke, K. Impactor design. *Atmos. Environ.* **1976**, *10* (10), 891–896.
- (98) Marple, V. A.; Chien, C. M. Virtual impactors: a theoretical study. *Environ. Sci. Technol.* **1980**, *14* (8), 976–985.
- (99) Chen, B. B.; Sverdlik, L. G.; Imashev, S. a.; Solomon, P. a.; Lantz, J.; Schauer, J. J.; Shafer, M. M.; Artamonova, M. S.; Carmichael, G. Empirical relationship between particulate matter and aerosol optical depth over Northern Tien-Shan, Central Asia. *Air Qual. Atmos. Heal.* **2012**, *6* (2), 385–396.
- (100) Hueglin, C.; Gehrig, R.; Baltensperger, U.; Gysel, M.; Monn, C.; Vonmont, H. Chemical characterisation of PM_{2.5}, PM₁₀ and coarse particles at urban, near-city and rural sites in Switzerland. *Atmos. Environ.* **2005**, *39* (4), 637–651.
- (101) Zappoli, S.; Andracchio, A.; Fuzzi, S.; Facchini, M. C.; Gelencse, A.; Kiss, G.; Kriva, Z.; Molna, A.; Me, E.; Hansson, H.; et al. Inorganic, organic and macromolecular components of fine aerosol in different areas of Europe in relation to their water solubility. *Atmos. Environ.* **1999**, *33*, 2733–2743.
- (102) Wang, Y.; Zhuang, G.; Tang, A.; Yuan, H.; Sun, Y.; Chen, S.; Zheng, A. The ion

- chemistry and the source of PM_{2.5} aerosol in Beijing. *Atmos. Environ.* **2005**, *39* (21), 3771–3784.
- (103) Barber, J. L.; Berger, U.; Chaemfa, C.; Huber, S.; Jahnke, A.; Temme, C.; Jones, K. C. Analysis of per- and polyfluorinated alkyl substances in air samples from Northwest Europe. *J. Environ. Monit.* **2007**, *9* (6), 530–541.
- (104) Arp, H. P. H.; Goss, K.-U. Irreversible sorption of trace concentrations of perfluorocarboxylic acids to fiber filters used for air sampling. *Atmos. Environ.* **2008**, *42* (28), 6869–6872.
- (105) Ahrens, L.; Shoeib, M.; Harner, T.; Lane, D. A.; Guo, R.; Reiner, E. J. Comparison of annular diffusion denuder and high volume air samplers for measuring per- and polyfluoroalkyl substances in the atmosphere. *Anal. Chem.* **2011**, *83* (24), 9622–9628.
- (106) Saxena, P.; Hildemann, L. M.; McMurry, P. H.; Seinfeld, J. H. Organics alter hygroscopic behavior of atmospheric particles. *J. Geophys. Res.* **1995**, *100* (95), 755–770.
- (107) Cabada, J. C.; Rees, S.; Takahama, S.; Khlystov, A.; Pandis, S. N.; Davidson, C. I.; Robinson, A. L. Mass size distributions and size resolved chemical composition of fine particulate matter at the Pittsburgh supersite. *Atmos. Environ.* **2004**, *38* (20), 3127–3141.
- (108) Zhuang, H.; Chan, C. K.; Fang, M.; Wexler, A. S. Formation of nitrate and non-sea-salt sulfate on coarse particles. *Atmos. Environ.* **1999**, *33* (26), 4223–4233.
- (109) Nie, W.; Wang, T.; Gao, X.; Pathak, R. K.; Wang, X.; Gao, R.; Zhang, Q.; Yang, L.; Wang, W. Comparison among filter-based, impactor-based and continuous

- techniques for measuring atmospheric fine sulfate and nitrate. *Atmos. Environ.* **2010**, *44* (35), 4396–4403.
- (110) Cuccia, E.; Massabò, D.; Ariola, V.; Bove, M. C.; Fermo, P.; Piazzalunga, a.; Prati, P. Size-resolved comprehensive characterization of airborne particulate matter. *Atmos. Environ.* **2013**, *67*, 14–26.
- (111) Geller, M. D.; Kim, S.; Misra, C.; Sioutas, C.; Olson, B. A.; Marple, V. A. A methodology for measuring size-dependent chemical composition of ultrafine particles. *Aerosol Sci. Technol.* **2002**, *36* (6), 748–762.
- (112) Pratt, K. A.; Prather, K. A. Mass spectrometry of atmospheric aerosols--recent developments and applications. Part I: Off-line mass spectrometry techniques. *Mass Spectrom. Rev.* **2012**, *31* (1), 1–16.
- (113) Marshall, A. G.; Hendrickson, C. L.; Jackson, G. S. Fourier transform ion cyclotron resonance mass spectrometry: a primer. *Mass Spectrom. Rev.* **1998**, *17*, 1–35.
- (114) Novotny, N. R.; Capley, E. N.; Stenson, A. C. Fact or artifact: the representativeness of ESI-MS for complex natural organic mixtures. *J. Mass Spectrom.* **2014**, *49* (4), 316–326.
- (115) Stenson, A. C.; Landing, W. M.; Marshall, A. G.; Cooper, W. T. Ionization and fragmentation of humic substances in electrospray ionization Fourier transform-ion cyclotron resonance mass spectrometry. *Anal. Chem.* **2002**, *74* (17), 4397–4409.
- (116) Jaoui, M.; Kleindienst, T. E.; Lewandowski, M.; Edney, E. O. Identification and quantification of aerosol polar oxygenated compounds bearing carboxylic or hydroxyl groups. 1. Method development. *Anal. Chem.* **2004**, *76* (16), 4765–4778.
- (117) Sullivan, A. P.; Weber, R. J. Chemical characterization of the ambient organic

- aerosol soluble in water: 1. Isolation of hydrophobic and hydrophilic fractions with a XAD-8 resin. *J. Geophys. Res. Atmos.* **2006**, *111* (5), 1–9.
- (118) Wozniak, A. S.; Willoughby, A. S.; Gurganus, S. C.; Hatcher, P. G. Distinguishing molecular characteristics of aerosol water soluble organic matter from the 2011 trans-North Atlantic US GEOTRACES cruise. *Atmos. Chem. Phys. Discuss.* **2014**, *14*, 6427–6470.
- (119) Kendrick, E. A Mass Scale Based on $CH_2 = 14.0000$ for High Resolution Mass Spectrometry of Organic Compounds. *Anal. Chem.* **1963**, *35* (13), 2146–2154.
- (120) Jobst, K. J.; Shen, L.; Reiner, E. J.; Taguchi, V. Y.; Helm, P. A.; McCrindle, R.; Backus, S. The use of mass defect plots for the identification of (novel) halogenated contaminants in the environment. *Anal. Bioanal. Chem.* **2013**, *405* (10), 3289–3297.
- (121) Kim, S.; Kramer, R. W.; Hatcher, P. G. Graphical Method for Analysis of Ultrahigh-Resolution Broadband mass spectra of Natural Organic Matter, the Van Krevelen diagram. *Anal. Chem.* **2003**, *75* (20), 5336–5344.
- (122) Stevenson, F. J. *Humus Chemistry: Genesis, Composition, Reactions*; Wiley-Interscience: New York, NY, **1982**.
- (123) Swift, R. S. Organic matter characterization. In *Methods of soil analysis. Part 3. Chemical Methods (Soil Science Society of America Book Series, No. 5)*; Sparks, D. L., Ed.; Soil Science Society of America: Madison, WI, **1996**; pp 1018–1020.
- (124) Sullivan, A. P.; Weber, R. J.; Clements, A. L.; Turner, J. R.; Bae, M. S.; Schauer, J. J. A method for on-line measurement of water-soluble organic carbon in ambient aerosol particles: Results from an urban site. *Geophys. Res. Lett.* **2004**, *31* (13), n/a-n/a.

- (125) Harris, D. C.; Lucy, C. A. *Quantitative Chemical Analysis*, 9th ed.; W. H. Freeman & Co.: New York, NY, **2015**.
- (126) Her, N.; Amy, G.; Foss, D.; Cho, J.; Yoon, Y.; Kosenka, P. Optimization of Method for Detecting and Characterizing NOM by HPLC–Size Exclusion Chromatography with UV and On-Line DOC Detection. *Environ. Sci. Technol.* **2002**, *36* (5), 1069–1076.
- (127) Her, N.; Amy, G.; Foss, D.; Cho, J. Variations of molecular weight estimation by HP-size exclusion chromatography with UVA versus online DOC detection. *Environ. Sci. Technol.* **2002**, *36* (15), 3393–3399.
- (128) Perminova, I. V; Frimmel, F. H.; Kovalevskii, D. V; Abbt-Braun, G.; Kudryavtsev, A. V.; Hesse, S. Development of a predictive model for calculation of molecular weight of humic substances. *Water Res.* **1998**, *32* (3), 872–881.

**2 Comprehensive mass spectral analysis of an aged biomass burning
aerosol sample**

2.1 Abstract

An aged biomass burning sample was analyzed using a multitude of ionization techniques, including electrospray ionization (ESI) in positive and negative mode, atmospheric pressure photo ionization (APPI) in positive mode, and electron ionization (EI), combined with Orbitrap, Time-Of-Flight (TOF) and Fourier transform ion cyclotron resonance (FTICR) mass analyzers, respectively. Thousands of molecular formulae were assigned containing C, H, N, O and S atoms with a high degree of heterogeneity and oxidation. Compound class variability and complexity, as identified through the use of Van Krevelen diagrams, show that BB-aerosols are quite different from humic acid standards and, as such, the term humic-like substances (HULIS) may be a misnomer. Species ionized by APPI are more representative of the light-absorbing BrC fraction than those ionized by ESI. It is concluded, through experiments coupled to size exclusion chromatography, that compounds identified by each ionization technique have been fragmented during ionization.

2.2 Introduction

The characterization of the organic fraction of aerosol particles represents an ongoing and concerted effort in the atmospheric community due to the complexity of the matrix¹⁻³. This complexity arises from the vast array of sources to the environment including primary emissions from biomass and fossil fuel combustion, and secondary organic aerosol (SOA) formation from a multitude of anthropogenic and biogenic gas-phase emissions⁴. It is common to detect thousands of individual organic species within this fraction⁵⁻⁸. There is no single method that will allow for the characterization of the complete array of molecules

comprising the organic aerosol (OA) fraction. As such, these organic species remain poorly characterized.

Combustion, particularly from biomass burning (BB) represents a dominant contributor to total OA, with emissions on the order of 50-100 Tg per year⁴. These combustion-derived organic aerosols commonly have light-absorbing properties⁹⁻¹⁶, containing species such as black carbon (BC) and brown carbon (BrC), which contribute to climate change through their positive radiative forcing effect^{17,18}. BC and BrC are operationally characterized by absorption and solubility characteristics, where BC shows a lack of water solubility and a relatively wavelength independent absorption with graphite-like molecular character and BrC is commonly correlated with aqueous solubility and a largely wavelength dependent absorption increasing into the UV^{19,20}. The molecular level characterization, particularly of BrC, is poorly constrained. It is of utmost importance to characterize the BrC fraction in order to better constrain models, since BrC potentially represents the difference between calculated negative radiative forcing and experimentally positive radiative forcing for atmospheric particles on the whole²¹.

Ultra-high resolution mass spectrometry (UHRMS), defined as a mass spectrometric technique with a resolving power (RP) greater than 100 000²², has been frequently used for molecular level characterization of natural organic matter (NOM)²³⁻²⁸ and OA^{5,7,29,30}. Due to the large RP, molecules differing by masses on the order of millidaltons can be resolved, including isobars differing between a C₃ (36.0000 Da) and SH₄ (36.0034 Da) unit. Instruments with lower RP still have the capability of assigning molecular formulae³¹⁻³³ if some degree of selectivity or chromatography prior to analysis to reduce spectral complexity is employed, or the matrix is low in S-containing organics.

No single ionization technique is capable of detecting the full spectrum of organic molecules present in natural organic matter samples. All ionization methods are selective to some extent. Electrospray ionization (ESI) operated in negative mode is the most commonly employed ionization technique employed for the detection of NOM²⁴⁻²⁶ and OA^{5,7,30}. This is not only due to the common availability of ESI-capable instruments, but also because it is believed that the OA-fraction is primarily acidic in nature^{1,34,35} for which ESI(-) is highly amenable. It is frequently the case that ESI(-) is the only ionization technique used for characterization. In this way, alkaline components could be potentially underrepresented if complementary experiments using ESI(+) or other ionization techniques are not undertaken. It has been shown that the representativeness of an ESI spectrum to the true mixture comes with the trade-off of increased selectivity, which is undesirable for full characterization³⁶. Few studies have employed alternative, less common ionization techniques in conjunction with UHRMS, but those that do have been shown to better represent different fractions of NOM, for example the use of atmospheric pressure photo ionization (APPI) for the detection of nitrogenous organics in marine organic matter²⁷.

The objectives of this study were to analyze an aged aerosol sample collected from a real-world boreal wildfire using multiple ionization methods, including ESI, APPI and electron ionization (EI) in order to molecularly characterize the complex mixture and assess the relevancy of the detected molecules to the identity of the contained BrC chromophores.

2.3 Methods

2.3.1 Sample Collection

Aged BB aerosol were collected in St. John's (47.572° N, 52.722° W, 42 m above sea level) two days after a large scale forest fire erupted in northern Quebec and Labrador on July 4, 2013. Multiple PM_{2.5} samples (n=6) were collected in parallel on pre-muffled (500 °C, 4 h) 47 mm quartz fibre filters (Pall Life Sciences, Washington, NY, USA) using a multi-channel, medium volume air sampler (URG-3000ABC, URG Corp., Chapel Hill, NC, USA) for a total collection time of 25.5 h during the intrusion of the BB plume. Filters were stored in the dark at -20 °C until analysis.

2.3.2 Sample Preparation

2.3.2.1 Direct Solvent Extraction

Each filter was sub-sampled using a 10 mm diameter arch punch. Punches from each filter were placed in a glass vial and sealed with an acid washed cap containing a Teflon-lined septum. Per 10 mm subsample, 1.0 mL of ultrapure deionized water (Barnstead Infinity Ultrapure Water System, Thermo Scientific, Waltham, MA, USA) was added and the samples were sonicated at room temperature for 45 minutes. Humic acids (Suwannee River Humic Acid (SRHA) from the International Humic Substances Society, Denver, CO, USA and a humic acid standard obtained from Sigma Aldrich, St. Louis, MI, USA) were prepared to a concentration of 1.25 mg/mL in H₂O via 45-minute sonication in pre-muffled glass vials. After sonication, all extracts were filtered with 0.2 µm PTFE syringe filters (Iso-Disc, Supelco, Bellefonte, PA, USA), transferred to pre-muffled glass sample vials and stored at 4 °C until analysis.

2.3.2.2 HULIS Extraction

The HULIS fraction of BB aerosols was isolated according to the solid phase extraction (SPE) procedure outlined by Lin et al⁷. Briefly, aqueous extracts, as prepared above, were acidified to pH = 2 with concentrated HCl and loaded onto pre-rinsed mixed mode SPE cartridges (Oasis HLB, 3cc, 60 mg sorbent, 30 µm particle size, Waters Corp., Milford, MA, USA). The cartridge was then washed with one column volume of deionized H₂O. Analytes were eluted with methanol containing 2% (v/v) NH₄OH. The extract was evaporated to dryness under a gentle stream of N₂ and reconstituted in 1 mL/subsample of 1:1 acetonitrile:H₂O for analysis.

2.3.3 Mass Spectrometric Analysis

2.3.3.1 Ultra-High Resolution Mass Spectrometry with Electrospray Ionization

ESI-UHRMS analysis was performed using a hybrid quadrupole-Orbitrap mass spectrometer (Q Exactive, Thermo Fisher Scientific, Waltham, MA, USA). All spectra were acquired at a resolving power of 140 000 at full width half max (FWHM). Solvent extracted samples were diluted with methanol to a 35:10 methanol:water ratio to improve spray efficiency and were directly infused at a flow rate of 5 µL/min. ESI conditions were optimized for the most stable total ion current (TIC). Negative mode experiments were performed with the following conditions: capillary voltage: 3500 V, desolvation temperature: 300 °C, desolvation gas flow rate: 10 L/min. Positive mode experiments were performed with the following conditions: capillary voltage: 3800 V, desolvation temperature: 320 °C, desolvation gas flow rate: 8 L/min.

2.3.3.2 Ultra-High Resolution Mass Spectrometry with Direct Insertion Probe Electron Ionization

BB aerosols were analyzed using a custom hybrid gas chromatograph (GC)-triple quadrupole-Fourier transform ion cyclotron resonance (FTICR) MS (Varian 3800 GC, Varian 920 TQ-FTICR MS, 9.4 T superconducting magnet, Varian Inc., Walnut Creek, CA, USA). A direct insertion probe (DIP) was used to introduce a 1 μ L filter subsample that was inserted into a 3 μ L capillary to the mass spectrometer without the need for solvent extraction and to bypass GC separation. The DIP was slowly heated from room temperature to 300 $^{\circ}$ C over 5 minutes, then held for an additional 2.5 min to distribute compound desorption and minimize ion suppression. The FTICR was operated in electron ionization (EI) mode (70 eV) at a resolution of 100 000 to 150 000 (FWHM). Mass spectra were obtained using arbitrary waveform excitation and detection from m/z 50 – 650. Acquisition and cycle times were 500 ms and 1.0 s respectively.

2.3.3.3 High Resolution Mass Spectrometry with Atmospheric Pressure Photo Ionization coupled to Size Exclusion Chromatography and UV-vis Spectroscopy

Direct aqueous extracts of BB aerosols were separated using size exclusion chromatography. Chromatograms were acquired using an HPLC system (1260 Infinity, Agilent Technologies, Santa Clara, CA, USA) coupled to a diode array detector (1260, Agilent Technologies, Santa Clara, CA, USA) and time-of-flight (TOF) mass spectrometer (6230, Agilent Technologies, Santa Clara, CA, USA). Isocratic separations were performed using an aqueous gel filtration column (Polysep GFC P-3000, Phenomenex, Torrance, CA,

USA) at a flow rate of 500 $\mu\text{L}/\text{min}$ using a 1:1 mixture of methanol and water with a total ammonium acetate concentration of 12.5 mM. Compounds were ionized using atmospheric pressure photo ionization (APPI) operated in positive mode using the following conditions: drying gas temperature: 350 $^{\circ}\text{C}$, drying gas flow rate: 5 L/min, nebulizer pressure: 60 psi, vaporizer temperature: 450 $^{\circ}\text{C}$.

2.3.4 Data Handling

All ultra-high resolution mass spectra were internally calibrated with low-mass ions of only one possible molecular composition. With the aid of Kendrick Mass Defect (KMD) plots, representative formulae for internal calibration were then assigned across the entire mass range. The polynomial regressions (>30 points) resulted in sub-1ppm mass accuracy in all cases. All molecular formulae were assigned using a custom Excel macro in combination with an elemental composition calculator (Varian Inc., Walnut Creek, CA, USA) with a mass tolerance set to ± 0.001 Da. All spectral subtraction was performed with a custom excel template where subtraction windows were set to ± 0.001 Da. Subtraction was peak intensity independent to negate any differences in ionization efficiency and ion suppression between samples.

2.4 Results and Discussion

2.4.1 ESI

2.4.1.1 Negative Mode

ESI(-) experiments of all BB aerosol extracts showed vast spectral complexity, with the observation of up to 15000 spectral peaks and the assignment of over 5000 unique molecular formulae between m/z 100 and 1000, with an intensity maximum around 200-

300 Da in all cases. Peak assignments covered between 89-96% of the total summed peak intensity for all sample extracts, with the average deviation between peak assigned exact mass and measured mass being less than 1.5 ppm in all cases. The spectral complexity can be observed in the KMD plots of the aqueous BB aerosol extract in Figure 2-1. Molecular formulae assignments show the inclusion of nitrogen, sulfur and up to 16 oxygen atoms. Other heteroatoms were not included during formula assignments for simplification, since they are expected to be present at very low levels. The HULIS extract showed the most peaks and had the greatest number of assigned molecular formulae. Considering the HULIS fraction is a subset of the water soluble fraction, the increased spectral complexity must arise from the reduction of ion suppressors due to the SPE cleanup employed. Differences in spectra between aqueous, methanolic and HULIS extracts were minor and primarily arose from the least intense peaks; 85-95% of the total summed intensity was identical across samples. Comparing aqueous and methanolic extracts, the aqueous extract shows 7.7% unique intensity (~3000 unique peaks) and the methanolic extract shows 11.8% unique intensity (~1300 unique peaks). Comparing aqueous and HULIS extracts, the aqueous extract shows 6.4% unique intensity (~2300 unique peaks), and the HULIS extract shows 16.1% unique intensity (~4000 unique peaks). Comparing their KMD plots (Figure A-1), the differences in methanolic and HULIS extracts compared to aqueous extracts arose from the inclusion of more saturated aliphatic character.

ESI(-) spectra of HA (Figure 2-1) showed markedly less spectral complexity, lower degrees of oxidation and narrower molecular weight distributions than the BB aerosol extracts, with only 1700 assigned molecular formulae. The greatest difference arose in the CHNO_x fraction, where only 277 unique formulae were assigned, compared to the 1660

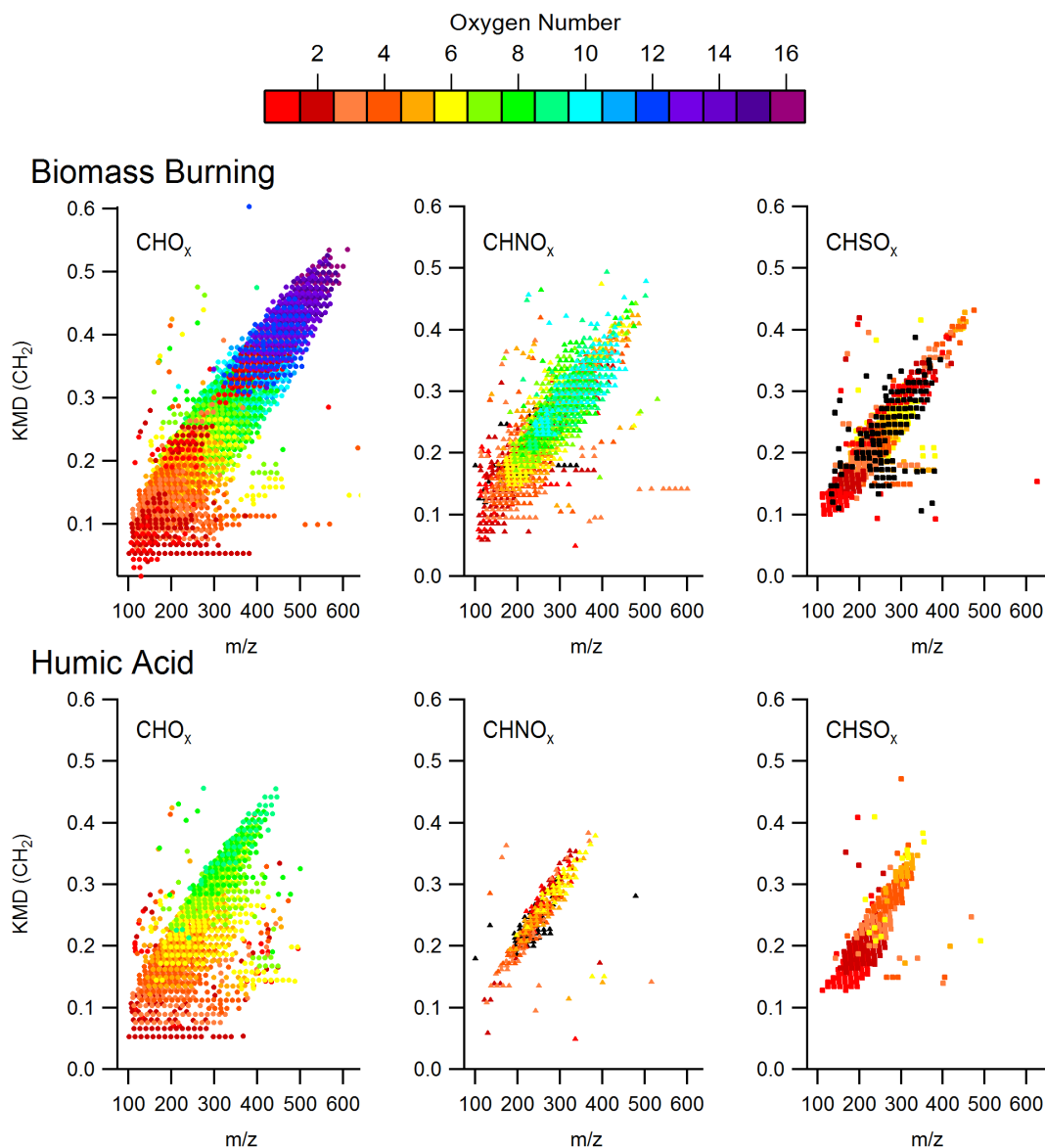


Figure 2-1: Kendrick mass defect plots for molecularly assigned peaks of (top) aqueous BB extract and (bottom) humic acid ionized using electrospray ionization in negative mode, coloured by the number of oxygens contained in the assigned molecular formula. Left panels correspond to peaks with assigned formulas containing C, H and O. Middle panels correspond to peaks with assigned formulas containing C, H, N and O. Right panels correspond to peaks with assigned formulas containing C, H, S and O. Black points correspond to formulas with no oxygen.

formulae assigned in the same fraction for the HULIS extract. The comparison between the compound class distribution between all BB aerosol extracts and HA is shown in Figure 2-2. HA is dominated by the O₂ and O₆ compound classes, but this is a result of the most abundant six to eight ions, which have been tentatively assigned to palmitic acid (C₁₆H₃₂O₂) and alkyl glucopyranose species for the O₂ and O₆ compound classes, respectively. Besides the O₂ and O₆ classes, the CHO_x class shows a uniform distribution with a maximum in the O₄ compound class. No compounds were observed to contain greater than 9 oxygens. All BB aerosol extracts showed similar distributions across CHO_x, CHNO_x and CHSO_x species. Intensity maxima are observed for the aqueous extract in the O₄ compound class, for the HULIS extract in the O₅ compound class, and for the methanolic extract in the O₆ compound class. All BB aerosol extracts showed a local maximum in the O₂ compound class, most likely due to the propensity of carboxylic acids to ionize in ESI(-).

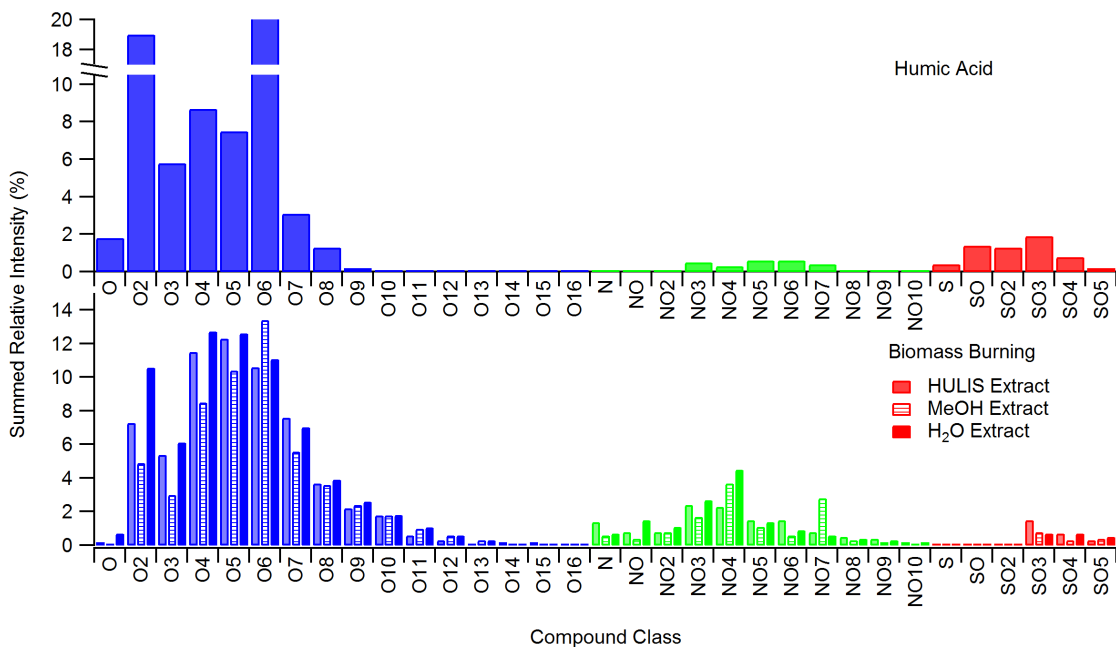


Figure 2-2: Summed relative intensity of each compound class of assigned peaks as ionized by electrospray ionization in negative mode. Top panel corresponds to HA. Bottom panel corresponds to HULIS, methanolic and aqueous BB extracts in shaded, hashed and filled bars respectively.

To further compare the types of compounds assigned between the BB and HA samples, the degree of unsaturation of assigned molecular formulae was investigated. Figure 2-3 shows the relative intensity of each assigned peak as a function of double bond equivalents (DBE) per carbon as determined from the molecular formulae as follows:

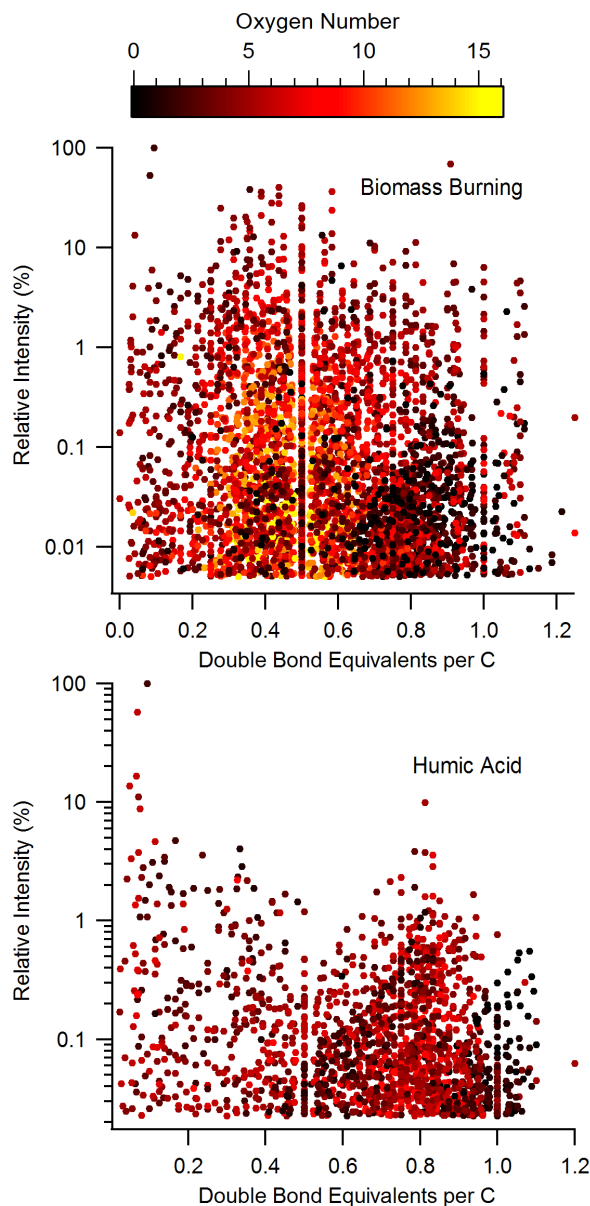


Figure 2-3: Distribution of double bond equivalents of assigned molecular formula for (top) an aqueous biomass burning extract and (bottom) humic acid. Points are coloured by degree of oxygenation as measured by number of oxygens in the assigned molecular formula

$$DBE = C + \frac{N - H}{2} + 1 \quad (2.1)$$

For the BB sample, the most abundant and most highly oxygenated peaks tended to be distributed around 0.5 DBE per carbon. The least oxygenated peaks showed a higher degree of unsaturation, centred on approximately 0.8 DBE per carbon. These less oxygenated and highly condensed species may represent compounds similar to functionalized polycyclic aromatic hydrocarbons (PAHs). In comparison to the BB aerosol extract, HA again showed less spectral complexity in the highly oxidized region centralized around 0.5 DBE per carbon compared to the the BB sample. The HA standard, however, did show similarity to the BB aerosol extract in the higher unsaturation region of lower oxygenation suggesting the condensed hydrocarbon species in the two samples may be comparable. This is consistent with previous studies that have observed that HA displays more aromaticity and lower degrees of oxygenation than HULIS³⁷.

The use of Van Krevelen diagrams is common in the speciation of natural organic matter as measured using UHRMS due to the complexity of the data set³⁸. Here, plotting H:C against O:C will yield regions in which common compound classes will fall. These regions are specific to the matrix from which the compounds are extracted, but are generally similar across naturally derived organic matrices such as soil, aquatic dissolved organic matter, and organic aerosol. Generally, eight zones have been identified including lipids, proteins, aminosugars, carbohydrates, unsaturated hydrocarbons, lignin, tannins, and condensed hydrocarbons. Van Krevelen diagrams for the BB and HA samples can be observed in Figure 2-4. The aqueous BB aerosol extract shows peaks arising in each zone, with the greatest number of peaks arising from formulas with lignin-like character. The

condensed hydrocarbon region primarily comprises CHNO_x species, potentially as a result of the formation of nitro-aromatics either directly from the BB source, or from reactivity with NO_x during transport^{39,40}. In comparison to the BB sample, HA is deficient in the aminosugar, carbohydrate and tannin regions. The condensed hydrocarbon region is

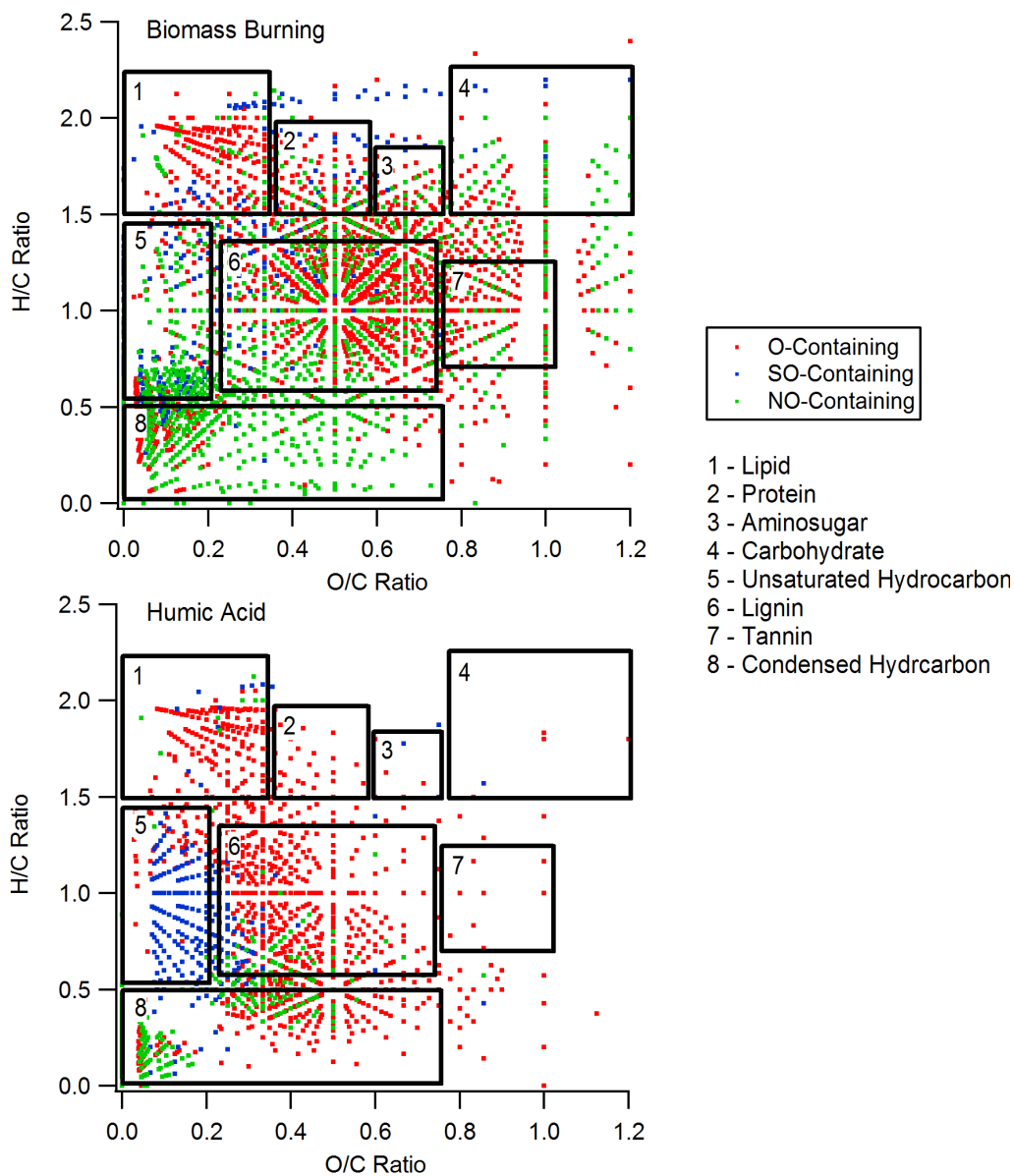


Figure 2-4: Van Krevelen diagrams for the assigned peaks from (top) an aqueous BB extract and (bottom) HA. Red dots correspond to formulas including C, H and O; blue dots correspond to formulas including C, H, O and S; green dots correspond to formulas including C, H, O and N.

dominated by CHO_x species, and the unsaturated hydrocarbon region is dominated by the inclusion of S.

From the ESI(-) experiments alone, it is evident that BB extracts and HA are quite different in their composition. Their similarity lies in the fact that they both are complex mixtures of oxidized organics, but it is clear that the acidic fractions differ greatly in their degree of oxidation, degree of unsaturation, heteroatom distribution and potential structural composition. The HULIS term may not aptly apply to describe the organic fraction of aerosols. Although the differences can be observed in this one fraction, ESI(-) alone cannot characterize the entire sample; alternative ionization sources are necessary if full characterization is to be achieved.

2.4.1.2 Positive Mode

Whereas ESI(-) selects for the acidic fraction of a mixture, ESI(+) will primarily select for compounds containing basic moieties. It is expected that the ESI(+) fraction of OA and HA would be less complex than the ESI(-) analyzed fraction due to the overall acidic nature of these mixtures. This was observed for the aqueous extracts of the BB sample (Figure 2-5), with the assignment of only 800 peaks, and HA, in which the spectral difference was negligible from the background (Figure A-2). It was expected that the HULIS extract would show even less spectral complexity due to the extraction method employed; the aqueous extract was acidified to load on to an SPE column and eluted in basic methanol, which would primarily select for acidic organic species. What was observed, however, was the assignment of over 4000 unique molecular formulae, as shown in Figure 2-5. It has been previously shown that HA, fulvic acid and large brown carbon

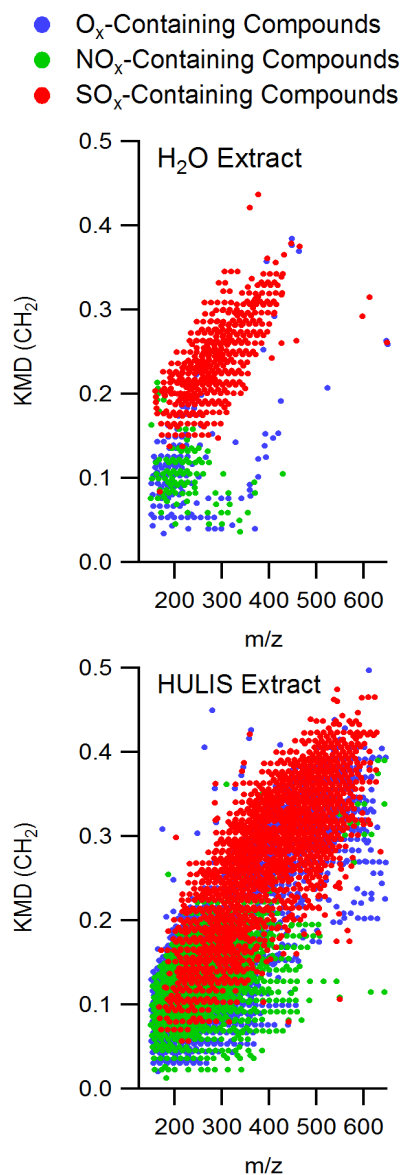


Figure 2-5: Kendrick mass defect plots for molecularly assigned peaks of (top) aqueous and (bottom) HULIS BB extract ionized using electrospray ionization in positive mode, coloured by heteroatom inclusion. Blue dots correspond to peaks with assigned formulas containing C, H and O. Green dots correspond to peaks with assigned formulas containing C, H, N and O. Red dots correspond to peaks with assigned formulas containing C, H, S and O.

(BrC) absorbing species have the propensity to fragment during ionization, even with soft techniques like ESI⁴¹⁻⁴³. The ESI(+) spectra may, therefore, be arising from the ionization

of basic fragments on an overall acidic oligomer or macromolecule. During the HULIS extraction, basic ion suppressors would be removed, thus allowing these potentially low-abundance basic fragments to be ionized and detected.

In comparison to ESI(-) experiments, although BB aerosol extracts analyzed by ESI(+) showed lower overall oxygenation, these spectra showed greater heteroatom variability as observed in the compound distributions show in Figure 2-6. Here, there was a large increase in the proportion of species containing S. Further, more highly oxygenated S-containing species were identified, up to SO₁₀. Compound class distributions were not dominated by the CHO_x compounds; relatively equal distributions of both summed intensity and number of assigned formulae were observed between CHO_x (1352 formulae), CHNO_x (1191 formulae) and CHSO_x (1558 formulae) species. The HULIS fraction showed a greater proportion of intensity due to CHNO_x species in comparison to the aqueous and methanolic extracts, with increasing intensity as the number of oxygens increased from 0 to 5.

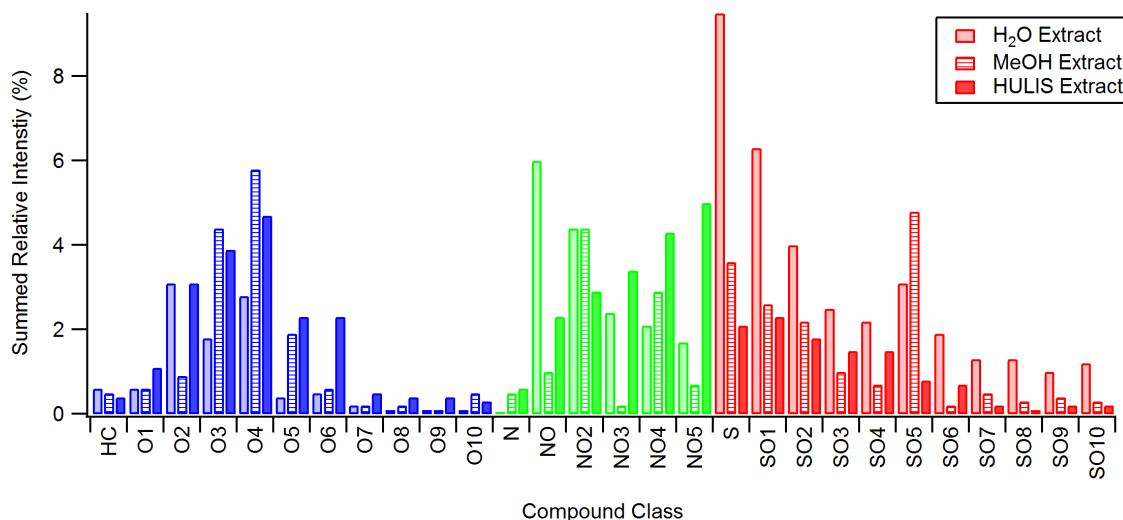


Figure 2-6: Summed relative intensity of each compound class of assigned peaks as ionized by electrospray ionization in positive mode. Shaded, hashed and filled bars correspond to aqueous, methanolic and HULIS extracts, respectively.

The stark difference between the profiles of BB aerosol extracts measured by ESI in positive and negative mode highlights the importance of using multiple ionization techniques for the mass spectral characterization of complex organic mixtures. ESI on the whole still selects for polar, ionizable molecules. Less polar species, or those without directly ionizable functional groups will not be observed, or will be of low abundance in these experiments; part of the mixture is still likely to be missed. The need for additional ionization techniques for full characterization is evident.

2.4.2 APPI

It has been shown that BB represents the dominant source of BrC to the atmosphere^{11,12,39}. It is difficult, if not impossible, to determine the species responsible for BrC absorption from molecular weights and calculated molecular formulae alone. Chapter 3 will show that ESI(-) analysis poorly represents the absorbing fraction from this BB sample. The selectivity of dopant-free APPI is towards molecules that have a propensity to absorb light. Thus, it is believed that this ionization technique would be best suited for the molecular characterization of BrC.

When placed in line with size exclusion chromatography (SEC) and UV-vis spectrophotometry, APPI was better able to match the profile distribution of absorbing species than ESI(-) for an aqueous BB aerosol extract (Figure 2-7). The spectra under each chromatographic peak showed a wider mass range, with peaks arising from 100 to over 1000 Da, and a greater degree of spectral complexity. Further, as SEC separates on the principle of molecular volume where the largest molecules elute first and subsequently smaller molecules elute later. For this reason, it is expected that earlier eluting peaks would

show a higher mass range in mass spectrometry experiments than later eluting peaks. This was not the case with ESI(-) experiments, where spectra were similar across the chromatographic range as highlighted in Chapter 3. APPI did show a lower mass range of

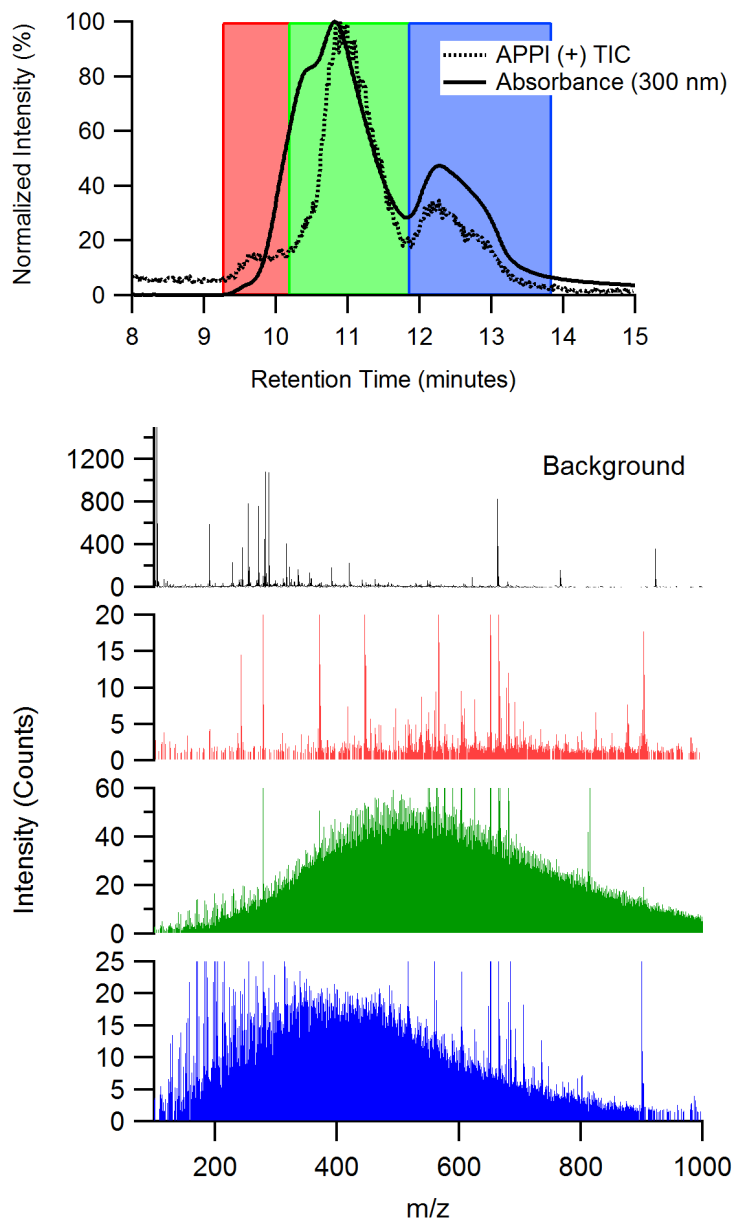


Figure 2-7: Top: Overlaid chromatograms from a size exclusion chromatography separation of an aqueous BB extract measured by APPI-MS in positive mode (solid black line) and by UV-vis absorbance spectrophotometry (dashed black line). Bottom: Summed and background subtracted APPI-MS spectra for each chromatographic region. Spectrum colour corresponds to the region in the above chromatogram: red – summed spectra from 9-10 min, green – from 10-12 min, blue – from 12-14 min. Black spectra corresponds to the background signal.

ionized peaks with increasing retention time. Molecular weight distributions, however, were still underestimated by APPI-MS in comparison to those measured by SEC. This suggests that there is potentially a lesser degree of fragmentation occurring during ionization by APPI than by ESI.

Unfortunately, molecular formula assignments and related analysis could not be performed with this data set due to the resolving power of the TOF-MS used for this analysis. Future experiments with APPI coupled to UHRMS instruments, for example Orbitrap or FTICR mass analyzers, have the potential to yield detailed molecular characterization of light-absorbing, particle-bound organic species.

2.4.3 EI

When attempting to characterize the entirety of a complex sample using mass spectrometry, a soft and completely non-selective ionization technique would be ideal. Although electron ionization (EI) is a notoriously hard ionization technique, nearly all organic species that can be desorbed can be ionized. Further, ionization efficiencies between molecules show minor variation in comparison to techniques like ESI, chemical ionization (CI) and atmospheric pressure photoionization (APPI), which can show drastically different ionization efficiencies based on the chemical and physical properties of a given molecule such as their pKa, electron or proton affinity and UV absorptivity, respectively. In this way, EI can be used to give a snapshot of representative molecular fragments and overall atomic ratios within a sample.

The common necessity for solvent extraction also introduces another level of potentially undesired selectivity during a non-targeted analysis. Ideally, samples would be

analyzed directly from the collection substrate. The use of a heated direct insertion probe (DIP) allows for compounds to be introduced into the ionization source and mass spectrometer via thermal desorption, negating the need for solvent extractions. A further benefit to DIP experiments is the minimal sample requirement, on the order of microliters. In the case of GC-MS analyses, 1 μ L injections are common, but sample volumes of 1 mL or more are often required to extract the sample; the majority of the extracted sample goes unanalyzed. With DIP experiments the entire subsample is analyzed. The absence of carrier solvent or gas further enhances ionization efficiency allowing for the analyses of these small subsamples.

The KMD plot for the direct analysis of the BB filter substrate can be observed in Figure 2-8. Compared to ESI analysis, the EI spectrum showed a lower overall molecular weight distribution as expected due to the propensity of fragmentation, and less spectral complexity with the assignment of a total of approximately 700 unique molecular formulae. The reduced spectral complexity compared to ESI experiments suggests that the many detected species in ESI arise from the assembly of common molecular fragments. This is expected from the polymeric nature of the major BB fuel sources lignin and cellulose, where incomplete combustion products will be scrambled combinations of lignin and cellulose pyrolysis fragments⁴⁴⁻⁴⁶. Compound class distributions (Figure 2-8) show the majority of the spectral intensity arises from hydrocarbon species. These may be a result of hydrocarbon-like side chain fragments of larger molecules. It may be interpreted that this compound class may also represent the black carbon (BC) fraction, which would have been lost in previous experiments due to its lack of water solubility and heteroatom functionality, but it is not expected that the BC would volatilize at these temperatures¹⁷.

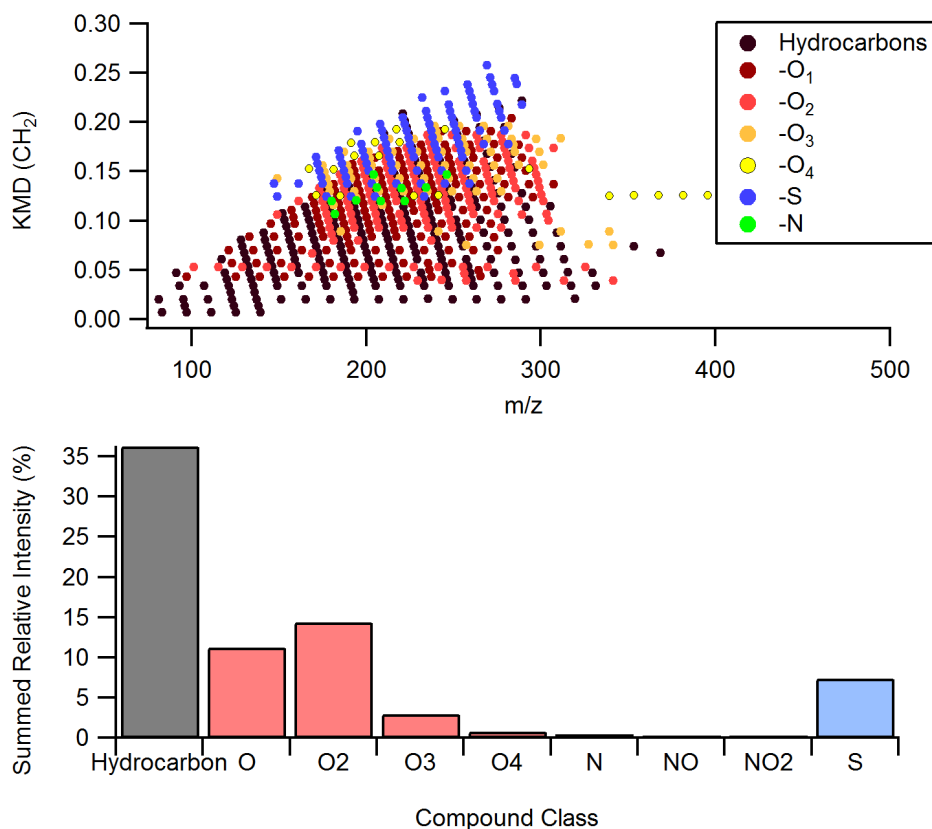


Figure 2-8: Top - Kendrick Mass Defect plot for BB aerosol as analyzed using EI-UHRMS introduced using a direct insertion probe. Bottom - Summed relative intensity of each compound class of assigned peaks.

Although used primarily to discriminate against ion suppression, the slow heating for the desorption of the compounds off the DIP yielded insight into the volatility of the detected species in a similar way to thermogravimetric analysis. The TIC plotted along with desorption temperature profile is shown in Figure 2-9, where two distinct populations with different volatilities can be observed. Nearly all of the mass spectral peaks arising from the lower volatility population, those that desorbed after four minutes at higher temperatures, were also present in the more volatile population, those that desorbed at lower temperatures before four minutes. This suggests that the species in both volatility regions are of similar

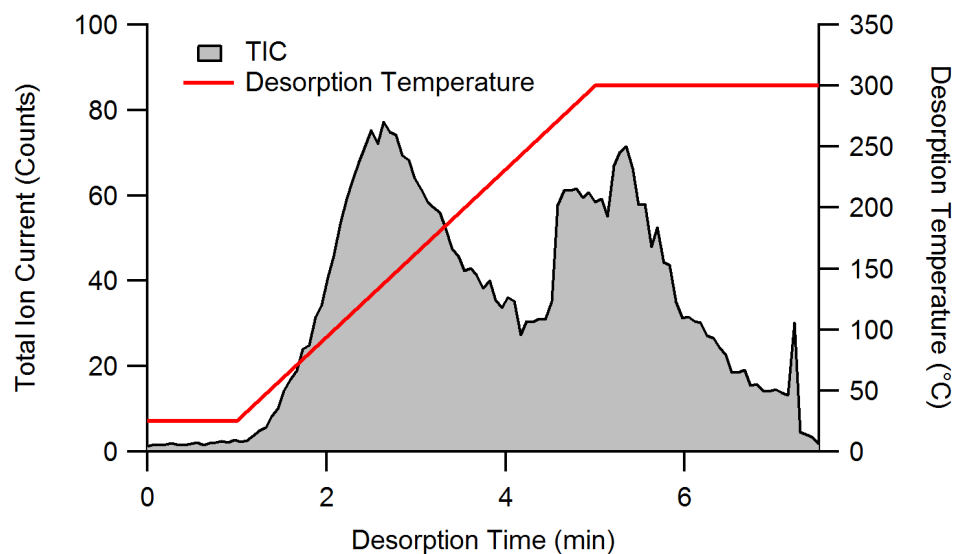


Figure 2-9: Total ion current (TIC) for EI-UHRMS analysis as a function of desorption time overlaid with the time dependent desorption temperature in red.

chemical structure, but primarily differ in their size, with the more volatile components being smaller molecules and the less volatile of higher molecular weight.

2.5 Conclusions

It is evidenced herein that no single mass spectral technique has the ability to fully characterize the suite of organics present in a BB aerosol sample. Although ESI(-) experiments showed the potential to identify the greatest number of individual species, it selects against basic species, and poorly represented light-absorbing organics. EI in conjunction with a DIP has the potential to ionize the entire suite of organics, but the resultant mass spectral peaks are mainly fragments of the original chemical species present in BrC. Although potential structural compound classes can be proposed to peaks with assigned molecular formulae with the aid of Van Krevelen diagrams, these are merely represented by atomic ratios; the identification of specific structural signatures of BB aerosol requires tandem MS. Although the acquisition of tandem MS spectra for the most

abundant peaks can be easily accomplished with the use of data dependent analysis, the structural elucidation for thousands of individual tandem MS spectra requires a large amount of manual labour or creativity for automation and should be the focus of further study.

2.6 References

- (1) Kanakidou, M.; Seinfeld, J. H.; Pandis, S. N.; Barnes, I.; Dentener, F. J.; Facchini, M. C.; Van Dingenen, R.; Ervens, B.; Nenes, A.; Nielsen, C. J.; et al. Organic aerosol and global climate modelling: a review. *Atmos. Chem. Phys.* **2005**, *5*, 1053–1123.
- (2) Pöschl, U. Atmospheric aerosols: composition, transformation, climate and health effects. *Angew. Chem. Int. Ed. Engl.* **2005**, *44* (46), 7520–7540.
- (3) Jimenez, J. L.; Canagaratna, M. R.; Donahue, N. M.; Prevot, a S. H.; Zhang, Q.; Kroll, J. H.; DeCarlo, P. F.; Allan, J. D.; Coe, H.; Ng, N. L.; et al. Evolution of organic aerosols in the atmosphere. *Science* **2009**, *326* (5959), 1525–1529.
- (4) Boucher, O.; Randall, D.; Artaxo, P.; Bretherton, C.; Feingold, G.; Forster, P. M.; Kerminen, V.-M.; Kondo, Y.; Liao, H.; Lohmann, U.; et al. Clouds and Aerosols. In *Climate Change 2013: The Physical Science Basis. Contribution of Working Group I to the Fifth Assessment Report of the Intergovernmental Panel on Climate Change*; Stocker, T. F., Qin, D., Plattner, G.-K., Tignor, M., Allen, S. K., Boschung, J., Nauels, A., Xia, Y., Bex, V., Midgley, P. M., Eds.; Cambridge University Press: Cambridge, United Kingdom and New York, NY, USA, **2013**.
- (5) Wozniak, A. S.; Bauer, J. E.; Sleighter, R. L.; Dickhut, R. M.; Hatcher, P. G. Technical Note: Molecular characterization of aerosol-derived water soluble organic carbon using ultrahigh resolution electrospray ionization Fourier transform ion cyclotron resonance mass spectrometry. *Atmos. Chem. Phys.* **2008**, *8* (17), 5099–5111.
- (6) Leclair, J. P.; Collett, J. L.; Mazzoleni, L. R. Fragmentation analysis of water-soluble atmospheric organic matter using ultrahigh-resolution FT-ICR mass spectrometry.

- Environ. Sci. Technol.* **2012**, *46* (8), 4312–4322.
- (7) Lin, P.; Rincon, A. G.; Kalberer, M.; Yu, J. Z. Elemental composition of HULIS in the Pearl River Delta Region, China: results inferred from positive and negative electrospray high resolution mass spectrometric data. *Environ. Sci. Technol.* **2012**, *46* (14), 7454–7462.
- (8) Hamilton, J. F.; Webb, P. J.; Lewis, A. C.; Hopkins, J. R.; Smith, S.; Davy, P. Partially oxidised organic components in urban aerosol using GCXGC-TOF/MS. *Atmos. Chem. Phys.* **2004**, *4*, 1279–1290.
- (9) Chen, Y.; Bond, T. C. Light absorption by organic carbon from wood combustion. *Atmos. Chem. Phys. Discuss.* **2009**, *9* (5), 20471–20513.
- (10) Bond, T. C.; Bergstrom, R. W. Light Absorption by Carbonaceous Particles: An Investigative Review. *Aerosol Sci. Technol.* **2006**, *40* (1), 27–67.
- (11) Lack, D. A.; Langridge, J. M.; Bahreini, R.; Cappa, C. D.; Middlebrook, A. M.; Schwarz, J. P. Brown carbon and internal mixing in biomass burning particles. *Proc. Natl. Acad. Sci.* **2012**, *109* (37), 14802–14807.
- (12) Washenfelder, R. A.; Attwood, A. R.; Brock, C. A.; Guo, H.; Xu, L.; Weber, R. J.; Ng, N. L.; Allen, H. M.; Ayres, B. R.; Baumann, K.; et al. Biomass burning dominates brown carbon absorption in the rural southeastern United States. *Geophys. Res. Lett.* **2015**, *42*, 653–664.
- (13) Liu, J.; Scheuer, E.; Dibb, J.; Ziemba, L. D.; Thornhill, K. L.; Anderson, B. E.; Wisthaler, A.; Mikoviny, T.; Devi, J. J.; Bergin, M.; et al. Brown carbon in the continental troposphere. *Geophysical Research Letters*. 2014, pp 2191–2195.
- (14) Yang, M.; Howell, S. G.; Zhuang, J.; Huebert, B. J. Attribution of aerosol light

- absorption to black carbon, brown carbon, and dust in China – interpretations of atmospheric measurements during EAST-AIRE. *Atmos. Chem. Phys. Discuss.* **2008**, *8* (3), 10913–10954.
- (15) Petzold, A.; Kramer, H.; Schönlinner, M. Continuous Measurement of Atmospheric Black Carbon Using a Multi-angle Absorption Photometer. *Environ. Sci. Pollut. Res. Int.* **2002**, *4* (4), 78–82.
- (16) Bahadur, R.; Praveen, P. S.; Xu, Y.; Ramanathan, V. Solar absorption by elemental and brown carbon determined from spectral observations. *Proc. Natl. Acad. Sci.* **2012**, *109* (43), 17366–17371.
- (17) Ramanathan, V.; Carmichael, G. Global and regional climate changes due to black carbon. *Nat. Geosci.* **2008**, *1* (4), 221–227.
- (18) Bond, T. C.; Doherty, S. J.; Fahey, D. W.; Forster, P. M.; Berntsen, T.; DeAngelo, B. J.; Flanner, M. G.; Ghan, S.; Kärcher, B.; Koch, D.; et al. Bounding the role of black carbon in the climate system: A scientific assessment. *J. Geophys. Res. Atmos.* **2013**, *118* (11), 5380–5552.
- (19) Kirchstetter, T. W.; Novakov, T.; Hobbs, P. V. Evidence that the spectral dependence of light absorption by aerosols is affected by organic carbon. *J. Geophys. Res. D Atmos.* **2004**, *109* (21), D21208.
- (20) Andreae, M. O.; Gelencsér, A. Black carbon or brown carbon? The nature of light-absorbing carbonaceous aerosols. *Atmos. Chem. Phys.* **2006**, *6* (10), 3131–3148.
- (21) Saleh, R.; Marks, M.; Heo, J.; Adams, P. J.; Donahue, N. M.; Robinson, A. L. Contribution of brown carbon and lensing to the direct radiative effect of carbonaceous aerosols from biomass and biofuel burning emissions. *J. Geophys.*

- Res. Atmos.* **2015**, *120* (19), 10,285-10,296.
- (22) Marshall, A. G.; Hendrickson, C. L.; Jackson, G. S. Fourier transform ion cyclotron resonance mass spectrometry: a primer. *Mass Spectrom. Rev.* **1998**, *17*, 1–35.
- (23) Hertkorn, N.; Harir, M.; Koch, B. P.; Michalke, B.; Schmitt-Kopplin, P. High-field NMR spectroscopy and FTICR mass spectrometry: powerful discovery tools for the molecular level characterization of marine dissolved organic matter. *Biogeosciences* **2013**, *10* (3), 1583–1624.
- (24) Zhang, H.; Zhang, Y.; Shi, Q.; Ren, S.; Yu, J.; Ji, F.; Luo, W.; Yang, M. Characterization of low molecular weight dissolved natural organic matter along the treatment trail of a waterworks using Fourier transform ion cyclotron resonance mass spectrometry. *Water Res.* **2012**, *46* (16), 5197–5204.
- (25) Altieri, K. E.; Turpin, B. J.; Seitzinger, S. P. Composition of dissolved organic nitrogen in continental precipitation investigated by ultra-high resolution FT-ICR mass spectrometry. *Environ. Sci. Technol.* **2009**, *43* (18), 6950–6955.
- (26) Stenson, A. C.; Landing, W. M.; Marshall, A. G.; Cooper, W. T. Ionization and fragmentation of humic substances in electrospray ionization Fourier transform-ion cyclotron resonance mass spectrometry. *Anal. Chem.* **2002**, *74* (17), 4397–4409.
- (27) Podgorski, D. C.; McKenna, A. M.; Rodgers, R. P.; Marshall, A. G.; Cooper, W. T. Selective ionization of dissolved organic nitrogen by positive ion atmospheric pressure photoionization coupled with Fourier transform ion cyclotron resonance mass spectrometry. *Anal. Chem.* **2012**, *84* (11), 5085–5090.
- (28) Ikeya, K.; Sleighter, R. L.; Hatcher, P. G.; Watanabe, A. Fourier transform ion cyclotron resonance mass spectrometric analysis of the green fraction of soil humic

- acids. *Rapid Commun. Mass Spectrom.* **2013**, *27* (22), 2559–2568.
- (29) Pratt, K. A.; Prather, K. A. Mass spectrometry of atmospheric aerosols--recent developments and applications. Part II: On-line mass spectrometry techniques. *Mass Spectrom. Rev.* **2012**, *31* (1), 17–48.
- (30) Rincón, A. G.; Calvo, A. I.; Dietzel, M.; Kalberer, M. Seasonal differences of urban organic aerosol composition - an ultra-high resolution mass spectrometry study. *Environ. Chem.* **2012**, *9* (3), 298.
- (31) O'Brien, R. E.; Laskin, A.; Laskin, J.; Liu, S.; Weber, R.; Russell, L. M.; Goldstein, A. H. Molecular characterization of organic aerosol using nanospray desorption/electrospray ionization mass spectrometry: CalNex 2010 field study. *Atmos. Environ.* **2013**, *68*, 265–272.
- (32) Smith, J. S.; Laskin, A.; Laskin, J. Molecular characterization of biomass burning aerosols using high-resolution mass spectrometry. *Anal. Chem.* **2009**, *81* (4), 1512–1521.
- (33) Laskin, A.; Smith, J. S.; Laskin, J. Molecular characterization of nitrogen-containing organic compounds in biomass burning aerosols using high-resolution mass spectrometry. *Environ. Sci. Technol.* **2009**, *43* (10), 3764–3771.
- (34) Jaoui, M.; Kleindienst, T. E.; Lewandowski, M.; Edney, E. O. Identification and quantification of aerosol polar oxygenated compounds bearing carboxylic or hydroxyl groups. 1. Method development. *Anal. Chem.* **2004**, *76* (16), 4765–4778.
- (35) Sullivan, A. P.; Weber, R. J. Chemical characterization of the ambient organic aerosol soluble in water: 1. Isolation of hydrophobic and hydrophilic fractions with a XAD-8 resin. *J. Geophys. Res. Atmos.* **2006**, *111* (5), 1–9.

- (36) Novotny, N. R.; Capley, E. N.; Stenson, A. C. Fact or artifact: the representativeness of ESI-MS for complex natural organic mixtures. *J. Mass Spectrom.* **2014**, *49* (4), 316–326.
- (37) Graber, E. R.; Rudich, Y. Atmospheric HULIS: how humic-like are they? A comprehensive and critical review. *Atmos. Chem. Phys. Discuss.* **2005**, *5*, 9801–9860.
- (38) Kim, S.; Kramer, R. W.; Hatcher, P. G. Graphical Method for Analysis of Ultrahigh-Resolution Broadband mass spectra of Natural Organic Matter, the Van Krevelen diagram. *Anal. Chem.* **2003**, *75* (20), 5336–5344.
- (39) Iinuma, Y.; Böge, O.; Gräfe, R.; Herrmann, H. Methyl-nitrocatechols: atmospheric tracer compounds for biomass burning secondary organic aerosols. *Environ. Sci. Technol.* **2010**, *44* (22), 8453–8459.
- (40) Lin, P.; Liu, J.; Shilling, J. E.; Kathmann, S. M.; Laskin, J.; Laskin, A. Molecular characterization of brown carbon (BrC) chromophores in secondary organic aerosol generated from photo-oxidation of toluene. *Phys. Chem. Chem. Phys.* **2015**, *17* (36), 23312–23325.
- (41) Reemtsma, T.; These, A.; Springer, A.; Linscheid, M. Differences in the molecular composition of fulvic acid size fractions detected by size-exclusion chromatography-on line Fourier transform ion cyclotron resonance (FTICR-) mass spectrometry. *Water Res.* **2008**, *42* (1–2), 63–72.
- (42) Reemtsma, T.; These, A. On-line coupling of size exclusion chromatography with electrospray ionization-tandem mass spectrometry for the analysis of aquatic fulvic and humic acids. *Anal. Chem.* **2003**, *75* (6), 1500–1507.

- (43) Di Lorenzo, R. A.; Young, C. J. Size separation method for absorption characterization in brown carbon: Application to an aged biomass burning sample. *Geophys. Res. Lett.* **2016**, *43* (1), 458–465.
- (44) Roberts, A. F. A review of kinetics data for the pyrolysis of wood and related substances. *Combust. Flame* **1970**, *14* (2), 261–272.
- (45) Alger, R. Pyrolysis and Combustion of Cellulosic Materials. In *The Mechanisms of Pyrolysis, Oxidation, and Burning of Organic Materials*; Wall, L. A., Ed.; National Bureau of Standards Special Publication, **1972**; pp 171–184.
- (46) Shafizadeh, F. The Chemistry of Pyrolysis and Combustion. In *The Chemistry of Solid Wood*; **1984**; pp 489–529.

3 Size separation method for absorption characterization in brown carbon: Application to an aged biomass burning sample

This chapter has been published as the following: Di Lorenzo, R. A. and Young, C. J.: Size separation method for absorption characterization in brown carbon: Application to an aged biomass burning sample, *Geophys. Res. Lett.*, 43(1), 458–465, doi:10.1002/2015GL066954, 2016.

3.1 Abstract

The majority of brown carbon (BrC) in atmospheric aerosols is derived from biomass burning (BB) and is primarily composed of extremely low volatility organic carbon (ELVOCs). We use two chromatographic methods to compare the contribution of large and small light-absorbing BrC components in aged BB aerosols with UV-Vis absorbance detection: 1) size exclusion chromatography (SEC) and 2) reverse-phase high performance liquid chromatography (RP-HPLC). We observe no evidence of small molecule absorbers. Most BrC absorption arises from large molecular weight components (>1000 Da). This suggests that although small molecules may contribute to BrC absorption near the BB source, analyses of aerosol extracts should use methods selective to large molecular weight compounds because these species may be responsible for long-term BrC absorption. Further characterization with electrospray ionization mass spectrometry (MS) coupled to SEC demonstrates an underestimation of the molecular size determined through MS as compared to SEC.

3.2 Introduction

Atmospheric aerosols represent the greatest factor underlying the total uncertainty of anthropogenically derived radiative forcing¹. Of particular importance are light absorbing aerosols, which exert a warming effect additive to those of gas phase absorbers. Aerosols that absorb in the ultraviolet and visible spectral region include black carbon (BC), mineral dust, and other organic absorbers classified as brown carbon (BrC), with BC being the dominant absorber². Although absorption by BC and mineral dust are fairly well understood, BrC is poorly characterized^{3,4} and consequently has only recently begun to be

parameterized in radiative forcing models^{5,6}. BrC differs from BC and mineral dust in its physical and chemical properties, thus can be analyzed offline independently. Where BC follows an approximate λ^{-1} dependency, the relationship is much stronger for BrC and mineral dust, following a λ^{-2} to λ^{-6} dependence into the near UV^{7,8}. BC can be separated due to its inherent lack of aqueous solubility. Inorganic mineral dust primarily exists as coarse mode aerosols, thus can be separated during the collection of predominantly fine mode BrC particles. Direct measurements of BrC absorption are inferred from small, wavelength-dependent spectral remainders after BC and mineral dust has been subtracted^{7,9}. Online analyses of water-extracted BrC have also been performed with a Particle into Liquid Sampler (PiLS) coupled to an ultraviolet and visible absorbance spectrometer⁹⁻¹¹.

Many laboratory experiments have proposed formation mechanisms of BrC, including formation from fossil fuel and biomass combustion¹², the production of polyimines from glyoxal in the presence of ammonium salts^{13,14}, the production of toluene secondary organic aerosol (SOA) in high NO_x environments to form aromatic, organo-nitrate absorbers¹⁵, and metal-mediated oxidative polymerization of catechol and guaiacol¹⁶. Although a recent, comprehensive review of atmospheric BrC illustrates that the majority of mechanistic studies on the formation BrC have focused on SOA formation and processing from gas-phase precursors¹⁷, field measurements have shown that BrC is most strongly correlated with biomass burning (BB) events^{18,19}. Some nitroaromatics, specifically substituted nitrocatechols, are visible light absorbers and correlated with BB events and have been estimated to contribute less than 10% of the total BrC absorption from fresh BB aerosol emissions^{9,12,20}. The remainder of the absorption has yet to be fully

characterized. Understanding the total radiative forcing (RF) impact of combustion-derived particles requires improved understanding of BrC characteristics, since BrC potentially represents the difference between model-derived negative RF and observationally-derived positive RF⁶.

It has been shown that BrC arising from both fresh and aged BB aerosols is primarily composed of extremely low volatility organic compounds (ELVOCs)⁴, defined in the volatility basis set as having a saturation concentration $< 3 \times 10^{-4} \text{ ug m}^{-3}$ ²¹. The ELVOC fraction includes highly oxidized, lower molecular weight species (7-10 carbons) with O:C ratios approaching 1:1 and oligomers. Measurements that have shown nitrocatechols to be the dominant individual absorbers of BB-derived BrC use C₁₈-based reverse phase high performance liquid chromatography (HPLC) separations coupled to UV-Vis detectors^{9,12,20}. It is suspected that ELVOCs will be strongly, if not irreversibly, retained on a C₁₈-HPLC column, and subsequently omitted from or poorly characterized by the detection methodology. For this reason, it is important to develop a BrC analysis method that is inclusive of the widest possible range of molecules, specifically conducive to large molecular weight ELVOCs. In this study, we compare SEC to C₁₈-HPLC for the analysis of both large and small molecular weight components of aged BB-derived BrC to identify potential gaps in current approaches to BrC characterization. The absorbing species are characterized through the use of inline UV-Vis and mass spectrometric detectors. The methods will be applied to samples from an aged biomass burning plume derived from a boreal wildfire.

3.3 Methods

3.3.1 Sample Collection

On July 4, 2013, a large fire started in the boreal forests of northern Quebec and Labrador. Smoke plumes travelled eastward over Atlantic Canada and on to Scandinavia over the following six days²². BB aerosol samples were collected in central St. John's, NL (47.572° N, 52.722° W, 42 m above sea level) on July 6, 2013, where PM_{2.5} reached concentrations of 120 µg/m³ (Figure B-2, Figure B-3). Six PM_{2.5} samples were collected in parallel with a multi-channel, medium volume sampler (URG-3000ABC, URG Corp, Chapel Hill, NC, USA) on pre-muffled (500 °C, 4 h) 47 mm quartz fiber filters (Tissuquartz2500QAT-UP, Pall Life Sciences, Washington, NY, USA). Size-resolved aerosol samples were also collected with 13-stage cascade impactor (nanoMOUDI II, model 122-R, MSP Corp., Shoreview, MN, USA) on pre-muffled (500 °C, 4 h) aluminum substrates. The total collection time for both sets of samples was 25.5 h. Filters and substrates were stored in the dark at -20 °C until analysis. Only results from the medium volume PM_{2.5} samples are discussed below. MOUDI sample preparation, analysis and selected results can be found in the SI (Text B.3, Figure B-4).

3.3.2 Sample Preparation

Filters were sub-sampled using a 10 mm arch punch. Each punch was placed in a pre-muffled 4 mL glass vial where 500 µL of either water (Barnstead Infinity Ultrapure Water System, Thermo Scientific, Waltham, MA, USA) or methanol (OmniSolv grade, EMD Millipore, Billerica, MA, USA) was added. Vials were sealed with acid-washed, Teflon-lined caps and parafilm and sonicated for 40 min at room temperature. After sonication,

extracts were filtered with 0.2 μm PTFE syringe filters (Iso-Disc, Supelco, Bellefonte, PA, USA), transferred to pre-muffled glass sample vials and diluted to 1.00 mL with either methanol or water to match initial chromatographic conditions. Samples were stored at 4 $^{\circ}\text{C}$ until analysis.

3.3.3 Sample Analysis

3.3.3.1 Size Exclusion Chromatography with UV-Vis (SEC-UV) Analysis

SEC-UV absorption density measurements were acquired using an HPLC system (1260 Infinity, Agilent Technologies, Santa Clara, CA, USA) coupled to a diode array detector (1260, Agilent Technologies, Santa Clara, CA, USA). Separations were performed using an aqueous gel filtration column (molecular weight range = 75 000 - 250 Da, Polysep GFC P-3000, Phenomenex, Torrance, CA, USA). Isocratic elutions were performed at a flow rate of 1 mL/min using a 1:1 mixture of methanol and water with an ammonium acetate concentration of 25 mM.

3.3.3.2 Size Exclusion Chromatography with UV-Vis and Mass Spectrometry (SEC-UV-MS) Analysis

Chromatograms were acquired using the same HPLC pump and column as the SEC-UV experiments. Isocratic elutions were performed at a flow rate of 500 $\mu\text{L}/\text{min}$ using a 1:1 mixture of methanol and water with total ammonium acetate concentration of 12.5 mM. The lower flow rate and salt concentration were used to increase MS sensitivity. Mass spectra were acquired following the diode array detector using a time of flight (TOF) MS (6230, Agilent Technologies, Santa Clara, CA, USA) operated with electrospray ionization in negative mode (ESI-) with the following acquisition parameters: Capillary voltage: 3.5

kV, gas temperature: 350 °C, gas flow: 12 L/min, nebulizer pressure: 35 psi, cone voltage: 125 V. Cone voltages were varied from 125 V to 325 V to determine the effect on fragmentation.

3.3.3.3 Reverse Phase High Performance Liquid Chromatography with UV-Vis and Mass Spectrometry (RP-HPLC-UV-MS) Analysis

Chromatograms were acquired on the same HPLC pump and diode array detector as the SEC-UV experiments. Separation was performed using a C18 column (2.1 mm x 50 mm x 5 µm, Kinetex, Phenomenex, Torrance, CA, USA). A long, slow gradient was used to elute and separate as many components as possible. The mobile phase consisted of A) 0.1% acetic acid in water and B) methanol and was programmed as follows: Initial condition of 95% A was held for 5 minutes and linearly decreased over the next 20 minutes until a solvent composition of 5% A was reached. This composition was held for 15 minutes. Conditions were returned back to the initial 95% A in one minute and held to reequilibrate for a total run time of 45 minutes.

3.4 Results and Discussion

Of the few studies employing chromatographic separations of BrC extracts for the molecular-level characterization of BrC components, only RP-HPLC has been explored^{9,12,20}. Although this is an excellent technique for the separation of small molecules, it is not suitable for the analysis of oligomeric or polymeric species, with the exception of highly hydrophilic proteins²³. If large, hydrophobic ELVOCs can be eluted from the column using this technique, it is suspected that there will be little to no resolution between components. In contrast, size exclusion chromatography (SEC) has successfully

been used to characterize large molecular weight components of environmentally-derived natural organic matter, such as humic acids, thought to be compositionally similar to light absorbing ELVOCs²⁴⁻²⁹. SEC separates components based solely on their molecular volume, which is primarily a function of the molecular weight of a compound. Secondary interactions between the column and analytes are assumed to be negligible, although this is difficult to prove with environmental samples. If this assumption is invalid, calculated molecular weights would represent a lower limit; analyte-column interactions will increase the retention of analytes leading to an underestimation of their molecular weight.

The use of an inline UV-Vis absorption detector coupled to SEC separation allows for the determination of absorbing species as a function of molecular size. UV-Vis detection is selective to absorbing species, independent of their structure or other molecular properties.

SEC absorption density of an aqueous extract of Suwannee River Humic Acid (SRHA, Figure 3-1b), a standard commonly considered structurally similar to atmospheric BrC, shows a single population with an absorption front at roughly 20 000 Da, with an absorption maximum at 4500 Da (Text B.1). The SRHA size observations are consistent with previous studies²⁴⁻²⁷. The SEC absorption density plot for the aqueous BB extract in Figure 3-1a also shows appreciable absorption into the visible region. From total organic carbon measurements (Text B.2), it can be calculated that approximately 1.5 $\mu\text{g C}$ was injected for each chromatographic analysis. The trace for the absorption at 300 nm shows that there are at least three populations of absorbing compounds. The front of the absorption peak has been estimated to correspond to roughly 10 000 Da, with absorption maxima occurring at 2750 Da, 1900 Da and 500 Da. Although the absorption intensity as a function

of wavelength and molecular weight is similar between the BB extract and the SRHA standard, it is clear that their composition is different based on both their average size and population homogeneity. Because the mass distribution as a function of molecular weight could not be determined for these samples, it is uncertain whether the variability in absorption intensity is governed by the relative abundance of different molecular weight fractions or by differences in relative absorption efficiencies. Previous studies have shown that methanol extracts of BB aerosol show greater absorption than the same samples extracted into water as measured by bulk UV-vis absorption^{9,30}. There was no discernible difference in the molecular weight distribution and no statistical difference in quantity of light absorption (paired t-test, $P < 0.46$) between water and methanol extracts as measured by SEC-UV in this study (Figure B-5).

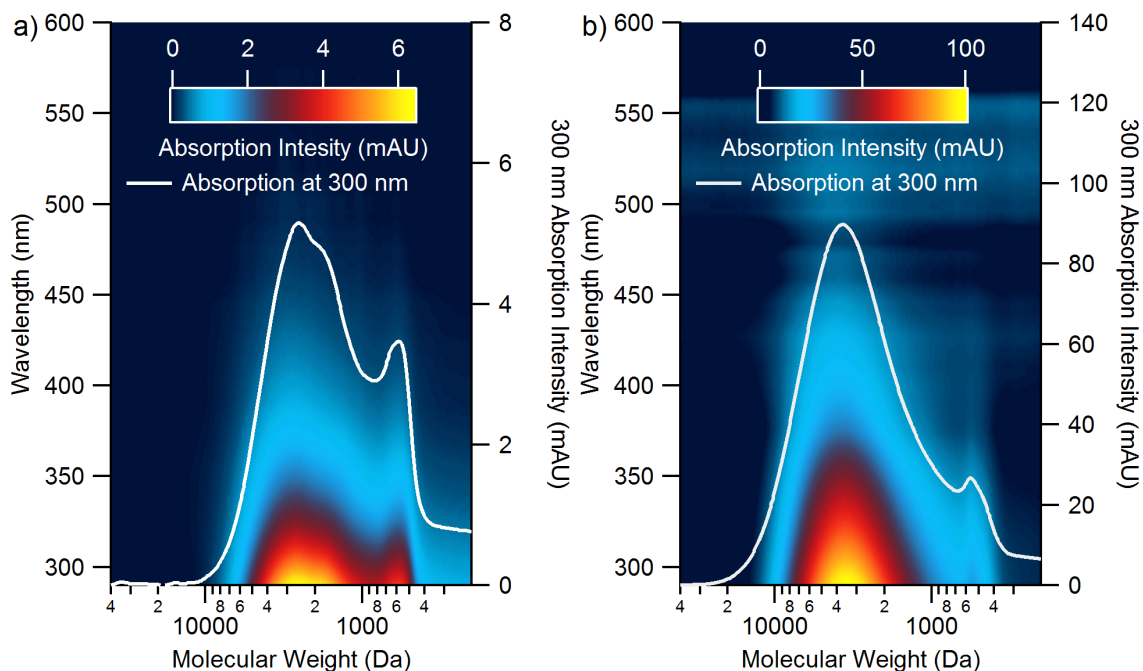


Figure 3-1: Absorption density plots for (a) an aqueous extract of biomass burning PM_{2.5} and (b) an aqueous extract of Suwannee River Humic Acid. The chromatogram extracted from absorption at 300 nm is overlaid to highlight the molecular weight distribution of absorbing species in each sample.

Absorption density at 365 nm is commonly used as a measure of the amount of BrC present in a sample^{9,19,31-33}. Although BC also absorbs at 365 nm, it is not expected to be present in an aqueous extract due to its inherent insolubility. Further, samples were filtered prior to analysis to remove any entrained BC particles if present. RP-HPLC chromatograms, measured at 365 nm, show little evidence of small molecule absorption, indicated by the lack of distinct individual absorption features (Figure B-6). Rather, the bulk of the absorption in these analyses is derived from a large, unresolved component that is reminiscent of a matrix artifact from a complex mixture. An integration comparison between this unresolved feature and that of the SEC-UV analysis at 305 nm, 365 nm, and 405 nm shows that the total absorption between the two analyses are identical within integration error (± 26 - 58% relative standard deviation (RSD) for RP-HPLC analysis, ± 6 - 10% RSD for SEC analysis) and are not statistically different (paired t-test, $P < 0.23$) (Figure B-7). This suggests that the unresolved mass in the RP-HPLC separation corresponds to the same large molecules as separated by SEC and that the absorbing fraction in these aged BB aerosols is comprised mostly of large molecules. The error associated with integrating such a broad, unresolved feature as in the RP-HPLC analysis is inherently large, as observed by the increased variability compared to SEC analysis. Assumptions must be made about where the absorption begins and ends, as well as the shape of the baseline under the feature. Furthermore, little information about the components contributing to this unresolved absorption feature can be derived from a RP-HPLC-UV analysis. For this reason, it is imperative that offline separations include SEC to more accurately quantify and characterize the light absorbing ELVOCs comprising BrC. An early study looking for species of comparable structure to humic acids in aerosol

extracts from rural Japan saw a molecular size distribution very similar to that observed here, with molecular weights ranging from 500 to 10,000 Da³⁴. The large molecules observed in that study accounted for up to 3% of the total carbon and the source was tentatively assigned as background agricultural burning. This suggests that large molecules may be common to aged biomass burning aerosols.

Substituted nitrocatechols are commonly used as tracers for BB-derived BrC since they have been found in appreciable concentrations in fresh BB aerosol¹². However, nitrocatechols have not been observed to be important in all previous measurements of fresh BB aerosol. For example, BB aerosols derived from fires that produced high BC show that BrC absorption is dominated by ELVOCs in both fresh and aged aerosols⁴. Further, large molecular weight organic species, with polycarboxylate and polysaccharide-like character, have been found to be internally mixed with carbon soot when derived from a combustion source³⁵. Evidence for the presence of 4-nitrocatechol in these BrC extracts from forest fires in Quebec and Labrador was sought, but not found (Figure B-8). Previous studies where 4-nitrocatechol was demonstrated to be a considerable absorber looked at fresh BB aerosols^{9,12,20}, while those sampled from this BB plume were aged over approximately two days. It has been recently shown that the organic species in BB aerosols, the BrC fraction in particular, rapidly oxidize during transport, with a half-life on the order of 9 to 15 hours^{33,36}. Nitrophenols, nitrocatechols and imine-based products from the condensation of glyoxal and ammonia are also photochemically processed to non-absorbing products on the order of hours³⁷. The transport time between generation and sampling of these particular samples is sufficient for nitrocatechols to be degraded. Although under certain burning conditions, nitrocatechols and other small molecules may

be an important contributor to BrC near the source, they do not appear to impact BrC absorption in these aged BB aerosols.

In order to further refine the effect of atmospheric aging on BB-BrC absorption, the imaginary component of the wavelength dependent refractive index, k , was calculated according to Sun et al.³⁸ using a particle density of 1.4 g/cm^3 ³⁹ (Figure B-9). Unfortunately, the calculated values are difficult to compare since all BC has been effectively removed during the extraction process. This is demonstrated by the calculated k at 550 nm of 0.002 and a wavelength dependence of 5.11. In both cases, this would correspond to a BC-to-OA ratio of much less than 0.01^4 . These values can, however, be compared to the BB-derived ELVOC specific k values determined by Saleh et al.⁴. Since the majority of the absorption in our samples arises from large molecular weight species, we can estimate an ELVOC-specific k . Assuming ELVOCs comprise 10% of the particle mass in Saleh et al.⁴, our calculated k values fall within the range of the low end of reported values. Discrepancies may arise from differences in fuel source, burn conditions and the atmospheric aging of samples. The agreement with literature values suggests that atmospheric processing of ELVOCs may not considerably alter their absorption properties.

Mass spectral analysis has commonly been applied to BrC extracts⁴⁰⁻⁴⁵. Although this technique can provide detailed structural information, it does not discriminate between species that absorb and those that do not. Instead, detection is selective to specific molecular properties that influence their ionization efficiency and is heavily subject to matrix effects. In order to characterize the chemical nature of the large molecular weight absorbing species, the mass spectra of the compounds separated by SEC was measured. For the chemical speciation of organics in aerosols, electrospray ionization operated in negative

mode (ESI-) is most commonly employed⁴⁰⁻⁴⁸. The total absorbing feature was split into two sections according to the local absorbance maxima in the total ion current (TIC) as shown in Figure 3-2a.

The majority of peaks in the BB extract observed by mass spectrometry, between m/z 100 and 400, is much lower than $MW >1000$ Da determined by SEC. A mismatch between the molecular weights inferred from SEC and measured by MS could be caused by multiply charged ions, which we have ruled out due to ion clusters and ^{13}C isotope peaks being separated by 1 m/z (Figure B-10). If multiply charged species dominated the spectra, ion clusters and isotope peaks would be closer together than 1 m/z . The mass discrepancy could also arise from fragmentation of compounds during the ionization process and from selective ionization. Kendrick Mass Defect plots for the two chromatographic regions as displayed in Figure 3-2b show substantial spectral overlap. The most abundant ions, the mass defect of the most prevalent homologous CH_2 series, and the molecular weight range of the most complex spectral region are similar under both peaks. This suggests that both size populations are composed of similar subunits and that the observed spectra are fragments of the total molecule. The cone voltage was altered to determine whether the degree of fragmentation would change. A high cone voltage is generally required to direct larger species to the source inlet after ion formation, but also results in a greater propensity for ion fragmentation. The TIC intensities were reduced with increasing cone voltage (Figure B-11). This has been observed for similar studies on humic and fulvic acids, indicating that fragmentation of the large, absorbing BrC molecules can occur^{49,50}.

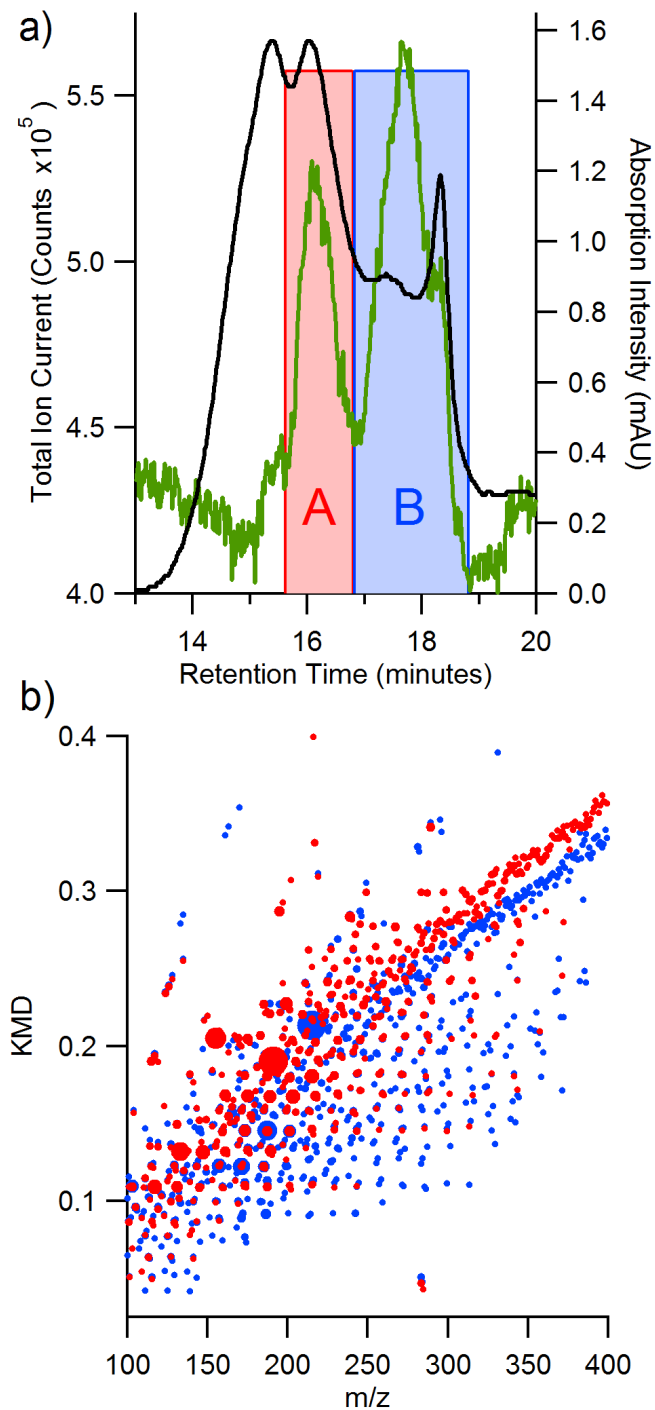


Figure 3-2: a) Comparison of the TIC as measured by ESI(-)-MS (green) and absorption profile at 300 nm (black) as separated by SEC showing a mismatch between molecules responsible for absorption and those detected by ESI(-)-MS. b) Overlaid Kendrick Mass Defect Plots (CH₂-normalized) of the individual TIC peaks A (red) and B (blue) highlighting spectral similarity across the range of species separated by SEC.

Most importantly, the MS TIC and UV-Vis absorption profiles do not match, which suggests the populations that are most amenable to analyses via ESI-MS are not those that are causing the greatest absorption. Other MS techniques that are rarely applied to aerosol extracts, but for which molecular absorption facilitates ionization (e.g. atmospheric pressure photoionization), could provide greater structural information about absorbing BrC species.

The majority of the BrC absorption in these samples of aged BB aerosols derived from a boreal forest fire can be attributed to the large molecular weight ELVOCs, of either primary or secondary origin. This large molecular fraction must be more resistant to photochemical degradation leading to a decrease in absorption. Boreal forests account for roughly one third of the global forested area, and a large proportion of fires occurring in the boreal forest are of natural origin⁵¹. It has been shown that increasing wildfire activity in recent decades can be attributed to higher mean annual temperatures as a result of climate change⁵². Although anthropogenically-initiated BB has the potential to be reduced through bans and mandates, naturally derived wildfires will continue to represent a strong global contributor to BrC. Thus, it is critical to understand the climate impacts of biomass burning in the boreal forest. This study focused on one set of aged samples from a boreal biomass burning fire, which was shown to have a similar molecular size distribution as extracts from aerosols collected in an agricultural area of Japan³⁴. The presence of large molecular weight compounds may be a common component of aged biomass burning BrC. Although small molecules can be important to BrC absorption in freshly emitted BB aerosols, large, long-lived absorbing molecules may have important climate impacts and are worthy of further study.

3.5 Acknowledgements

Additional information on SEC calibration and TOC analysis, as well as additional figures can be found in Appendix B. Funding was provided by a Natural Science and Engineering Research Council of Canada Discovery Grant. The authors gratefully acknowledge the NOAA Air Resources Laboratory (ARL) for the provision of the HYSPLIT transport and dispersion model and READY website (<http://www.ready.noaa.gov>) used in this publication. The authors thank Joseph Bautista, Teles Furlani, John MacInnis and Trevor VandenBoer for experimental support.

3.6 References

- (1) Myhre, G.; Shindell, D.; Bréon, F.-M.; Collins, W.; Fuglestvedt, J.; Huang, J.; Koch, D.; Lamarque, J.-F.; Lee, D.; Mendoza, B.; et al. Anthropogenic and Natural Radiative Forcing. In *Climate Change 2013: The Physical Science Basis. Contribution of Working Group I to the Fifth Assessment Report of the Intergovernmental Panel on Climate Change*; Stocker, T. F., Qin, D., Plattner, G.-K., Tignor, M., Allen, S. K., Boschung, J., Nauels, A., Xia, Y., Bex, V., Midgley, P. M., Eds.; Cambridge University Press: Cambridge, United Kingdom and New York, NY, USA, **2013**; Vol. AR5.
- (2) Ramanathan, V.; Carmichael, G. Global and regional climate changes due to black carbon. *Nat. Geosci.* **2008**, *1* (4), 221–227.
- (3) Bond, T. C.; Doherty, S. J.; Fahey, D. W.; Forster, P. M.; Berntsen, T.; DeAngelo, B. J.; Flanner, M. G.; Ghan, S.; Kärcher, B.; Koch, D.; et al. Bounding the role of black carbon in the climate system: A scientific assessment. *J. Geophys. Res. Atmos.* **2013**, *118* (11), 5380–5552.
- (4) Saleh, R.; Robinson, E. S.; Tkacik, D. S.; Ahern, A. T.; Liu, S.; Aiken, A. C.; Sullivan, R. C.; Presto, A. a.; Dubey, M. K.; Yokelson, R. J.; et al. Brownness of organics in aerosols from biomass burning linked to their black carbon content. *Nat. Geosci.* **2014**, *7* (9), 647–650.
- (5) Kodros, J. K.; Scott, C. E.; Farina, S. C.; Lee, Y. H.; L'Orange, C.; Volckens, J.; Pierce, J. R. Uncertainties in global aerosols and climate effects due to biofuel emissions. *Atmos. Chem. Phys.* **2015**, *15* (15), 8577–8596.

- (6) Saleh, R.; Marks, M.; Heo, J.; Adams, P. J.; Donahue, N. M.; Robinson, A. L. Contribution of brown carbon and lensing to the direct radiative effect of carbonaceous aerosols from biomass and biofuel burning emissions. *J. Geophys. Res. Atmos.* **2015**, *120* (19), 10,285-10,296.
- (7) Kirchstetter, T. W.; Novakov, T.; Hobbs, P. V. Evidence that the spectral dependence of light absorption by aerosols is affected by organic carbon. *J. Geophys. Res. D Atmos.* **2004**, *109* (21), D21208.
- (8) Andreae, M. O.; Gelencsér, A. Black carbon or brown carbon? The nature of light-absorbing carbonaceous aerosols. *Atmos. Chem. Phys.* **2006**, *6* (10), 3131–3148.
- (9) Zhang, X.; Lin, Y. H.; Surratt, J. D.; Weber, R. J. Sources, composition and absorption Ångström exponent of light-absorbing organic components in aerosol extracts from the Los Angeles basin. *Environ. Sci. Technol.* **2013**, *47* (8), 3685–3693.
- (10) Hecobian, A.; Zhang, X.; Zheng, M.; Frank, N.; Edgerton, E. S.; Weber, R. J. Water-Soluble Organic Aerosol material and the light-absorption characteristics of aqueous extracts measured over the Southeastern United States. *Atmos. Chem. Phys.* **2010**, *10* (13), 5965–5977.
- (11) Zhang, X.; Lin, Y. H.; Surratt, J. D.; Zotter, P.; Prévôt, A. S. H.; Weber, R. J. Light-absorbing soluble organic aerosol in Los Angeles and Atlanta: A contrast in secondary organic aerosol. *Geophys. Res. Lett.* **2011**, *38* (21), 2–5.
- (12) Iinuma, Y.; Böge, O.; Gräfe, R.; Herrmann, H. Methyl-nitrocatechols: atmospheric tracer compounds for biomass burning secondary organic aerosols. *Environ. Sci.*

- Technol.* **2010**, *44* (22), 8453–8459.
- (13) Shapiro, E. L.; Szprengiel, J.; Sareen, N.; Jen, C. N.; Giordano, M. R.; McNeill, V. F. Light-absorbing secondary organic material formed by glyoxal in aqueous aerosol mimics. *Atmos. Chem. Phys.* **2009**, *9* (7), 2289–2300.
- (14) Lee, A. K. Y.; Zhao, R.; Li, R.; Liggio, J.; Li, S. M.; Abbatt, J. P. D. Formation of light absorbing organo-nitrogen species from evaporation of droplets containing glyoxal and ammonium sulfate. *Environ. Sci. Technol.* **2013**, *47* (22), 12819–12826.
- (15) Lin, P.; Liu, J.; Shilling, J. E.; Kathmann, S. M.; Laskin, J.; Laskin, A. Molecular characterization of brown carbon (BrC) chromophores in secondary organic aerosol generated from photo-oxidation of toluene. *Phys. Chem. Chem. Phys.* **2015**, *17* (36), 23312–23325.
- (16) Slikboer, S.; Grandy, L.; Blair, S. L.; Nizkorodov, S. A.; Smith, R. W.; Al-Abadleh, H. A. Formation of Light Absorbing Soluble Secondary Organics and Insoluble Polymeric Particles from the Dark Reaction of Catechol and Guaiacol with Fe(III). *Environ. Sci. Technol.* **2015**, *49* (13), 7793–7801.
- (17) Laskin, A.; Laskin, J.; Nizkorodov, S. A. Chemistry of atmospheric brown carbon. *Chem. Rev.* **2015**, *115* (10), 4335–4382.
- (18) Lack, D. A.; Langridge, J. M.; Bahreini, R.; Cappa, C. D.; Middlebrook, A. M.; Schwarz, J. P. Brown carbon and internal mixing in biomass burning particles. *Proc. Natl. Acad. Sci.* **2012**, *109* (37), 14802–14807.
- (19) Washenfelder, R. A.; Attwood, A. R.; Brock, C. A.; Guo, H.; Xu, L.; Weber, R. J.; Ng, N. L.; Allen, H. M.; Ayres, B. R.; Baumann, K.; et al. Biomass burning

- dominates brown carbon absorption in the rural southeastern United States. *Geophys. Res. Lett.* **2015**, *42*, 653–664.
- (20) Claeys, M.; Vermeylen, R.; Yasmineen, F.; Gómez-González, Y.; Chi, X.; Maenhaut, W.; Mészáros, T.; Salma, I. Chemical characterisation of humic-like substances from urban, rural and tropical biomass burning environments using liquid chromatography with UV/vis photodiode array detection and electrospray ionisation mass spectrometry. *Environ. Chem.* **2012**, *9* (3), 273.
- (21) Donahue, N. M.; Kroll, J. H.; Pandis, S. N.; Robinson, A. L. A two-dimensional volatility basis set – Part 2: Diagnostics of organic-aerosol evolution. *Atmos. Chem. Phys.* **2012**, *12* (2), 615–634.
- (22) NASA. Smoke and Wildfires in Quebec: Natural Hazards <http://earthobservatory.nasa.gov/NaturalHazards/view.php?id=81613> (accessed Jul 17, 2013).
- (23) Issaq, H. J. The role of separation science in proteomics research. *Electrophoresis* **2001**, *22* (17), 3629–3638.
- (24) Her, N.; Amy, G.; Foss, D.; Cho, J.; Yoon, Y.; Kosenka, P. Optimization of Method for Detecting and Characterizing NOM by HPLC–Size Exclusion Chromatography with UV and On-Line DOC Detection. *Environ. Sci. Technol.* **2002**, *36* (5), 1069–1076.
- (25) Her, N.; Amy, G.; Foss, D.; Cho, J. Variations of molecular weight estimation by HP-size exclusion chromatography with UVA versus online DOC detection. *Environ. Sci. Technol.* **2002**, *36* (15), 3393–3399.

- (26) Klaus, U.; Pfeifer, T.; Spiteller, M. APCI-MS/MS: A powerful tool for the analysis of bound residues resulting from the interaction of pesticides with DOM and humic substances. *Environ. Sci. Technol.* **2000**, *34* (16), 3514–3520.
- (27) Wang, Y.; Chiu, C.-A.; Westerhoff, P.; Valsaraj, K. T.; Herckes, P. Characterization of atmospheric organic matter using size-exclusion chromatography with inline organic carbon detection. *Atmos. Environ.* **2013**, *68*, 326–332.
- (28) Janoš, P. Separation methods in the chemistry of humic substances. *J. Chromatogr. A* **2003**, *983* (1–2), 1–18.
- (29) Mukai, H.; Ambe, Y. Characterization of a humic acid-like brown substance in airborne particulate matter and tentative identification of its origin. *Atmos. Environ.* **1986**, *20* (5), 813–819.
- (30) Chen, Y.; Bond, T. C. Light absorption by organic carbon from wood combustion. *Atmos. Chem. Phys. Discuss.* **2009**, *9* (5), 20471–20513.
- (31) Liu, J.; Scheuer, E.; Dibb, J.; Ziemba, L. D.; Thornhill, K. L.; Anderson, B. E.; Wisthaler, A.; Mikoviny, T.; Devi, J. J.; Bergin, M.; et al. Brown carbon in the continental troposphere. *Geophysical Research Letters*. 2014, pp 2191–2195.
- (32) Desyaterik, Y.; Sun, Y.; Shen, X.; Lee, T.; Wang, X.; Wang, T.; Collett, J. L. Speciation of “brown” carbon in cloud water impacted by agricultural biomass burning in eastern China. *J. Geophys. Res. Atmos.* **2013**, *118* (13), 7389–7399.
- (33) Forrister, H.; Liu, J.; Scheuer, E.; Dibb, J.; Ziemba, L.; Thornhill, K. L.; Anderson, B.; Diskin, G.; Perring, A. E.; Schwarz, J. P.; et al. Evolution of brown carbon in wildfire plumes. *Geophys. Res. Lett.* **2015**, *42* (11), 4623–4630.

- (34) Mukai, H.; Ambe, Y. Characterization of a humic acid-like brown substance in airborne particulate matter and tentative identification of its origin. *Atmos. Environ.* **1986**, *20* (5), 813–819.
- (35) Gaffney, J. S.; Marley, N. A.; Smith, K. J. Characterization of Fine Mode Atmospheric Aerosols by Raman Microscopy and Diffuse Reflectance FTIR. *J. Phys. Chem. A* **2015**, 150203151218000.
- (36) Vakkari, V.; Kerminen, V. M.; Beukes, J. P.; Tiitta, P.; Van Zyl, P. G.; Josipovic, M.; Venter, A. D.; Jaars, K.; Worsnop, D. R.; Kulmala, M.; et al. Rapid changes in biomass burning aerosols by atmospheric oxidation. *Geophys. Res. Lett.* **2014**, *41*, 2644–2651.
- (37) Zhao, R.; Lee, A. K. Y.; Huang, L.; Li, X.; Yang, F.; Abbatt, J. P. D. Photochemical processing of aqueous atmospheric brown carbon. *Atmos. Chem. Phys.* **2015**, *15* (11), 6087–6100.
- (38) Sun, H.; Biedermann, L.; Bond, T. C. Color of brown carbon: A model for ultraviolet and visible light absorption by organic carbon aerosol. *Geophys. Res. Lett.* **2007**, *34* (17), L17813.
- (39) Hand, J. L.; Kreidenweis, S. M. A New Method for Retrieving Particle Refractive Index and Effective Density from Aerosol Size Distribution Data. *Aerosol Sci. Technol.* **2002**, *36* (10), 1012–1026.
- (40) Laskin, A.; Smith, J. S.; Laskin, J. Molecular characterization of nitrogen-containing organic compounds in biomass burning aerosols using high-resolution mass spectrometry. *Environ. Sci. Technol.* **2009**, *43* (10), 3764–3771.

- (41) Laskin, J.; Laskin, A.; Nizkorodov, S. A.; Roach, P.; Eckert, P.; Gilles, M. K.; Wang, B.; Lee, H. J.; Hu, Q. Molecular selectivity of brown carbon chromophores. *Environ. Sci. Technol.* **2014**, *48* (20), 12047–12055.
- (42) Lin, Y.; Budisulistiorini, S. H.; Chu, K.; Siejack, R. A.; Zhang, H.; Riva, M.; Zhang, Z.; Gold, A.; Kautzman, K. E.; Surratt, J. D. Light-absorbing oligomer formation in secondary organic aerosol from reactive uptake of isoprene epoxydiols. *Environ. Sci. Technol.* **2014**, *48* (20), 12012–12021.
- (43) Smith, J. S.; Laskin, A.; Laskin, J. Molecular characterization of biomass burning aerosols using high-resolution mass spectrometry. *Anal. Chem.* **2009**, *81* (4), 1512–1521.
- (44) Nguyen, Q. T.; Kristensen, T. B.; Hansen, A. M. K.; Skov, H.; Bossi, R.; Massling, A.; Sørensen, L. L.; Bilde, M.; Glasius, M.; Nøjgaard, J. K. Characterization of humic-like substances in Arctic aerosols. *J. Geophys. Res. Atmos.* **2014**, *119* (8), 5011–5027.
- (45) Lin, P.; Rincon, A. G.; Kalberer, M.; Yu, J. Z. Elemental composition of HULIS in the Pearl River Delta Region, China: results inferred from positive and negative electrospray high resolution mass spectrometric data. *Environ. Sci. Technol.* **2012**, *46* (14), 7454–7462.
- (46) Wozniak, A. S.; Bauer, J. E.; Sleighter, R. L.; Dickhut, R. M.; Hatcher, P. G. Technical Note: Molecular characterization of aerosol-derived water soluble organic carbon using ultrahigh resolution electrospray ionization Fourier transform ion cyclotron resonance mass spectrometry. *Atmos. Chem. Phys.* **2008**, *8* (17), 5099–

5111.

- (47) Ikeya, K.; Sleighter, R. L.; Hatcher, P. G.; Watanabe, A. Fourier transform ion cyclotron resonance mass spectrometric analysis of the green fraction of soil humic acids. *Rapid Commun. Mass Spectrom.* **2013**, *27* (22), 2559–2568.
- (48) Leclair, J. P.; Collett, J. L.; Mazzoleni, L. R. Fragmentation analysis of water-soluble atmospheric organic matter using ultrahigh-resolution FT-ICR mass spectrometry. *Environ. Sci. Technol.* **2012**, *46* (8), 4312–4322.
- (49) Reemtsma, T.; These, A.; Springer, A.; Linscheid, M. Differences in the molecular composition of fulvic acid size fractions detected by size-exclusion chromatography-on line Fourier transform ion cyclotron resonance (FTICR-) mass spectrometry. *Water Res.* **2008**, *42* (1–2), 63–72.
- (50) Reemtsma, T.; These, A. On-line coupling of size exclusion chromatography with electrospray ionization-tandem mass spectrometry for the analysis of aquatic fulvic and humic acids. *Anal. Chem.* **2003**, *75* (6), 1500–1507.
- (51) Forster, P.; Ramaswamy, V.; Artaxo, P.; Berntsen, T.; Betts, R.; Fahey, D. W.; Haywood, J.; Lean, J.; Lowe, D. C.; Myhre, G.; et al. Changes in Atmospheric Constituents and in Radiative Forcing. In *Climate Change 2007: The physical Science Basis. Contribution of Working Group I to the Fourth Assessment Report of the Intergovernmental Panel on Climate Change*; Solomon, S., Qin, D., Manning, M., Chen, Z., Marquis, M., Averyt, K. B., Tignor, M., Miller, H. L., Eds.; Cambridge University Press: Cambridge, United Kingdom and New York, NY, USA, **2007**; p 165.

- (52) Westerling, A. L. Warming and Earlier Spring Increase Western U.S. Forest Wildfire Activity. *Science* (80-.). **2006**, 313 (5789), 940–943.

**4 Size-resolved composition of aged biomass burning aerosols derived
from a real-world boreal wildfire**

4.1 Abstract

Size resolved aerosols between 18 μm and 10 nm collected into 13 different size bins were obtained from an aged biomass burning (BB) plume derived from a boreal wildfire. Aerosol extracts were analyzed for a multitude of analytes including biomass burning molecular markers, common particulate cations and anions, ammonium species and brown carbon (BrC) absorption to identify their size distribution and mixing state. It was found that BrC absorption arose entirely in the submicron fraction, but that common molecular markers including levoglucosan, potassium and acetate were not internally mixed with BB-derived BrC. The low levels of iron and silicon suggest that soil inclusion is minimal to the composition of these BB-derived aerosols. It was found that the observance of ammonium and two dialkyl ammonium species (dimethy- and diethyl-) correlated strongly with BrC absorption. This is the first observation of diethylammonium being the dominant amine in an aerosol sample.

4.2 Introduction

Biomass burning (BB) represents a dominant source of organic aerosols to the atmosphere, second in magnitude only to the atmospheric processing of biogenic volatile organic compounds (VOCs) to form secondary organic aerosol (SOA)¹. Although much work has gone into mechanistically understanding the BB combustion process²⁻⁴ and characterizing gas- and particle-phase molecular markers⁵⁻⁷, the majority of BB-derived organics remain uncharacterized. Currently, the presence of biomass burning organic aerosol (BBOA) is assessed using various particle-bound molecular markers including levoglucosan⁸ and potassium⁹, and gas-phase markers including carbon monoxide¹⁰ and

acetonitrile¹¹. Although these species are primarily emitted as a result of BB, single molecules are being used to represent the entirety of a complex mixture. For example, using an aerosol mass spectrometer, the entire BBOA fraction is determined using positive matrix factorization primarily based on fragment ions of levoglucosan¹²⁻¹⁴. Further, some markers are potentially influenced by alternative sources; for example, mineral dust and fireworks interfere in the use of potassium^{15,16}. Nearly 2 Tg of nitrogen are emitted annually in the form of ammonia and methylamines as a result of biomass burning¹⁷, particularly during smouldering events¹⁰. As efficient particle nucleators, these amines potentially represent additional BBOA markers in regions where alternative sources are negligible.

Combustion processes, including BB, are of importance to climate models due to their ability to produce aerosols that absorb ultraviolet and visible light. Although black carbon (BC) is the dominant absorbing species produced via combustion, light absorbing organic species, called brown carbon (BrC), have been shown to be of increasing importance. Their brown appearance arises from wavelength-dependent absorption in contrast to the relatively constant absorption across wavelengths for BC¹⁸⁻²⁰. Although many SOA-mediated formation mechanisms of BrC from biogenic and anthropogenic gas-phase precursors have been proposed²¹⁻²⁵, field studies demonstrate that primary particles derived from combustion processes, BB in particular, are the dominant atmospheric source of BrC²⁶⁻³². BrC is being consistently reported to have the potential to modify an overall negative radiative forcing (RF) aerosol budget (i.e. net cooling) to one that is positive (i.e. net warming)³³. Estimates of a positive RF influence indicate that BrC could be equal to a third of the positive RF exerted by atmospheric CO₂³³, but the few studies that have included BrC in climate models³⁴⁻³⁸ commonly report that the accuracy of their predictions

is hindered by the large variability of measured BrC absorption efficiencies^{20,29,39,40}. This uncertainty largely arises from the fact that the identity of BrC chromophores are generally unknown. It has been shown that BB-derived BrC is primarily composed of extremely low volatility organic compounds (ELVOCs)⁴¹, with molecular weights as high as 10000 Da²⁷, but the structural identity of the compounds has not been elucidated. These large molecules could have a vast range of molar absorptivities, dependent on their chemical connectivity, conjugation and functionality. For example, ammonia and monoalkyl amines have the ability to participate in Schiff base reactions with ketones to form strongly absorbing imine oligomers, which have been proposed to be important reactions during the formation of SOA-derived BrC^{23,24}. Molecular characterization of real BrC-containing particles from globally important emission sources is therefore necessary to reduce modelled RF uncertainty.

Traditional BB markers do not show strong absorption in the visible and near UV regions, and thus are categorically not part of the BrC fraction. Although their emission ratios may be constant with BBOA on the whole, it is important to determine their mixing state with BrC chromophores in the absence of full molecular characterization of BrC. Models that include BB-derived BrC generally use a single scaling factor to BBOA, which may be erroneous if the BB markers used to assess the presence of BBOA and BrC are not internally mixed. Understanding the distribution of these markers molecular markers across a range of particle diameters will give insight to their mixing state. Few studies have assessed the particle size distribution of BB markers^{9,42}, but none have done so in relationship to BrC absorption. This work describes the size-resolved characterization of various biomass burning markers, amines, elemental species and common particulate

components in reference to large molecular weight BrC absorption from an aged BB plume in order to assess their mixing state and quality as BrC markers.

4.3 Methods

Aged BB particulate samples were collected in St. John's, NL (47.572°N, 52.722°W, 42 m above sea level) two days after a large-scale boreal forest fire erupted in northern Quebec and Labrador, Canada on July 4, 2013. Particle concentrations at the sample site reached over 100 $\mu\text{g}/\text{m}^3$ with a corresponding rise in CO concentrations, indicating the plume intrusion originated from a combustion source (Figure C-1). Computed back trajectories using the Hybrid Single Particle Lagrangian Integrated Trajectory (HYSPPLIT) model confirmed the air mass origin and indicated a transport time of roughly 48 h (Figure C-2).

4.3.1 Sample Collection and Extraction

Size-resolved aerosol samples with aerodynamic diameters ranging from 18 μm to 10 nm were collected with 13-stage cascade impactor (nanoMOUDI II, model 122-R, MSP Corp., Shoreview, MN, USA) at 30 L/min on pre-combusted aluminum substrates (500 °C, 4 h). The total collection time for the size resolved aerosols was 25.5 h corresponding to a total air sample volume of 45.9 m^3 . Filters were stored in the dark at -20°C until extraction. Substrates were sub-sampled using 10% “pie slices”. Pie slices were used instead of punches, as described in previous chapters, due to the radial uniformity of the particles collected onto MOUDI substrates. Each subsample was placed in i) a pre-combusted glass vial or ii) a polypropylene centrifuge which was acid-washed with 10% (v/v) HCl and rinsed 8 times with deionised water (18 M Ω , Barnstead Infinity Ultrapure Water System,

Thermo Scientific, Waltham, MA, USA). For each extraction, an aliquot of deionized water was added according to analysis requirements below. Vials were sealed and sonicated for 40 min at room temperature. After sonication, extracts were filtered with 0.2 μm PTFE syringe filters (Iso-Disc, Supelco, Bellefonte, PA, USA), transferred to muffled glass or clean polypropylene sample vials. Sample extracts were stored at 4 °C until analysis.

4.3.2 Sample Analysis

4.3.2.1 Size Exclusion Chromatography with UV-Vis Analysis (SEC-UV)

Samples were analyzed according to the procedure outlined in Chapter 3 (Di Lorenzo and Young²⁷). Briefly, samples were separated using high performance liquid chromatography (HPLC) (1260 Infinity, Agilent Technologies, Santa Clara, CA, USA) on an aqueous gel filtration column (Polysep GFC P-3000, Phenomenex, Torrance, Ca, USA) with a 25 mM aqueous ammonium acetate eluent at a flow rate of 1 mL/min. Compounds were detected using a diode array detector (1260, Agilent Technologies, Santa Clara, CA, USA). Integrations of total absorbance were calculated at 300 nm, 365 nm and 405nm. Multiple wavelengths were chosen to assess absorption dependence, where the specific wavelengths were chosen for direct literature comparison^{20,28,29,43,44}. Absorbance peak areas, in units of AU·min, were converted to absorption coefficients, in units of Mm^{-1} (Text C.1).

4.3.2.2 Ion Chromatography Analysis

Ion chromatographic analysis was performed using a Dionex ICS 2100 Ion Chromatography System. The instrument and all related products were obtained from Thermo Scientific, Mississauga, ON, Canada. Briefly, 1 mL samples were injected using

an autosampler (Dionex AS-DV) and the cations therein preconcentrated on a cation-exchange column (TC-UPL1, 5 mm x 23 mm). Cations were separated on a cation exchange column (CS19, 4 mm x 250 mm) with a guard column (CG19, 4 mm x 50 mm) using gradient elution with continuously generated methane sulfonic acid (MSA) as the solvent modifier (EGC II MSA Generator Cartridge). Eluent ions were selectively suppressed (Dionex CSRS 300 Ion Suppressor, 4mm) before the analytes were measured using conductivity detection (DS6 heated conductivity cell). Anions were separated on an anion exchange column (AS19, 4 mm x 250 mm) with a guard column (AG19, 4 mm x 50 mm) using gradient elution with potassium hydroxide. The eluent was suppressed (AERS 500 ion suppressor, 4mm) before the analytes were detected by conductivity (DS6 heated conductivity cell).

4.3.2.3 Inductively Coupled Plasma Optical Emission Spectroscopy (ICP-OES)

Analysis

Inductively coupled plasma optical emission spectroscopy (ICP-OES) analysis was performed using an iCap 6500 Series ICP-OES (Thermo Scientific, Mississauga, ON, Canada). Samples were acidified to 2% (v/v) HNO₃ prior to analysis. The instrument was calibrated at the start of the analysis, with two check standards and a reagent blank run every 20 samples. Yttrium was added inline as an internal standard. A drift check was performed every 15 samples and re-calibrated if the drift check failed. Each sample was analyzed four times using the following settings: nebulizer pump flush rate: 100 rpm, analysis pump rate: 50 rpm, pump relaxation time: 20 s, RF power: 1150 W, nebulizer flow: 0.55 L/min, auxiliary gas: 0.5 L/min

4.3.2.4 Levoglucosan Analysis

Samples were separated using high performance liquid chromatography (HPLC) (1260 Infinity, Agilent Technologies, Santa Clara, CA, USA) on a hydrophilic interaction chromatography (HILIC) column (X-Bridge BEH Amide, 2.5 μm x 4.6 mm x 100 mm, Waters Corporation, Milford, MA, USA) with a mobile phase consisting of (A) 0.1% acetic acid in water and (B) acetonitrile. A gradient elution was used for the separation of 10 μL injections with the following program: Initial conditions of 10% A were held for 0.1 min and linearly increased to 80% A over the next 0.9 minutes. This composition was held for 5 minutes. Conditions were returned back to the initial 10% A in 0.1 min and held to reequilibrate for a total run time of 10 min.

Compounds were detected using a time-of-flight mass spectrometric detector (6230, Agilent Technologies, Santa Clara, CA, USA) with electrospray ionization in positive mode (ESI+) with the following acquisition parameters: capillary voltage: 3.5 kV, gas temperature: 350 $^{\circ}\text{C}$, gas flow: 12 L/min, nebulizer pressure: 35 psig, and cone voltage of 175 V. Quantification was performed via external calibration using peak areas from extracted ion chromatograms with a 0.002 Da mass window. The sodiated adduct of levoglucosan ($m/z = 185.0426$) was used for quantification. The sodiated adduct of methyl β -D-xylopyranoside ($m/z = 187.0582$) was used as an internal standard to track ionization efficiency. A five-point calibration between 0.1 - 10 $\mu\text{g}/\text{mL}$ was used to quantify levoglucosan in each sample. Calibration was run before and after the sample analysis.

4.4 Results and Discussion

4.4.1 Size Distribution of Measured Species

4.4.1.1 Biomass Burning Markers

Many markers are used as proxies for detecting BB influence in particle composition. Since BrC is commonly linked to BB activity in real world particles, it is useful to assess the size distribution of some of these common markers. Figure 4-1 shows mass concentrations of the common BB markers, potassium, levoglucosan and acetate, as a function of particle diameter.

Potassium (Figure 4-1A) was found in all size fractions between 18 nm and 5.6 μm , with the majority of mass found in the submicron fraction. Particle diameter-normalized mass loadings ranged between 0.059 – 0.75 $\mu\text{g}/\text{m}^3$. Potassium showed a bimodal distribution with maxima at submicron stages corresponding to 18 – 32 nm (0.56 $\mu\text{g}/\text{m}^3$) and 0.56 – 1.0 μm . (0.75 $\mu\text{g}/\text{m}^3$). Levoglucosan (Figure 4-1B) was found in all size fractions between 18 nm and 5.6 μm with the exception of the stage corresponding to particle diameters ranging from 100 – 180 nm. Particle diameter-normalized mass loadings ranged between 0.059 – 0.34 $\mu\text{g}/\text{m}^3$. Levoglucosan also showed a bimodal distribution with local maxima in submicron stages corresponding to 32 – 56 nm (0.14 $\mu\text{g}/\text{m}^3$) and 0.56 – 1.0 μm (0.34 $\mu\text{g}/\text{m}^3$). The majority of levoglucosan mass was also in the submicron fraction, but showed greater relative mass in supermicron aerosols than potassium. The total mass of levoglucosan across all stages was similar to that of potassium. Acetate (Figure 4-1C) was found in all size fractions between 10 nm and 10 μm with the exception of the stage corresponding to 180 – 320 nm. Particle diameter-normalized mass loadings ranged

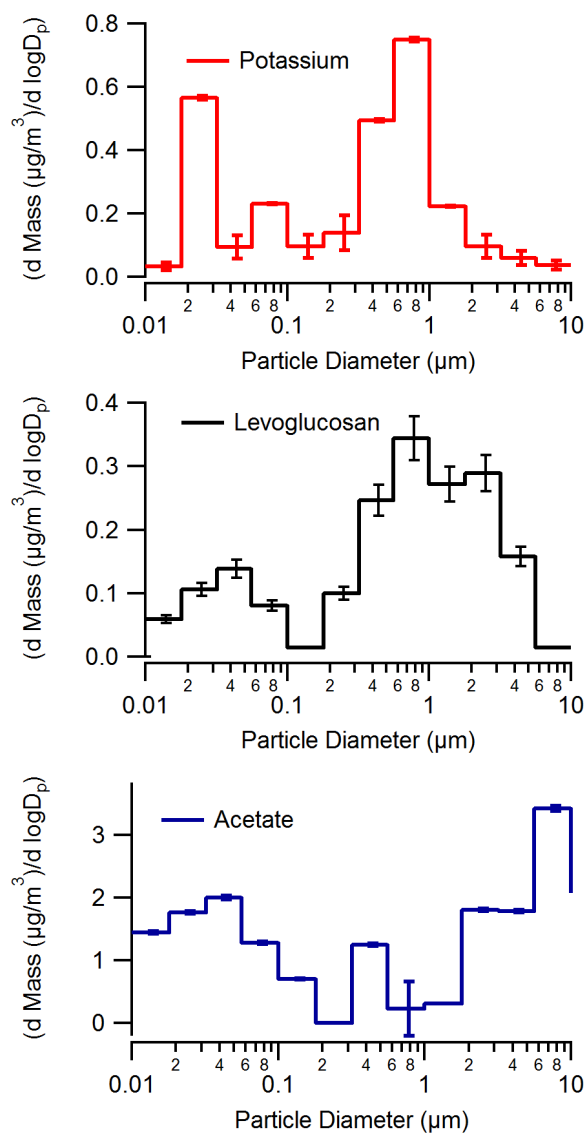


Figure 4-1: Particle size distributions of (top) potassium, (middle) levoglucosan, and (bottom) acetate. between $0.22 - 3.4 \mu\text{g}/\text{m}^3$. Acetate showed local maxima in the superfine mode at the stage corresponding to $32 - 56 \text{ nm}$ ($2.0 \mu\text{g}/\text{m}^3$) and in the coarse mode at the stage corresponding to $5.6 - 10 \mu\text{m}$ ($3.4 \mu\text{g}/\text{m}^3$), with local minima surrounding $1 \mu\text{m}$. Total acetate mass across all stages was roughly 10 times higher than both potassium and levoglucosan.

4.4.1.2 Coastally-Derived Ionic Species

A suite of cationic, anionic and elemental species concentrations was also measured. The most abundant ions are shown in Figure 4-2. The entire data set can be observed in Table C-1. Here we describe the distribution of the most common ions expected in water extracts of coastal atmospheric aerosol samples. Sulfate was found in all size fractions between 18 nm and 10 μm , with a uni-modal distribution. Particle diameter-normalized mass loadings ranged between 0.20 – 1.5 $\mu\text{g}/\text{m}^3$ with a maximum at the stage representing particles between 0.56 – 1.0 μm . Chloride showed negligible submicron abundance, with the majority of mass appearing in stages with particles greater than 1.0 μm . Supermicron particle diameter-normalized mass loadings ranged between 0.43 – 1.7 $\mu\text{g}/\text{m}^3$ with a

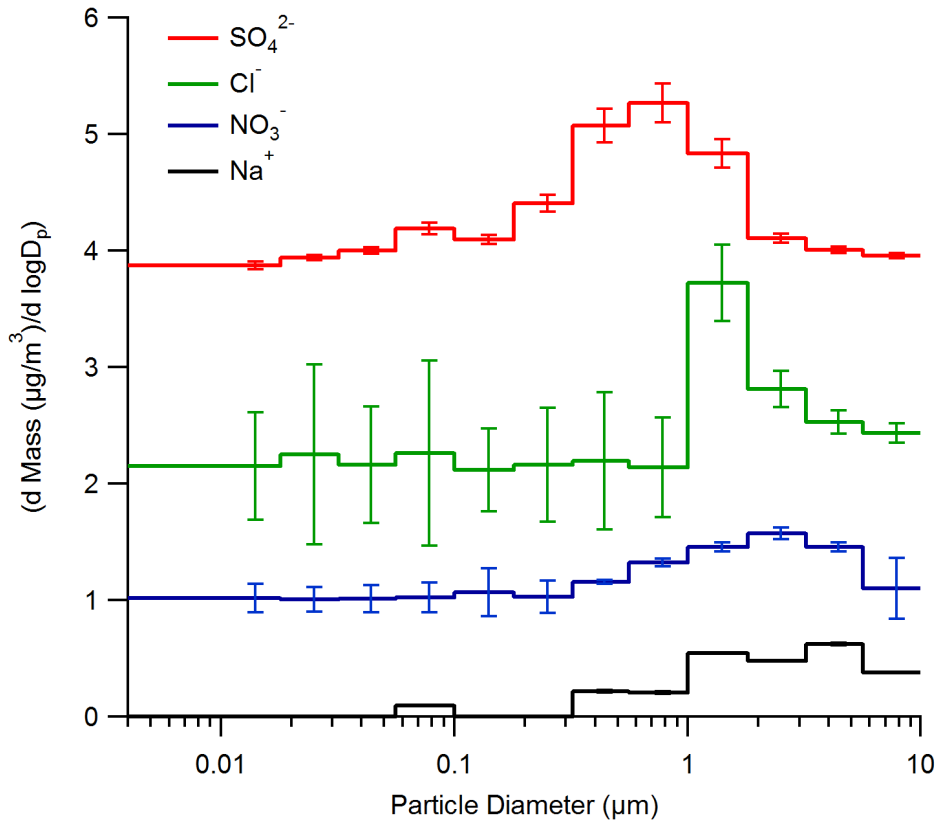


Figure 4-2: Particle size distributions of (red) sulfate, (green) chloride, (blue) nitrate and (black) sodium ions. Traces are offset for clarity.

maximum at the stage corresponding to 1.0 – 1.8 μm . Nitrate was found in size fractions between 0.056 – 5.6 μm with a unimodal distribution. Particle diameter-normalized mass loadings ranged between 0.08 and 0.63 $\mu\text{g}/\text{m}^3$ with a maximum occurring at the stage corresponding to 1.8 – 3.2 μm . Sodium showed a similar distribution to nitrate, being detected in particles between 0.056 – 10 μm , with the exclusion of 0.10 – 0.32 μm . Concentrations ranged between 0.095 – 0.62 $\mu\text{g}/\text{m}^3$, with a maximum occurring between 3.2 – 5.6 μm .

4.4.1.3 Ammonium and Alkyl Ammonium Species

Figure 4-3 shows the size distribution of particulate ammonium and most abundant alkyl ammonium species in this aged BB plume. The distribution of the remaining quantified alkyl ammonium species can be seen in Table C-1. The size distribution was similar across all detected amines, with species being detected in all size fractions between

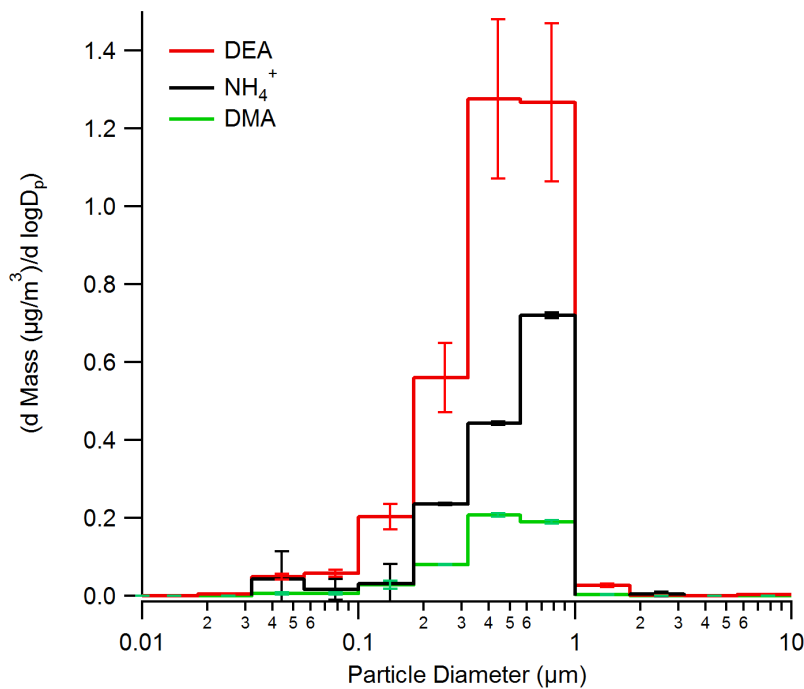


Figure 4-3: Particle size distributions of the most abundant ammonium species: (red) diethyl ammonium, (black) ammonium and (green) dimethyl ammonium.

0.018 and 1.8 μm . Diethylammonium (DEA) was the most abundant ammonium species detected in the sample, with particle diameter-normalized mass loadings ranging between 0.004 – 1.2 $\mu\text{g}/\text{m}^3$. DEA concentration maximum was observed in particles ranging between 0.32 – 0.56 μm . Ammonium concentrations ranged between 0.004 – 0.79 $\mu\text{g}/\text{m}^3$ with a maximum at the stage corresponding to 0.56 – 1.0 μm . Dimethylammonium (DMA) concentrations ranged between 0.006 – 0.021 $\mu\text{g}/\text{m}^3$, with a maximum occurring at the stage corresponding to particles between 0.32 – 0.56 μm

4.4.2 Size Distribution of BrC Absorption

Figure 4-4 depicts the distribution of BrC absorption as a function of particle size as measured by SEC-UV. OA absorption was entirely in the submicron fraction with a modal maximum between 0.56 and 1.0 μm . The molecular weight maxima of absorbing species

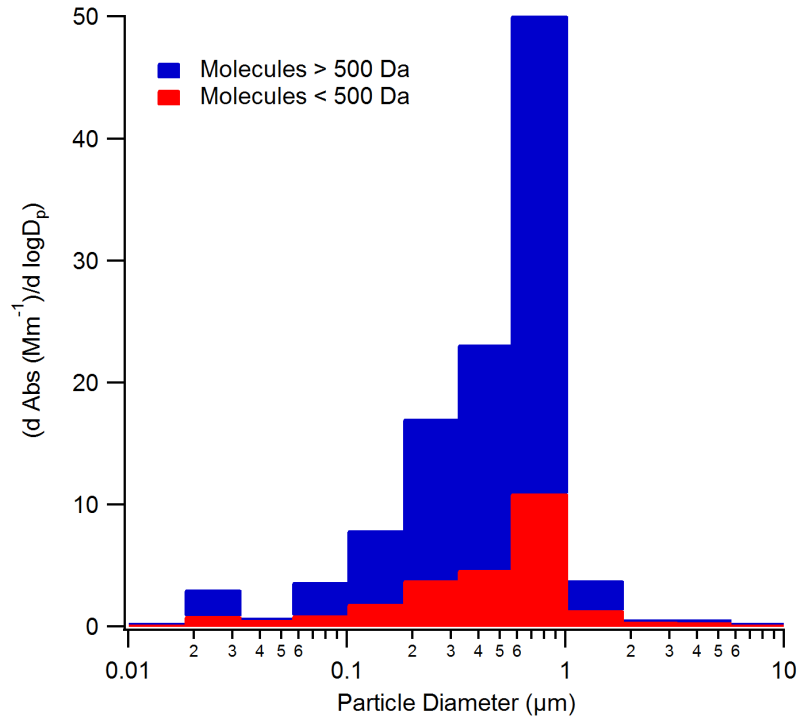


Figure 4-4: Particle size distributions of BrC absorption by (blue) molecules larger than 500 Da and (red) molecules less than 500 Da. Traces are stacked to reflect total absorption at each size fraction

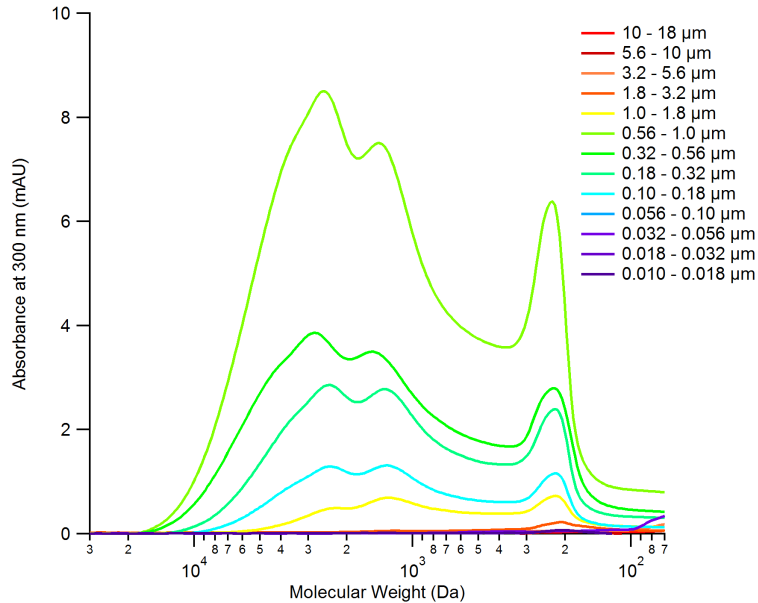


Figure 4-5: BrC molecular size distribution across particle stages as measured using SEC-UV

are identical across all particle sizes, including the ultrafine mode, with maxima occurring at 2800 Da, 1800 Da and 250 Da as depicted in Figure 4-5. The maximum at 250 Da is an artifact of the chromatographic column used, as all compounds less than 250 Da elute simultaneously at this value.

This submicron distribution is consistent with the production of primary BB aerosol^{45,46}. Freshly emitted BB aerosols have been known to rapidly oxidize and grow during transport^{46,47}. Accumulation mode particles contained 93% of the total absorption, with a sharp decrease in absorption after 1 μm , suggesting that absorbing species are highly aged and oxidized, as expected from the calculated transport time; freshly emitted primary particles would likely be distributed in the ultrafine region. A local modal maximum in the ultrafine region, between 0.18 and 0.32 μm was also observed, suggesting a secondary formation mechanism in which absorbers potentially arise from the nucleation of precursor gases or subsequent condensation of co-emitted gases also generated in the biomass

burning plume. Although the species responsible for absorption may be consistent across all particle sizes, Figure 4-6 shows that in the fine mode as particle size decreases, the smaller molecular weight fractions are increasingly responsible for the total absorption. This is consistent with single particle mass spectrometric measurements showing that smaller molecular weight fractions of BBOA are in greater proportion in smaller diameter aerosols⁹. This may also be suggestive of the primary emission size range of BB-derived particles, where high molecular weight components may be too large to condense into ultrafine particles.

Average absorption coefficients across each aerosol size fraction are within the same order of magnitude as the absorption by bulk PM_{2.5} aerosol measured at the same site²⁷

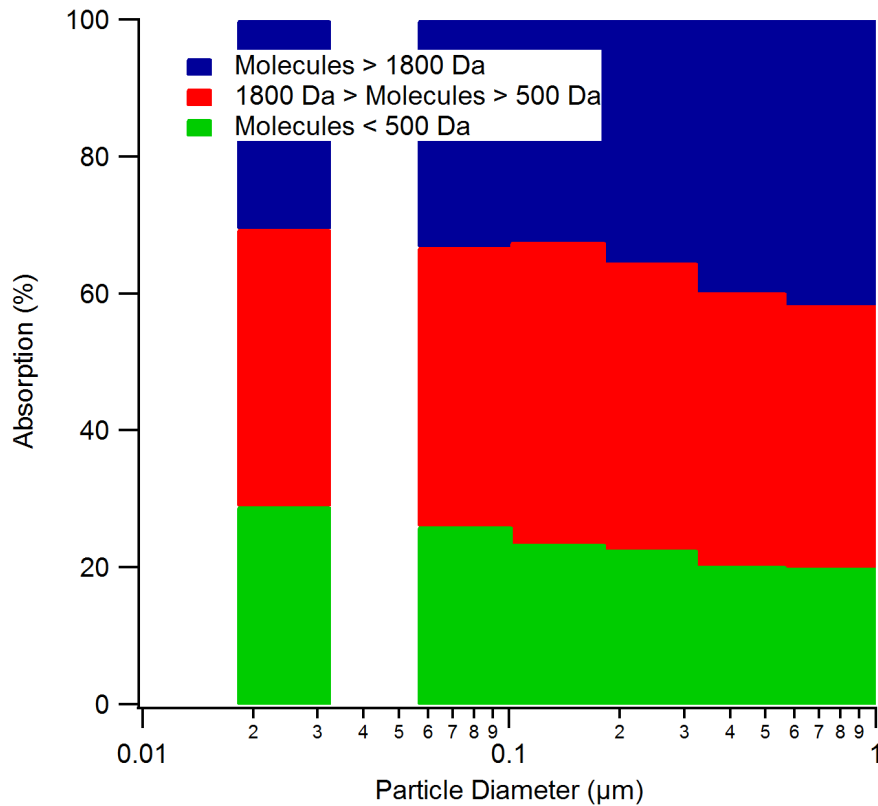


Figure 4-6: Relative contribution of different sized molecules to the total absorption as a function of particle diameter

further suggesting that the molecular composition of the absorbing species are consistent across all particle sizes. Previous studies have shown that the complex component of the particle refractive index, k , varies minimally over the range particle diameters⁴⁸. It has also been shown that the k value of aqueous extracted PM_{2.5} OA from the same BB plume are 0.0186, 0.0056 and 0.0031 at 350 nm, 450 nm and 571 nm respectively²⁷. These complex components are more consistent with previously reported size-resolved absorption by methanol extracts of organic aerosol⁴⁸. Methanol extracted OA has generally been shown to more strongly absorb than corresponding aqueous extracts when rapid solubilisation mechanisms are employed, such as with inertial impaction plates on Particle into Liquid Sampler instruments^{28,30,44,49}, but this phenomenon is not observed when an exhaustive method, such as a 45-minute ultrasonication extraction, is used to extract particle samples. The increase in absorption in methanolic extracts has been attributed to the inclusion of larger molecular weight species in addition to the polar species extracted into water. The methods employed here show that the majority of the absorption is due to large molecular weight species and these are observed in both aqueous and methanolic extracts across all submicron particle diameters.

4.4.3 Comparison between BrC Absorption and Measured Species

4.4.3.1 Biomass Burning Markers

Although potassium (Figure 4-1A) seemingly tracks BrC absorption well in the fine mode ($100 \text{ nm} < D_p < 1 \text{ }\mu\text{m}$) ($R^2=0.820$ and $R^2=0.810$, for correlations with molecular absorption greater than and less than 500 Da, respectively. Figure C-3) and is the most strongly correlated biomass burning marker (Figure 4-7), single particle mass spectrometer

measurements in this size region with more highly resolved particle diameter have shown that potassium distributions have a modal maximum roughly 100 nm smaller than BBOA⁹. In these single particle measurements, potassium was more closely distributed with BBOA that gave a higher proportion of low mass fragments, indicating smaller molecular weight organics. This indicates that potassium inclusion into BB particles may be as a result of a different formation mechanism than BrC, or that potassium may be co-emitted with a

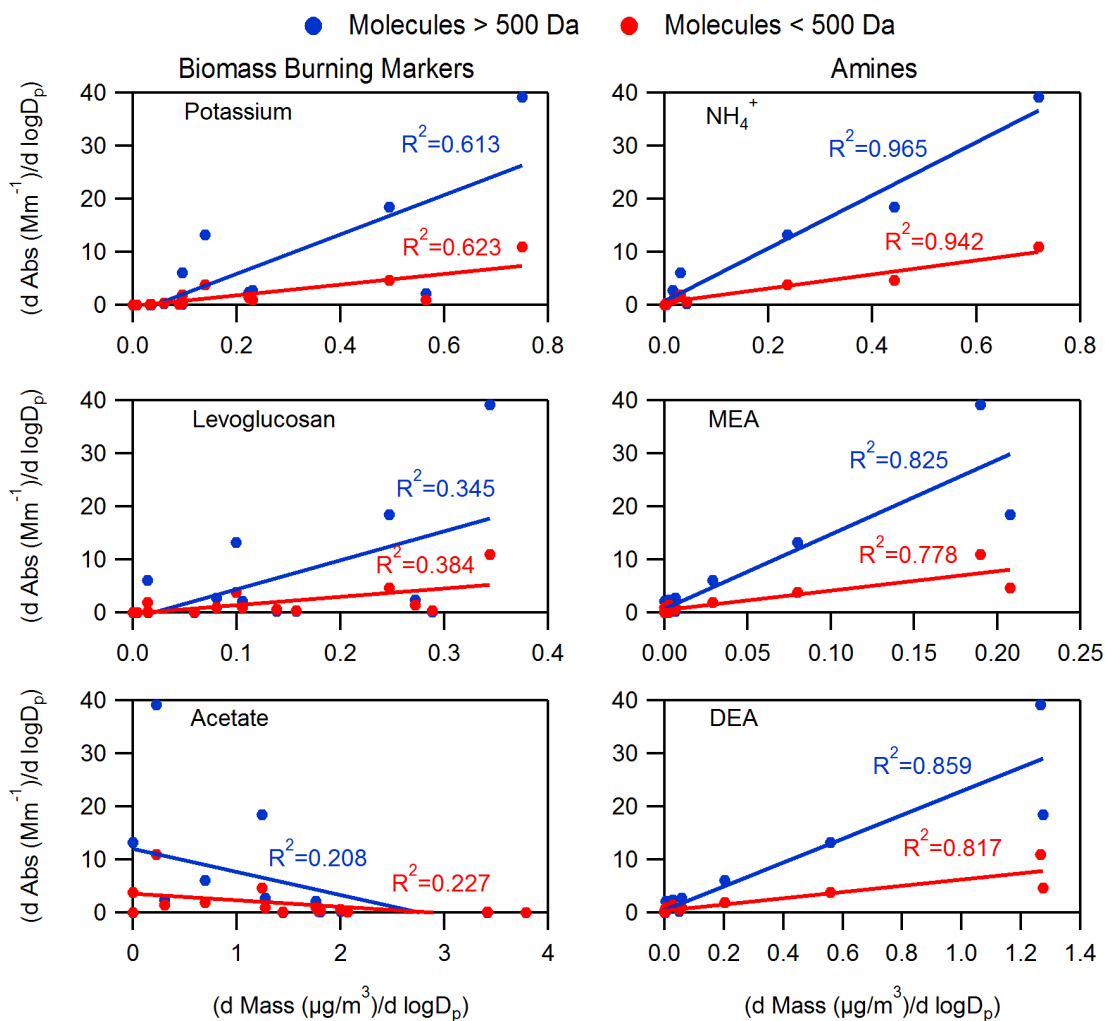


Figure 4-7: Correlation between various (left) biomass burning markers (top - potassium, middle - levoglucosan, bottom - acetate) and (right) ammonium species (top - ammonium, middle - monoethyl ammonium, bottom - diethyl ammonium). Blue markers and lines correspond to correlations made with molecular absorption greater than 500 Da, where red markers and lines correspond to correlations made with molecular absorption < 500 Da.

particular fraction, such as with low molecular weight species, of the total BrC. In the ultrafine mode ($D_p < 100$ nm), although the observation of a potassium signal coincides with the observation of BrC absorption, 32% of the total potassium exists in these particles whereas only 7% of the total absorbance arises in the same fraction. The variability in the ratio between potassium and BrC absorption is primarily a result of the differences in the ultrafine mode ($R^2 = 0.579$ and $R^2 = 0.625$ for correlations with molecular absorption greater than and less than 500 Da, respectively; Figure C-3). This emission ratio variability across particle diameters, therefore, makes scaling BrC absorption to bulk potassium levels for the purpose of climate modelling inaccurate. Proper scaling must include variable ratios with known size-resolved particle loadings.

Levoglucosan (Figure 4-1B) also tracks BrC absorption well in the fine mode, but shows larger relative concentrations in the ultrafine mode as with potassium. Levoglucosan also extends into the coarse mode ($D_p > 1$ μm), where BrC absorption does not. Although levoglucosan is an anhydrosugar directly produced from the combustion of cellulose, it is not internally mixed with BrC chromophores produced from the same fire. When BrC is detected, it coincides with the detection of levoglucosan, but there are many size fractions in which levoglucosan is present and BrC absorption is not. It is proposed that the formation of ELVOCs during combustion events is rapid⁴¹. Levoglucosan, although highly oxidized, is a semi-volatile species. It is suspected to be in the gas phase during the combustion events due to the high temperature environment, and later condense on to particles as the plume transports and cools⁵⁰. In this way, levoglucosan may track well with particle surface area from primary BB aerosol.

Lastly, acetate (Figure 4-1C) shows an anti-correlation with BrC absorption (Figure 4-7). The accumulation mode particles showed high concentrations of sulfate, which would be more thermodynamically favourable to form condensed phase salts with abundant amines present in the particle. In this way, sulfate may have replaced acetate salts produced during combustion. Further, BrC has been proposed to be chemically similar to humic acids, and thus is potentially acidic. Particle pH effects, therefore, could discourage the partitioning of acetate into BrC-rich particles, although their source is the same.

These distributions highlight the importance of understanding particle mixing when assessing the quality of a molecular marker, especially in bulk particle samples. The need for more single particle and size resolved measurements is apparent.

4.4.3.2 Coastally-Derived Ionic Species

Due to the age of the plume and the ubiquity of these ions from multiple origins, it is unsurprising that they are not internally mixed with BrC absorption. The coastal influence from the nearby Atlantic Ocean is apparent in the observed coarse mode distributions of magnesium, sodium and chloride ions. Sulfate as measured by ion chromatography and total sulfur measured by ICP-OES show nearly identical distributions and similar concentrations suggesting that sulfate comprises nearly all of the total sulfur in these aged particles. Total mass concentrations of sulfate, nitrate, chloride and sodium are equal to or slightly higher than that of potassium, suggesting a non-negligible influence of secondary species condensing onto primary BB particles or plume mixing from an oceanic source, which is expected from the age of the collected particles. We calculated that sea-salt derived sulfate, calculated from known oceanic sodium:sulfate ion ratio⁵¹, comprises less than 1%

of the total observed sulfate. The common distributions of nitrate and sodium suggest sea salt interaction with nitric acid to form HCl and NaNO₃ as observed in the literature^{52,53}. Chloride shows a sharp drop-off in concentration into the fine mode with the appearance of BrC absorbers. Chloride may also interact with the acidic moieties of BrC, leading to a reduction in free chloride⁵². Previous work has identified that soil-bound species may be entrained in BB plumes and be incorporated into BB-derived particles^{54,55}. Low concentrations of silicon and iron suggest that inclusion of soil-bound species are not a major contributor to the composition of these aged BB-particles. It is the inclusion of these metals that extend the macromolecular structure of soil organics; the large organic species detected in these samples must therefore have little non-covalent macromolecular character due to the low metal levels contained these samples.

4.4.3.3 Ammonium and Alkyl Ammonium Species

Each of these ammonium species is highly correlated with the occurrence of BrC absorption (Figure 4-7), suggesting they are of similar origin and mechanistic formation. Dimethyl ammonium (DMA) has been used previously in the literature as a BB molecular marker⁵⁶, but diethyl ammonium (DEA) is the dominant amine in this sample. Mono- and tri-alkyl amines were minor components. DEA is in greater mass concentration and nearly equal molar concentration to ammonium in each size bin. This is surprising, as ammonium is commonly found to be in excess of alkyl amines by two to three orders of magnitude⁵⁶. Further, although gas phase alkyl amines have half-lives against hydroxyl radical and ozone oxidation on the order of hours⁵⁷, particulate ammonium species are likely to be more resistant to oxidation than their gas-phase deprotonated analogues.

The similarity in profile distribution between BrC absorption and ammonium and dialkyl ammonium species gives support for their use as BrC markers, but it is important to assess their mechanism of particle partitioning. Particle charge balance between ammonium, alkyl ammonium species, sulfate and nitrate shows a cationic excess in these particles when alkyl ammonium concentrations are high (0.18 – 1.0 μm). Two potential mechanisms may explain this excess. First, as mentioned previously, BrC species are proposed to be similar to humic acids, and this have the potential to deprotonate and charge balance the particles. It is reported that ammonium has a high affinity for humic substances and is difficult to remove during analysis⁵⁸, so ammonium may have preferential partitioning into particles already containing BrC. Second, it is suspected that there may be reactive uptake of ammonium into these particles through reaction with carbonyls on the highly oxidized BrC species to form imines as reported in the literature (Figure 4-8)^{23,24,59}. These imines may be subsequently hydrolysed during aqueous extractions yielding the detected ammonium. This reactive uptake allows for the partitioning of additional ammonium into particles, for example the reported dialkyl ammonium above. The low

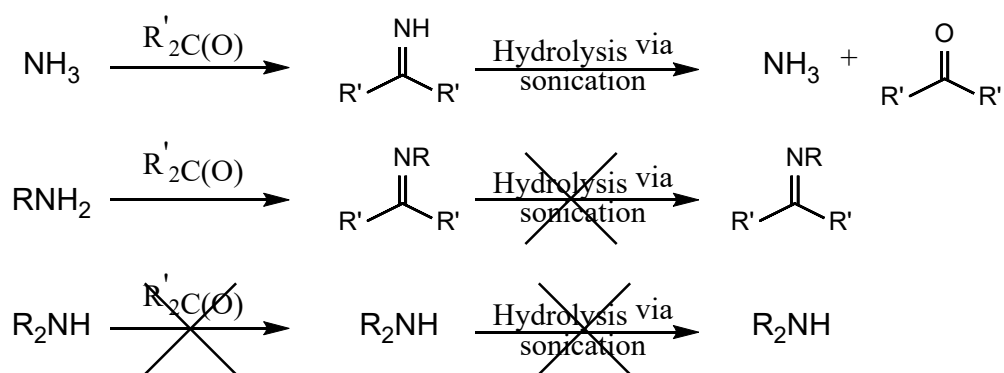


Figure 4-8: Reaction scheme outlining potential atmospheric imine formation and hydrolysis during sonication. Ammonia potentially reacts with carbonyl species to form an imine, and is hydrolysed back during extraction. Primary amines can undergo the same Schiff base reaction as ammonia, but may not be hydrolysed during extraction, leading to negatively biased primary amine concentrations. Secondary amines cannot undergo Schiff base reactions with carbonyls, and are thus not hydrolysed

concentration of monoalkyl amines observed in these samples may also be due to this reactive uptake, where the produced monoalkyl imines may not have been hydrolysed during extraction to give back the corresponding monoalkyl amine species.

It is important to also assess secondary sources of the detected ammonium species in order to assess their relevance as BrC markers. Terrestrial sources of amines primarily include animal husbandry (125 Gg methylamines/year), but another large source of amines to the environment is from the oceanic biological activity (80 Gg methylamines/year)⁵⁶. Calculated particle back-trajectories via the HYSPLIT model show that the sampled BB plume may have transported over the open ocean before being sampled²⁷. Measurements by the NASA MODIS-Aqua satellite show oceanic activity during the plume transport. Here, biologically produced amines may have preferentially partitioned into BrC containing particles long after particle formation at the BB source.

4.5 Conclusions

It is evidenced herein that understanding the mixing state of particulate bound species is important when assessing the quality of a proposed molecular marker. Although the use of size resolved aerosol samples cannot confirm internal mixing, these samples can identify external mixing when the size distributions between species differ. In contrast to online single particle measurements, the offline analysis of size-resolved aerosol allows for a wide gamut of particulate bound species to be assessed. This type of analysis yields excellent complementary data when single-particle measurements can simultaneously be made. It has been shown that common BB molecular markers do not accurately reflect the distribution of absorbing species generated during combustion in aged particles. In this

way, BrC scaling to traditional markers as used during climate modelling or in the field may be erroneous as the size distributions are not consistent and suggest BrC exists in an aerosol population that is externally mixed with other co-emitted particles in a BB plume, even after extensive aging. It is potentially ammonium and alkyl ammonium species that may play a role during the formation of BB-derived BrC, or may secondarily interact with BrC chromophores during transport. Although studies have examined the influence of ammonium on BrC formation from biogenically derived SOA containing glyoxal^{23,24,59}, it may be worthwhile to mechanistically study the interaction of ammonium species with freshly emitted BB aerosol. More discrete observations of the size distribution of BrC, relevant markers and their evolution during aging are required to help constrain the approaches used to describe BrC in climate models.

4.6 References

- (1) Boucher, O.; Randall, D.; Artaxo, P.; Bretherton, C.; Feingold, G.; Forster, P. M.; Kerminen, V.-M.; Kondo, Y.; Liao, H.; Lohmann, U.; et al. Clouds and Aerosols. In *Climate Change 2013: The Physical Science Basis. Contribution of Working Group I to the Fifth Assessment Report of the Intergovernmental Panel on Climate Change*; Stocker, T. F., Qin, D., Plattner, G.-K., Tignor, M., Allen, S. K., Boschung, J., Nauels, A., Xia, Y., Bex, V., Midgley, P. M., Eds.; Cambridge University Press: Cambridge, United Kingdom and New York, NY, USA, **2013**.
- (2) Roberts, A. F. A review of kinetics data for the pyrolysis of wood and related substances. *Combust. Flame* **1970**, *14* (2), 261–272.
- (3) Alger, R. Pyrolysis and Combustion of Cellulosic Materials. In *The Mechanisms of Pyrolysis, Oxidation, and Burning of Organic Materials*; Wall, L. A., Ed.; National Bureau of Standards Special Publication, **1972**; pp 171–184.
- (4) Shafizadeh, F. The Chemistry of Pyrolysis and Combustion. In *The Chemistry of Solid Wood*; **1984**; pp 489–529.
- (5) Simoneit, B. R. T. Biomarker PAHs in the Environment. In *PAHs and Related Compounds*; Neilson, A. H., Ed.; Springer Berlin Heidelberg: Berlin, Heidelberg, **1998**; Vol. 3, pp 175–221.
- (6) Oros, D. R.; Simoneit, B. R. T. Identification and emission factors of molecular tracers in organic aerosols from biomass burning Part 2 . Deciduous trees. *Appl. Geochemistry* **2001**, *16*, 1513–1544.
- (7) Oros, D. R.; Simoneit, B. R. T. Identification and emission factors of molecular tracers in organic aerosols from biomass burning Part 2 . Deciduous trees. *Appl.*

- Geochemistry* **2001**, *16*, 1545–1565.
- (8) Simoneit, B. R. T. Biomass burning - A review of organic tracers for smoke from incomplete combustion. *Appl. Geochemistry* **2002**, *17* (3), 129–162.
- (9) Lee, A. K. Y.; Willis, M. D.; Healy, R. M.; Wang, J. M.; Jeong, C.-H.; Wenger, J. C.; Evans, G. J.; Abbatt, J. P. D. Single particle characterization of biomass burning organic aerosol (BBOA): evidence for non-uniform mixing of high molecular weight organics and potassium. *Atmos. Chem. Phys. Discuss.* **2015**, *15* (22), 32157–32183.
- (10) Yokelson, R. J.; Susott, R.; Ward, D. E.; Reardon, J.; Griffith, D. W. T. Emissions from smoldering combustion of biomass measured by open-path Fourier transform infrared spectroscopy. *J. Geophys. Res.* **1997**, *102* (D15), 18865.
- (11) Andreae, M. O.; Merlet, P. Emission of trace gases and aerosols from biomass burning. *Global Biogeochem. Cycles* **2001**, *15* (4), 955–966.
- (12) Alfarra, M. R.; Prevot, A. S. H.; Szidat, S.; Sandradewi, J.; Lanz, V. a; Schreiber, D.; Mohr, M.; Baltensperger, U. Identification of the Mass Spectral Signature of Organic Aerosols from Wood Burning Emissions Identification of the Mass Spectral Signature of Organic Aerosols from Wood Burning Emissions. *Environ. Sci. Technol.* **2007**, *41* (16), 5770–5777.
- (13) Shrivastava, M. K.; Subramanian, R.; Rogge, W. F.; Robinson, A. L. Sources of organic aerosol: Positive matrix factorization of molecular marker data and comparison of results from different source apportionment models. *Atmos. Environ.* **2007**, *41* (40), 9353–9369.
- (14) Xu, L.; Guo, H.; Boyd, C. M.; Bougiatioti, A.; Cerully, K. M.; Hite, J. R.; Isaacman-vanwertz, G.; Kreisberg, N. M.; Olson, K.; Koss, A.; et al. Effects of anthropogenic

- emissions on aerosol formation from isoprene and monoterpenes in the southeastern United States: Fig. 1. *Proc. Natl. Acad. Sci.* **2015**, *112* (32), E4506–E4507.
- (15) Zhang, X.; Hecobian, A.; Zheng, M.; Frank, N. H.; Weber, R. J. Biomass burning impact on PM_{2.5} over the southeastern US during 2007: Integrating chemically speciated FRM filter measurements, MODIS fire counts and PMF analysis. *Atmos. Chem. Phys.* **2010**, *10* (14), 6839–6853.
- (16) Liu, D.; Rutherford, D.; Kinsey, M.; Prather, K. A. Real-Time Monitoring of Pyrotechnically Derived Aerosol Particles in the Troposphere. **1997**, *69* (10), 1808–1814.
- (17) Lobert, J. M.; Scharffe, D. H.; Hao, W. M.; Crutzen, P. J. Importance of biomass burning in the atmospheric budgets of nitrogen-containing gases. *Nature* **1990**, *346* (6284), 552–554.
- (18) Andreae, M. O.; Gelencsér, A. Black carbon or brown carbon? The nature of light-absorbing carbonaceous aerosols. *Atmos. Chem. Phys.* **2006**, *6* (10), 3131–3148.
- (19) Hoffer, A.; Gelencsér, A.; Guyon, P.; Kiss, G.; Schmid, O.; Frank, G.; Artaxo, P.; Andreae, M. O. Optical properties of humic-like substances (HULIS) in biomass-burning aerosols. *Atmospheric Chemistry and Physics Discussions*. 2005, pp 7341–7360.
- (20) Kirchstetter, T. W.; Novakov, T.; Hobbs, P. V. Evidence that the spectral dependence of light absorption by aerosols is affected by organic carbon. *J. Geophys. Res. D Atmos.* **2004**, *109* (21), D21208.
- (21) Laskin, A.; Laskin, J.; Nizkorodov, S. A. Chemistry of atmospheric brown carbon. *Chem. Rev.* **2015**, *115* (10), 4335–4382.

- (22) Slikboer, S.; Grandy, L.; Blair, S. L.; Nizkorodov, S. A.; Smith, R. W.; Al-Abadleh, H. A. Formation of Light Absorbing Soluble Secondary Organics and Insoluble Polymeric Particles from the Dark Reaction of Catechol and Guaiacol with Fe(III). *Environ. Sci. Technol.* **2015**, *49* (13), 7793–7801.
- (23) Shapiro, E. L.; Szprengiel, J.; Sareen, N.; Jen, C. N.; Giordano, M. R.; McNeill, V. F. Light-absorbing secondary organic material formed by glyoxal in aqueous aerosol mimics. *Atmos. Chem. Phys.* **2009**, *9* (7), 2289–2300.
- (24) Lee, A. K. Y.; Zhao, R.; Li, R.; Liggio, J.; Li, S. M.; Abbatt, J. P. D. Formation of light absorbing organo-nitrogen species from evaporation of droplets containing glyoxal and ammonium sulfate. *Environ. Sci. Technol.* **2013**, *47* (22), 12819–12826.
- (25) Lin, P.; Liu, J.; Shilling, J. E.; Kathmann, S. M.; Laskin, J.; Laskin, A. Molecular characterization of brown carbon (BrC) chromophores in secondary organic aerosol generated from photo-oxidation of toluene. *Phys. Chem. Chem. Phys.* **2015**, *17* (36), 23312–23325.
- (26) Iinuma, Y.; Böge, O.; Gräfe, R.; Herrmann, H. Methyl-nitrocatechols: atmospheric tracer compounds for biomass burning secondary organic aerosols. *Environ. Sci. Technol.* **2010**, *44* (22), 8453–8459.
- (27) Di Lorenzo, R. A.; Young, C. J. Size separation method for absorption characterization in brown carbon: Application to an aged biomass burning sample. *Geophys. Res. Lett.* **2016**, *43* (1), 458–465.
- (28) Washenfelder, R. A.; Attwood, A. R.; Brock, C. A.; Guo, H.; Xu, L.; Weber, R. J.; Ng, N. L.; Allen, H. M.; Ayres, B. R.; Baumann, K.; et al. Biomass burning dominates brown carbon absorption in the rural southeastern United States.

- Geophys. Res. Lett.* **2015**, *42*, 653–664.
- (29) Lack, D. A.; Langridge, J. M.; Bahreini, R.; Cappa, C. D.; Middlebrook, A. M.; Schwarz, J. P. Brown carbon and internal mixing in biomass burning particles. *Proc. Natl. Acad. Sci.* **2012**, *109* (37), 14802–14807.
- (30) Forrister, H.; Liu, J.; Scheuer, E.; Dibb, J.; Ziemba, L.; Thornhill, K. L.; Anderson, B.; Diskin, G.; Perring, A. E.; Schwarz, J. P.; et al. Evolution of brown carbon in wildfire plumes. *Geophys. Res. Lett.* **2015**, *42* (11), 4623–4630.
- (31) Liu, J.; Scheuer, E.; Dibb, J.; Diskin, G. S.; Ziemba, L. D.; Thornhill, K. L.; Anderson, B. E.; Wisthaler, A.; Mikoviny, T.; Devi, J. J.; et al. Brown carbon aerosol in the North American continental troposphere: Sources, abundance, and radiative forcing. *Atmos. Chem. Phys.* **2015**, *15* (14), 7841–7858.
- (32) Xu, L.; Guo, H.; Boyd, C. M.; Klein, M.; Bougiatioti, A.; Cerully, K. M.; Hite, J. R.; Isaacman-VanWertz, G.; Kreisberg, N. M.; Knote, C.; et al. Effects of anthropogenic emissions on aerosol formation from isoprene and monoterpenes in the southeastern United States. *Proc. Natl. Acad. Sci.* **2015**, *112* (1), 37–42.
- (33) Saleh, R.; Marks, M.; Heo, J.; Adams, P. J.; Donahue, N. M.; Robinson, A. L. Contribution of brown carbon and lensing to the direct radiative effect of carbonaceous aerosols from biomass and biofuel burning emissions. *J. Geophys. Res. Atmos.* **2015**, *120* (19), 10,285–10,296.
- (34) Lin, G.; Penner, J. E.; Flanner, M. G.; Sillman, S.; Xu, L.; Zhou, C. Radiative forcing of organic aerosol in the atmosphere and on snow: Effects of SOA and brown carbon. *J. Geophys. Res. Atmos.* **2014**, *119*, 7453–7476.
- (35) Jacobson, M. Z. Investigating cloud absorption effects: Global absorption properties

- of black carbon, tar balls, and soil dust in clouds and aerosols. *J. Geophys. Res. Atmos.* **2012**, *11* (D6).
- (36) Jacobson, M. Z. Effects of biomass burning on climate, accounting for heat and moisture fluxes, black and brown carbon, and cloud absorption effects. *J. Geophys. Res. Atmos.* **2014**, *119*, 8980–9002.
- (37) Wang, X.; Heald, C. L.; Ridley, D. A.; Schwarz, J. P.; Spackman, J. R.; Perring, A. E.; Coe, H.; Liu, D. Exploiting simultaneous observational constraints on mass and absorption to estimate the global direct radiative forcing of black carbon and brown carbon. *Atmos. Chem. Phys.* **2014**, *14*, 10989–11010.
- (38) Feng, Y.; Ramanathan, V.; Kotamarthi, V. R. Brown carbon: a significant atmospheric absorber of solar radiation? *Atmos. Chem. Phys.* **2013**, *13*, 8607–8621.
- (39) Alexander, D. T. L.; Crozier, P. a.; Anderson, J. R. Brown Carbon Spheres in East Asian Outflow and Their Optical Properties. *Science (80-.)*. **2008**, *321* (5890), 833–836.
- (40) Chen, Y.; Bond, T. C. Light absorption by organic carbon from wood combustion. *Atmos. Chem. Phys. Discuss.* **2009**, *9* (5), 20471–20513.
- (41) Saleh, R.; Robinson, E. S.; Tkacik, D. S.; Ahern, A. T.; Liu, S.; Aiken, A. C.; Sullivan, R. C.; Presto, A. a.; Dubey, M. K.; Yokelson, R. J.; et al. Brownness of organics in aerosols from biomass burning linked to their black carbon content. *Nat. Geosci.* **2014**, *7* (9), 647–650.
- (42) Youn, J.-S.; Crosbie, E.; Maudlin, L. C.; Wang, Z.; Sorooshian, A. Dimethylamine as a major alkyl amine species in particles and cloud water: Observations in semi-arid and coastal regions. *Atmos. Environ.* **2015**, *122*, 250–258.

- (43) Zhang, X.; Lin, Y. H.; Surratt, J. D.; Zotter, P.; Prévôt, A. S. H.; Weber, R. J. Light-absorbing soluble organic aerosol in Los Angeles and Atlanta: A contrast in secondary organic aerosol. *Geophys. Res. Lett.* **2011**, *38* (21), 2–5.
- (44) Zhang, X.; Lin, Y. H.; Surratt, J. D.; Weber, R. J. Sources, composition and absorption Ångström exponent of light-absorbing organic components in aerosol extracts from the Los Angeles basin. *Environ. Sci. Technol.* **2013**, *47* (8), 3685–3693.
- (45) Park, S.-S.; Sim, S. Y.; Bae, M.-S.; Schauer, J. J. Size distribution of water-soluble components in particulate matter emitted from biomass burning. *Atmos. Environ.* **2013**, *73*, 62–72.
- (46) Vakkari, V.; Kerminen, V. M.; Beukes, J. P.; Tiitta, P.; Van Zyl, P. G.; Josipovic, M.; Venter, A. D.; Jaars, K.; Worsnop, D. R.; Kulmala, M.; et al. Rapid changes in biomass burning aerosols by atmospheric oxidation. *Geophys. Res. Lett.* **2014**, *41*, 2644–2651.
- (47) Capes, G.; Johnson, B.; McFiggans, G.; Williams, P. I.; Haywood, J.; Coe, H. Aging of biomass burning aerosols over West Africa: Aircraft measurements of chemical composition, microphysical properties, and emission ratios. *J. Geophys. Res. Atmos.* **2008**, *113* (23), 1–13.
- (48) Liu, J.; Bergin, M.; Guo, H.; King, L.; Kotra, N.; Edgerton, E.; Weber, R. J. Size-resolved measurements of brown carbon in water and methanol extracts and estimates of their contribution to ambient fine-particle light absorption. *Atmos. Chem. Phys.* **2013**, *13*, 12389–12404.
- (49) Hecobian, A.; Zhang, X.; Zheng, M.; Frank, N.; Edgerton, E. S.; Weber, R. J. Water-

- Soluble Organic Aerosol material and the light-absorption characteristics of aqueous extracts measured over the Southeastern United States. *Atmos. Chem. Phys.* **2010**, *10* (13), 5965–5977.
- (50) Donahue, N. M.; Kroll, J. H.; Pandis, S. N.; Robinson, A. L. A two-dimensional volatility basis set – Part 2: Diagnostics of organic-aerosol evolution. *Atmos. Chem. Phys.* **2012**, *12* (2), 615–634.
- (51) Sciare, J.; Bardouki, H.; Moulin, C.; Mihalopolous, N. Aerosol sources and their contribution to the chemical composition of aerosols in the Eastern Mediterranean Sea during summertime. *Atmos. Chem. Phys.* **2003**, *3*, 291–302.
- (52) Maudlin, L. C.; Wang, Z.; Jonsson, H. H.; Sorooshian, A. Impact of wildfires on size-resolved aerosol composition at a coastal California site. *Atmos. Environ.* **2015**, *119*, 59–68.
- (53) Pakkanen, T. a.; Kerminen, V.-M.; Hillamo, R. E.; Makinen, M.; Makela, T.; Virkkula, A. Distribution of nitrate over sea-salt and soil derived particles: Implications from a field study. *J. Atmos. Chem.* **1996**, *24* (2), 189–205.
- (54) Popovicheva, O.; Kistler, M.; Kireeva, E.; Persiantseva, N.; Timofeev, M.; Kopeikin, V.; Kasper-Giebl, A. Physicochemical characterization of smoke aerosol during large-scale wildfires: Extreme event of August 2010 in Moscow. *Atmos. Environ.* **2014**, *96* (August 2011), 405–414.
- (55) Kavouras, I. G.; Nikolich, G.; Etyemezian, V.; DuBois, D. W.; King, J.; Shafer, D. In situ observations of soil minerals and organic matter in the early phases of prescribed fires. *J. Geophys. Res. Atmos.* **2012**, *117* (D12), n/a-n/a.
- (56) Ge, X.; Wexler, A. S.; Clegg, S. L. Atmospheric amines - Part I. A review. *Atmos.*

Environ. **2011**, *45* (3), 524–546.

- (57) Schade, G. W.; Crutzen, P. J. Emission of aliphatic amines from animal husbandry and their reactions: Potential source of N₂O and HCN. *J. Atmos. Chem.* **1995**, *22* (3), 319–346.
- (58) Stevenson, F. J. *Humus Chemistry: Genesis, Composition, Reactions*; Wiley-Interscience: New York, NY, **1982**.
- (59) Zhao, R.; Lee, A. K. Y.; Huang, L.; Li, X.; Yang, F.; Abbatt, J. P. D. Photochemical processing of aqueous atmospheric brown carbon. *Atmos. Chem. Phys.* **2015**, *15* (11), 6087–6100.

5 Molecular size separated brown carbon absorption for fresh and aged biomass burning plumes at multiple field sites

5.1 Abstract

Biomass burning is a known source of brown carbon aerosol in the atmosphere. We collected filter samples of biomass burning emissions at three locations in Canada and the United States, with transport times of 10 h to >3 days. We analyzed the samples with size exclusion chromatography coupled to molecular absorbance spectroscopy to determine absorbance as a function of molecular size. The majority of absorption was due to molecules >500 Da, and these contributed an increasing fraction of absorption as the biomass burning aerosol aged. This suggests that the smallest molecular weight fraction is more susceptible to degradation leading to reduced light absorption, while larger molecular weight species may represent recalcitrant BrC. We calculate that these highly-oxidized, large molecular weight species are composed of more than 20 carbons with as few as 2 oxygens, and would be classified as extremely low volatility organic compounds (ELVOCs).

5.2 Introduction

The role of atmospheric aerosol in the global radiative budget is important, but poorly quantified¹. Direct aerosol absorption is particularly important, because it is responsible for positive radiative forcing (RF) and net warming, in contrast to negative RF impacts of light scattering and indirect cloud effects. Although black carbon (BC) dominates carbonaceous particle absorption, organic aerosol (OA) may also include absorbing species that absorb light and are described as brown carbon (BrC). BrC has greater chemical functionality, water solubility, and absorption that increases rapidly in the near ultraviolet spectral region, with a λ^{-2} to λ^{-6} dependency, but its molecular composition is poorly characterized^{2,3}. The

contribution of BrC to total particle absorption potentially represents the difference between model-derived negative RF and experimentally determined positive RF of atmospheric PM⁴. Only recently has BrC determined from field samples been included in global RF models^{4,5}. Many primary and secondary sources for BrC have been proposed, and the majority of mechanistic laboratory studies have focused on secondary organic aerosol (SOA) formation and processing⁶. Potential BrC sources include various polymerization mechanisms from gas-phase sources⁷⁻⁹, NO_x processing of toluene SOA¹⁰, and production from combustion sources¹¹. Improved knowledge of BrC sources, composition, and optical properties is necessary for accurate global RF models.

A few spectroscopic detection methods exist for field measurements of BrC. First, photoacoustic spectroscopy or aethalometry can directly measure total absorption by an aerosol sample. BrC absorption can be inferred from measurements at multiple wavelengths, with the assumption that absorption at visible wavelengths can be attributed to BC, while absorption in the near-UV is due to both BrC and BC¹²⁻¹⁴. Second, because BrC is more volatile than BC, BrC can be selectively removed by thermal denuding. A photoacoustic spectrometer, cavity ringdown spectrometer, or broadband cavity enhanced spectrometer can be used to measure the difference between a denuded and undenuded sample. Each of these first two methods is challenging when BrC concentrations are low. Third, a Particle-into-Liquid Sampler (PILS) can be coupled to a liquid waveguide capillary cell (LWCC) and an absorbance spectrometer¹⁵. This is the only direct online field measurement of BrC that currently exists. A similar approach uses offline filter extracts where solubility differences between BC and BrC are exploited, such that only soluble aerosol components are dissolved and measured using a long pathlength absorbance

spectrophotometer. The BrC content is inferred from the average absorbance in the UV, such as between 360 and 370 nm (Abs_{365})¹⁵. None of the optical methods described here give any information about the chemical composition of BrC.

Our group has recently developed a method for offline determination of BrC absorption for molecules from 250-75,000 Da using size exclusion chromatography and molecular absorbance spectroscopy¹⁶. This method allows for quantification of BrC absorbance as a function of molecular weight, and provides new information about BrC composition. Our previous results showed BrC in a biomass burning (BB) plume was primarily composed of large molecular weight species¹⁶. This is consistent with a study showing that BrC from BB consists of extremely low volatility organic compounds (ELVOCs)¹⁷. The composition of BrC from biomass burning is important because field measurements have shown that water-soluble organic aerosol absorption is predominantly correlated with BB in the southeastern U.S., despite the larger mass contribution of biogenic SOA¹⁹⁻²³.

In this work, we apply our method to analyze filters from multiple locations with different aerosol sources. Fresh BB aerosol was collected during a wildfire event in Vancouver, British Columbia in July 2015, aged BB aerosol was collected in St. John's, Newfoundland and Labrador in July 2013, and background aerosol was acquired during the Southern Oxidant and Aerosol Study (SOAS) in Alabama during June and July of 2013 (Figure 5-1). We use these results together with the extensive instrumentation available at the SOAS field site and through the Fraser Valley Air Quality Monitoring Network to gain information about the molecular species that compose BrC.

5.3 Methods

5.3.1 Sampling Sites

Samples were collected at three locations to examine fresh biomass emissions, aged biomass burning emissions, and background air. A map of these sites is shown in Figure 5-1.

5.3.1.1 Fresh Biomass Burning Aerosol in Vancouver, British Columbia, Canada

Fresh BB emissions were collected during summer 2015 as part of the Lower Fraser Valley Air Quality Monitoring Network in British Columbia, Canada. These samples are of particular interest because they capture the early July wildfire events in the nearby Temperate Coniferous forest, where $PM_{2.5}$ concentrations exceeded $200 \mu\text{g}/\text{m}^3$ (Figure D-1). Samples were obtained from the Burnaby/Kensington Park (BKP) site (49.2792°N , 122.9707°W , 110 m above sea level) and North Vancouver/Second Narrows (NVSN) site (49.3015°N , 123.0204°W). The BKP site is situated in a mixed urban neighbourhood near residential, industrial, commercial and park land areas. The NVSN site is located in a busy commercial and industrial area, within 50 m of a chemical plant that is a known NO_x emitter. Both sampling sites were located approximately 100 km east of the main burn location.

At the Vancouver sites, aerosol samples were collected using real-time beta attenuation particle monitors (5030 SHARP Monitor at the BKP site, 5030i SHARP monitor at the NVSN site, Thermo Fisher Scientific, Waltham, MA, USA). Particles were collected at 16.67 L/min on glass microfiber filter tape at 8 h intervals. Filter tape was stored in the dark at -20°C until analysis.

5.3.1.2 Aged Biomass Burning Aerosol in Newfoundland, Canada

Aged BB particulate samples were collected in St. John's, Newfoundland (47.572°N, 52.722°W, 42 m above sea level) two days after a large-scale forest fire erupted in northern Quebec and Labrador, Canada on July 4. Further details for the collection and analysis conditions for this sample can be found in Di Lorenzo and Young¹⁶.

The collection of aged BB particles at the St. John's site is described in detail in Di Lorenzo and Young¹⁶. Briefly, multiple PM_{2.5} samples (n=6) were collected in parallel on 47 mm quartz fibre filters (Pall Life Sciences, Washington, NY, USA) using a multi-channel, medium volume air sampler (URG-3000ABC, URG Corp., Chapel Hill, NC, USA) for a total collection time of 25.5 h during the intrusion of the above described BB plume. Filters were stored in the dark at -20 °C until analysis.

5.3.1.3 Regional Background of Aged Biomass Burning Aerosol in the southeastern U.S.

Background air samples were collected over six weeks during the summer of 2013. PM_{2.5} samples were taken as part of the Southern Oxidant and Aerosol Study (SOAS) in the Talladega National Forest in Central Alabama (32.90328°N, 87.24994°W, 76.5 m above sea level). These samples represent typical rural air masses with no direct emissions other than the biogenic emissions of the surrounding forest and occasional intrusion from the neighboring urban areas of Birmingham and Tuscaloosa, AL¹⁹. The forest is primarily composed of pine and hardwoods with isoprene emissions representative of the southeastern US²⁴.

At the SOAS site, background PM_{2.5} samples were collected on the back filter assembly of a custom-built broadband cavity enhanced spectrometer (BBCEAS)²⁵ on 47 mm PTFE filters (Pall Life Sciences, Washington, NY, USA) housed in a molded PFA 47 mm filter assembly (Savillex Corp., Eden Prairie, MN, USA) across two channels. Each channel was sampled at 2035 standard cm³ min⁻¹ through black silicone tubing for 3, 12, or 24 h. It is suspected that the earliest samples (10 - 13 June 2013) were affected by contamination from the off-gassing of siloxanes from the black silicone tubing used in the instruments^{26,27}, based on the absorbance of these filters 300 nm²⁸. For this reason, these three filter samples were excluded from analysis.

Sampled filters were wrapped in pre-muffled aluminum foil (500 °C, 4 h), placed in anti-static bags (McMaster-Carr, Elmhurst, IL, USA) and stored in the dark at -20 °C until analysis. Three types of field blanks were acquired to assess contamination. Filters were 1) removed from packaging then immediately stored as above, 2) removed from packaging and placed into filter housing then removed and stored as above, and 3) removed from packaging, placed in series behind the sample filter to assess filter breakthrough during sampling, then stored as above. In total, 100 filters were collected.

This field campaign was co-located with the Electric Power Research Institute Southeastern Aerosol Research and Characterization Network (SEARCH), where a suite of gas- and particle-phase measurements were performed alongside the particle collection: CO as measured by non-dispersive infrared (NDIR) detection, K⁺ as measured by the Monitor for Aerosols and Gases in Ambient Air (MARGA)²⁹, and organic aerosol fractions as measured by an aerosol mass spectrometer (AMS)³⁰. Particle absorption was also measured in real time at the SOAS site using a PiLS-LWCC for water soluble organic

aerosol (OA) absorption¹⁵ and with a multi-angle absorption photometer (MAAP) for BC absorption³¹.

5.3.2 Fire Identification and Transport Time

Fire locations and burn areas, shown as red circles in Figure 5-1 were obtained from the British Columbia Air Data Archive and the Canadian National Fire Database for Vancouver and St. John's samples, respectively. Only fires erupting within seven days prior to the sampling time were included, as to represent potential BB sources of sampled aerosol.

Airmass back trajectories as computed using the Hybrid Single Particle Lagrangian Integrated Trajectory Model (HYSPLIT) are shown in coloured traces of Figure 5-1³². Back trajectories were computed using a ground-level sampling location, archived Global Data Assimilation System (GDAS1) meteorology. Vertical motion was computed using the vertical velocity field from the meteorological data. New trajectories were computed every 1 hour for a total run time of 48 and 72 hours for Vancouver and St. John's locations, respectively.

5.3.3 Sample Extraction and Analysis by Size Exclusion Chromatography Absorption Spectrophotometry (SEC-UV)

Each filter was sub-sampled using a 10 mm arch punch. Punches from each filter were placed in a glass vial and sealed with an acid washed cap containing a Teflon-lined septum. 750 μ L of ultrapure deionized water (Barnstead Infinity Ultrapure Water System, Thermo Scientific, Waltham, MA, USA) was added and the samples were sonicated for 45 minutes. For SOAS samples, seven punches from each filter were combined per extraction.

For the Vancouver samples, one punch from each filter spot was used per extraction. Due to the hydrophobicity of the Teflon filters of the SOAS samples, a 38 mm, 20-gauge needle (BD Precision Glide, Fisher Scientific, Waltham, MA, USA) was inserted through the septa to keep the filter media below the water surface during sonication. The exposed needle opening was wrapped in parafilm to prevent contamination. After sonication, all extracts were filtered with 0.2 μm PTFE syringe filters (Iso-Disc, Supelco, Bellefonte, PA, USA), transferred to pre-muffled glass sample vials and stored at 4 °C until analysis.

Samples were analyzed according to the procedure outlined in Di Lorenzo and Young¹⁶. Briefly, samples were separated using high performance liquid chromatography (HPLC) (1260 Infinity, Agilent Technologies, Santa Clara, CA, USA) on an aqueous gel filtration column (Polysep GFC P-3000, Phenomenex, Torrance, Ca, USA) with a 25 mM aqueous ammonium acetate eluent at a flow rate of 1 mL/min. Compounds were detected using a diode array detector (1260, Agilent Technologies, Santa Clara, CA, USA). Integrations of total absorbance were performed at 300 nm, 365 nm and 405nm. Conversion of absorption peak areas, in units of AU·min, to absorption coefficients, in units of Mm^{-1} can be found in the supporting information (Text C.1).

5.4 Results and Discussion

5.4.1 Calculated Ages for Biomass Burning Aerosol

HYSPLIT back trajectories and fire plume locations are shown in Figure 5-1. Although the back trajectories and transport can be uncertain, they give a useful indication of transport age for the biomass burning samples. Plume ages were estimated by determining the HYSPLIT-calculated age at which a plume traversed over a likely fire

source. Back trajectories for the Vancouver NVSN/BKP sites show aerosol transport times between 8 and 30 h during the study period. Air masses sampled at the St. John's site were

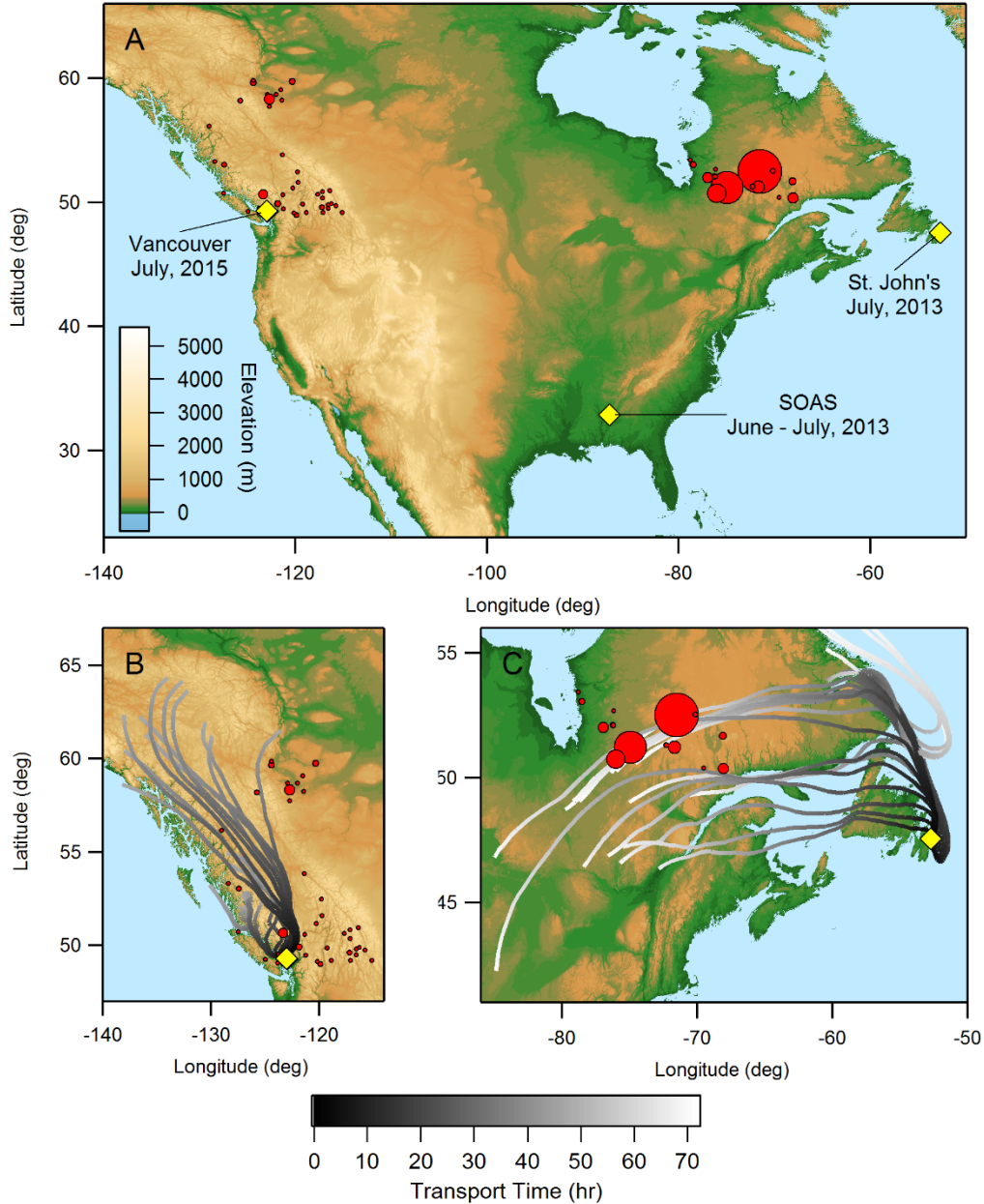


Figure 5-1: A) Locations of three sampling sites highlighted in yellow diamonds. Red circles denote locations of forest fires relevant to respective sampling periods with sizes of circles denoting size of forest fire from the Canadian National Fire Database. B) 48 h air mass back trajectories from the Vancouver sampling sites from 6 July 2015 as computed using the Hybrid Single Particle Lagrangian Trajectory (HYSPLIT) model. C) 72 h air mass back trajectories from the St. John's sampling site from 6 July 2013 as computed using the HYSPLIT mode. Trace color denotes air mass transport time.

more aged, with transport times between 48 and 72 h during the study period. Finally, the biomass burning aerosol at the SOAS field site was significantly aged, and was generally not associated with identifiable fires. Examination of MODIS fire locations and back trajectories showed that the SOAS site was not influenced by large, discrete fires, and more likely was affected by a regional background of small agricultural fires. In this case, aerosol age is difficult to quantify, but we estimate a value of up to 5 days using HYSPLIT back-trajectories.

5.4.2 BrC Absorbance as a Function of Molecular Weight

Absorbance density plots as a function of molecular weight of BrC for a freshly emitted subalpine/montane wildfire, an aged boreal plume, and a typical background rural aerosol sample are shown in Figure 5-2. Absorption density plots show marked similarity in molecular weight profile distribution across sample locations. Molecular weights of

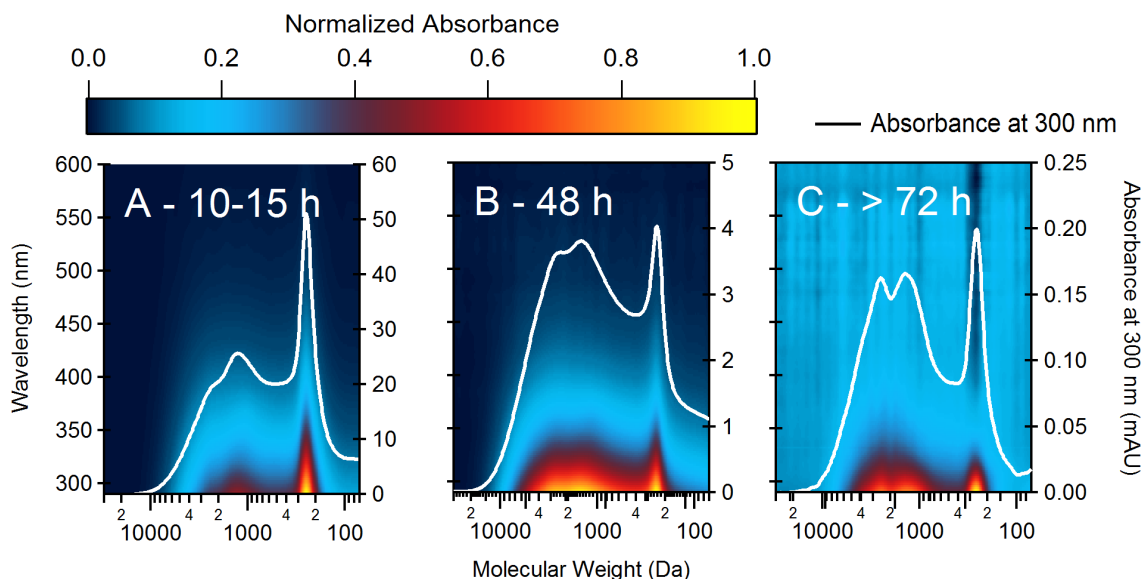


Figure 5-2: Absorption density of BrC as a function of molecular weight across different sampling regions. Image color corresponds to normalized absorbance intensity. White trace denotes absorption profile at 300 nm. Plume age increases moving from figures A to C. A) Freshly emitted BB aerosol (~10-15 h) at the BKP site. B) Aged BB-aerosol (~48 h) collected at the St. John's, NL site. C) Background emissions as collected at the SOAS site

absorbing species were estimated using the calibration method outlined in Di Lorenzo and Young¹⁶. Samples from each site contain three apparent populations with consistent molecular weight maxima of approximately 2400 Da, 1400 Da and 250 Da. Each sample shows a maximum observable molecular weight of 10,000 Da. Further, this molecular weight profile distribution remained constant throughout all days of the SOAS campaign (Figure 5-3). The only day in which the molecular weight profile was different was on 11 June 2013, highlighted by the grey trace in Figure 5-3. It is suspected that this is a result of siloxane contamination, as described above.

Previous studies have reported that the amount of BrC emitted from biomass burning depends on burn conditions, with a smaller influence from fuel type¹⁷. Although the two wildfire samples (Vancouver and St John's) are of separate origin, different age, and

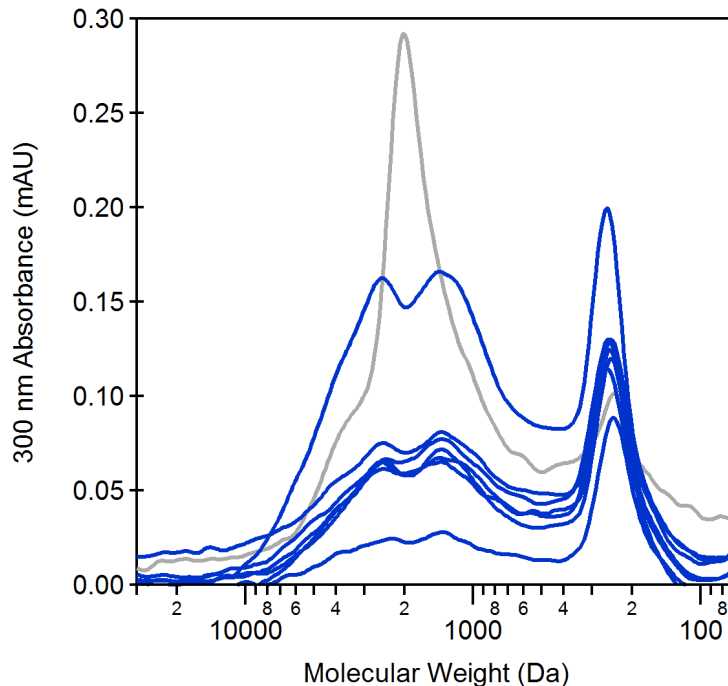


Figure 5-3: Absorbance distribution as a function of molecular weight for filters collected from 11 June 2013 – 13 July 2013 during the SOAS campaign. Each blue line represents a single analysis. The anomalous molecular weight profile from 11 June 2013 is shown in light grey.

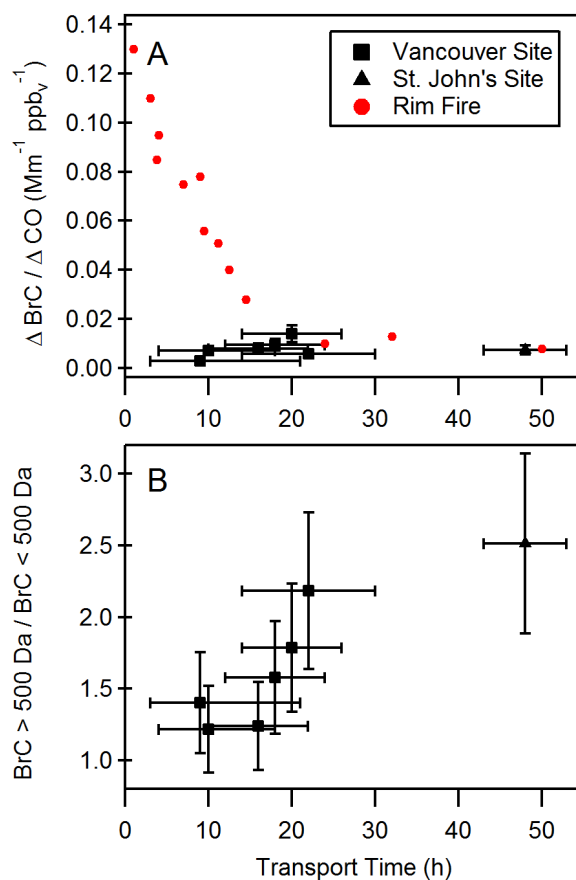


Figure 5-4: A) BrC absorbance at 365 nm relative to CO as a function of plume age. Black squares denote average $\Delta \text{BrC}/\Delta \text{CO}$ for both Vancouver sites, black triangle denotes the St. John's site, red circles denote values obtained from Rim 1 fire in Forrister et al.²¹ B) Absorbance ratio for large molecules (>500 Da) to small molecules (<500 Da) as a function of plume age. Transport times for the Vancouver and St. John's sites are estimated from back trajectories calculated using the HYSPLIT model.

different fuel source (boreal vs. temperate coniferous forests), they have similar absorption characteristics. This suggests that although the quantity of BrC produced is variable depending on the particular burning event, molecular characteristics of BB-derived BrC may be constant.

To assess the relative absorbance and aging of BB aerosol from each fire, the ratio of BrC to a conserved CO tracer ($\Delta \text{BrC}/\Delta \text{CO}$) was plotted as a function of aerosol transport time in Figure 5-4A³³. Background CO values were calculated from average ground-level

CO measurements made at the same site 8 h before plume intrusion. Background CO concentrations were calculated to be 0.15, 0.11 and 0.14 ppm_v for the BKP, NVSN and St. John's sites, respectively. Background CO values were calculated using the average of the eight consecutive hours containing the lowest CO concentrations five days prior and succeeding plume intrusions. Previous field and laboratory measurements have shown rapid initial transformation of individual absorbing BB-derived molecules³⁴, as well as the BrC fraction of BB plumes on the whole²¹ with half-lives on the order of 9 to 15 h³⁵. In Figure 5-4A, the $\Delta\text{BrC}/\Delta\text{CO}$ for the Vancouver and St. John's BB samples are overlaid with those reported by Forrister et al.²¹, where BrC absorption was measured as multiple BB-plumes were tracked via aircraft from their source. It is observed that the BB-derived particles collected at both Vancouver sites have already undergone sufficient oxidation leading to a reduction in absorption, as the measured plumes are at least 10 h old upon collection. Furthermore, the total BrC absorption at the Vancouver sites is the same as that of the St. John's site after correcting for plume dilution. Differences between values observed in this study and those measured by Forrister et al.²¹ may be because of uncertainty in determining plume ages from back trajectories, difficulty in determining background CO levels in comparison to aircraft flights in and out of BB plumes, or Forrister et al. BrC values are the sum of sequential methanol and water extracts.

Although the total absorption of measured BB-derived samples is seemingly constant with age, relative contributions of higher molecular weight components (>500 Da) increases in comparison to smaller molecular weight components (<500 Da) as the plume continues to age (Figure 5-4B). Further, the molecular weight profile of SOAS samples more closely resemble those sampled from an aged BB plume in comparison to a fresh BB

plume. This absorbance ratio is relatively constant throughout the SOAS campaign (Figure D-3), where large molecular weight species consistently contribute roughly three times the absorbance of small molecules measured by this method. These large molecule absorbers drive the correlations with other species, as described in the proceeding sections. The decreasing contribution of smaller molecules to total BrC absorbance as a function of plume age suggests that it is the lower molecular weight fraction that undergoes oxidative transformation resulting in decreased absorbance. The absorbance profile measured for SOAS samples potentially represents the recalcitrant, background BB-derived BrC absorption.

5.4.3 Comparison of Absorbance for SEC-UV Filter Samples and Online PiLS-LWCC

Figure 5-5 shows the time series of and relationship between offline BrC absorption as measured by SEC-UV and online PiLS-LWCC water soluble organic aerosol absorption. The higher-frequency absorbance data from the PiLS-LWCC was time-averaged to that of the filter samples in order to make the relevant correlations. Offline SEC-UV absorption measurements vs online OA absorption has a slope = 0.46 ± 0.08 , offset = 0.05 ± 0.02 , and $r^2 = 0.530$. Both the PiLS-LWCC and SEC-UV methods measure the water soluble absorbing component of SOAS aerosols, so the correlation between these two methods was expected to be stronger. One explanation is that different solubilisation methods are employed by the two techniques. For the offline SEC-UV absorption measurements, rigorous extraction via a 40-minute sonication in water was used, designed to be exhaustive for water soluble species. In situ OA absorption is expected to select for only the most

soluble components of aerosols, since particle collection relies on immediate unmediated solubilisation on collision with an impactation plate³⁶. Many of the species being detected by SEC-UV are large and would have comparatively lower solubility than small, oxidized molecules. Thus, they would not be expected to rapidly dissolve by the solubilisation

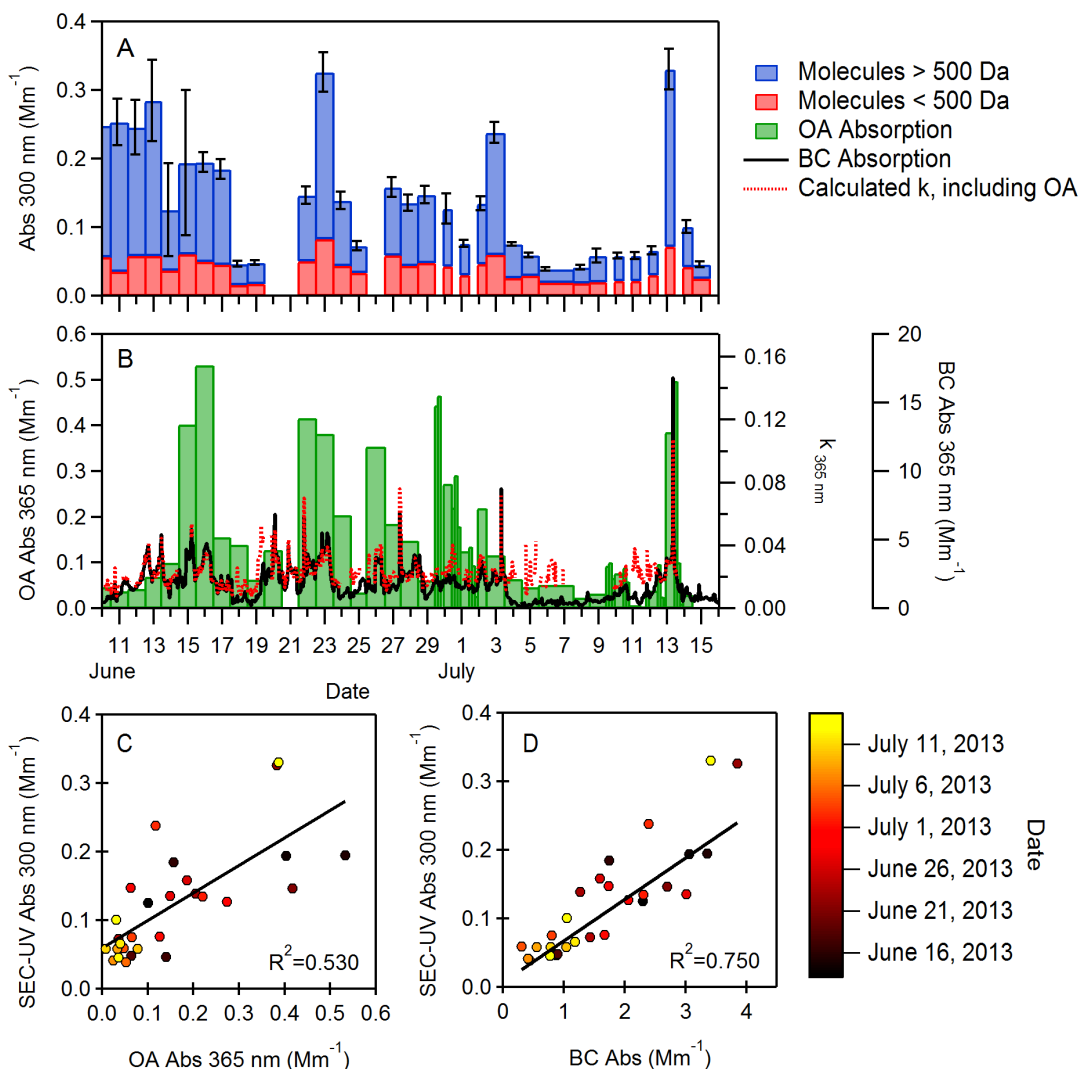


Figure 5-5: A) Absorbance as measured by SEC-UV for samples acquired from the SOAS campaign. Blue bars represent the absorbance by molecules greater than 500 Da, red bars represent the absorbance by molecules less than 500 Da. B) In-situ measured absorption at the SOAS campaign. Green bars show OA absorption, the black line represents absorption by BC, the red dotted line represents calculated k values, including OA absorption. C) Correlation between BrC absorption as measured by SEC-UV offline and by PiLS-LWCC online. Points colored by sampling date. D) Correlation between BrC absorption as measured by SEC-UV and BC absorption as measured by MAAP. Points also colored by sampling date.

mechanisms employed by the PiLS-LWCC. It has been previously reported that methanolic extracts under similar conditions to those employed with the PiLS-LWCC show greater absorption than corresponding aqueous extracts^{37,38}. This absorption difference between methanolic and aqueous extracts was not observed when a sonication-based extraction method was employed¹⁶. This suggests that compounds extracted by sonication, whether in methanol or water, may represent a greater fraction of large molecular weight absorbers of BrC than by in-situ PiLS-LWCC. Further, filter measurements may suffer from losses of semivolatile BrC species, the abundance of which may vary based on the type of BrC in the ambient air at that time.

5.4.4 Sources of BrC in background aerosol at the SOAS site

Absorption spectra for aerosol samples acquired at the SOAS site are similar to those from known biomass burning aerosol collected in Vancouver and St. John's (Figure 5-2), although the SOAS site was not downwind of large discrete fires. The SOAS site was primarily influenced by isoprene emissions of the nearby forest, with minor periodic input of urban emissions of Tuscaloosa and Birmingham¹⁹. For this reason, BrC components have likely had sufficient time to age and internally mix with other particle phase components. BB has been previously shown to be an important contributor to absorption measured by PiLS-LWCC¹⁹. We examined the correlation between the SEC-UV absorption and other co-located measurements at the SOAS site to better identify the potential BrC sources.

5.4.4.1 Correlation of BrC with BB and combustion-based sources

Figure 5-5D shows a strong correlation of SEC-UV absorption with BC absorption ($r^2 = 0.750$), suggesting that both are emitted by a common combustion source. This is consistent with the correlation between SEC-UV absorption and CO ($r^2 = 0.623$, Figure 5-6). Further, SEC-UV absorption was poorly correlated with SO₂ ($r^2 = 0.029$), indicating that the bulk of BrC in the area is not a result of coal or diesel combustion.

Offline BrC measurements by SEC-UV showed a stronger correlation to BC absorption than did in situ BrC absorption measurements made by PiLS-LWCC, as seen in Figure 5-5C and D. This provides further evidence that the dominant contributor to large molecular

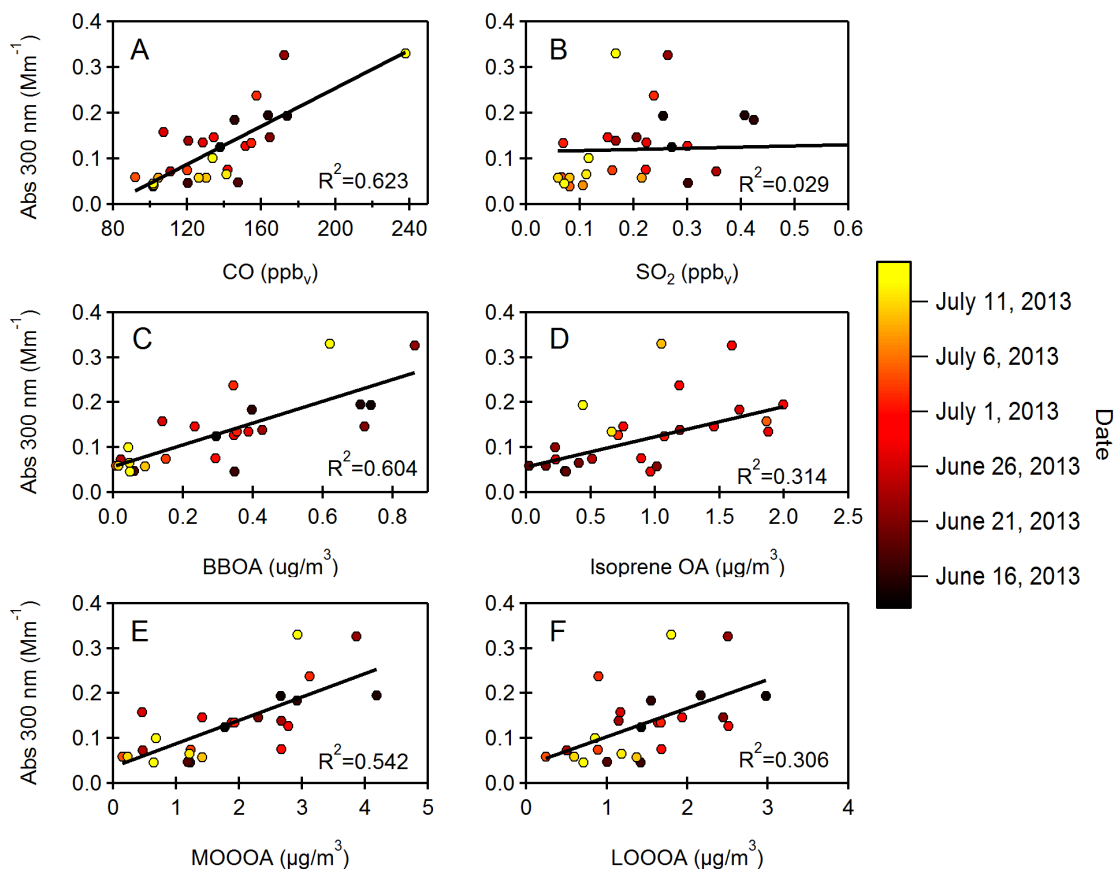


Figure 5-6: Correlation of BrC absorption as measured by SEC-UV to A) CO, B) SO₂, and organic aerosol fractions determined by PMF from AMS data in panels C-F. All points are colored by date.

weight BrC absorbers is combustion. The OA absorption measured by the PiLS-LWCC may be underrepresenting large molecular weight contributors.

We examined the correlation of SEC-UV absorbance with four AMS organic aerosol mass factors determined by positive matrix factorization, and found strongest correlation with biomass burning organic aerosol (BBOA; $r^2 = 0.604$), followed by more oxidized oxygenated organic aerosol (MOOOA; $r^2 = 0.542$). BBOA is partly indicated in the AMS using tracer ions of levoglucosan fragments (m/z 60, 73), a single, non-absorbing component of BB-derived particles³⁹⁻⁴¹. Although this may be a good indicator for BB-derived particles on the whole, it may not accurately represent absorbing components as levoglucosan has a relatively short atmospheric lifetime. MOOOA represents multi-origin, highly-aged species with O:C ratio of 0.8^{19,42}, which is expected of aged BB particles and has been previously observed^{43,44}. Not only would these particles be produced in a highly oxidizing environment, they will have had considerable time to oxidize in the atmosphere. Freshly emitted BB vapour and BBOA is expected to have a lower O:C ratio, but undergoes rapid oxidation with OH radicals, on the order of 6 h, to become highly oxidized⁴⁵. The other OA fractions represent either nighttime photochemical products of NO₃ oxidation of monoterpenes (LOOOA), or secondary organic aerosol (SOA) from isoprene oxidation^{23,41}, neither of which are known or expected to produce considerable amounts of light absorbing species.

5.4.4.2 Correlation of BrC with anthropogenic sources and total PM_{2.5}

Laboratory experiments have shown that processing of anthropogenically-derived SOA in high NO_x environments can lead to formation of coloured compounds, with spectral

characteristics similar to measured BrC¹⁰. In order to test whether this potential formation mechanism contributed to BrC formation at the SOAS site, our BrC absorption data was correlated with multiple markers of anthropogenic activity, such as SO₂, NO₂, and O₃ (Figure D-4). Poor correlation was observed with SO₂ and NO₂, suggesting anthropogenic activity is a minor contributor to formation of absorbing particulate species compared to combustion. Anthropogenic activity cannot be completely ruled out; however, as the MOOOA fraction may contain aged anthropogenic SOA. Although moderate correlation is seen with O₃, which is often used as a marker of anthropogenic activity, it has been observed at elevated levels in BB plumes and correlated with CO⁴⁶. Total PM_{2.5} mass shows moderate correlation with BrC, most likely because samples from the SOAS site represent well-mixed background aerosol. These poor correlations imply that SOA derived from anthropogenic activity is not a dominant contributor to these large molecular weight BrC species.

5.5 Conclusions

It is evident from multiple samples analyzed via the SOAS campaign and their comparison to concentrated BB plumes that combustion is the primary source of BrC in well-mixed, background aerosol. The molecular weight profile consistency of absorbing species across all sampling sites suggests BrC chemical composition is relatively constant. For BB-derived particles, this suggests chemical composition is independent of fuel type and burn conditions. It is the largest molecular weight fraction that comprises the bulk of BrC absorption and the contribution of the smaller molecular weight fraction to absorption decreases with plume age. The large molecular weight fraction, defined here as greater than

500 Da, would contain at least 20 to 30 carbons, whether the average carbon oxidation state was -2 or 1, respectively. According to the 2-D volatility basis set, these molecules would likely have a log saturation concentration ($\log_{10}C^{\circ}$) less than -5 and fall under the ELVOC category, even if they contained as few as 2 to 3 oxygens (Figure 5-7). Considering their water solubility, and the lack of chemical functionality defining BC, it is expected that these large absorbing BrC species are also highly oxidized. During aging, the entire BrC population is likely further oxidized, but it is seemingly the smallest components that rapidly lose their absorptive properties during this process. The BBOA species reported to undergo rapid oxidation by Donahue et al.⁴⁵ would correspond to molecules with molecular weights of approximately 250 Da, as observed when comparing fresh BB with aged BB and background samples above. Since the large molecular weight fraction of absorbing compounds is longer lived in the atmosphere, these are the species more likely to have long-term impacts on climate.

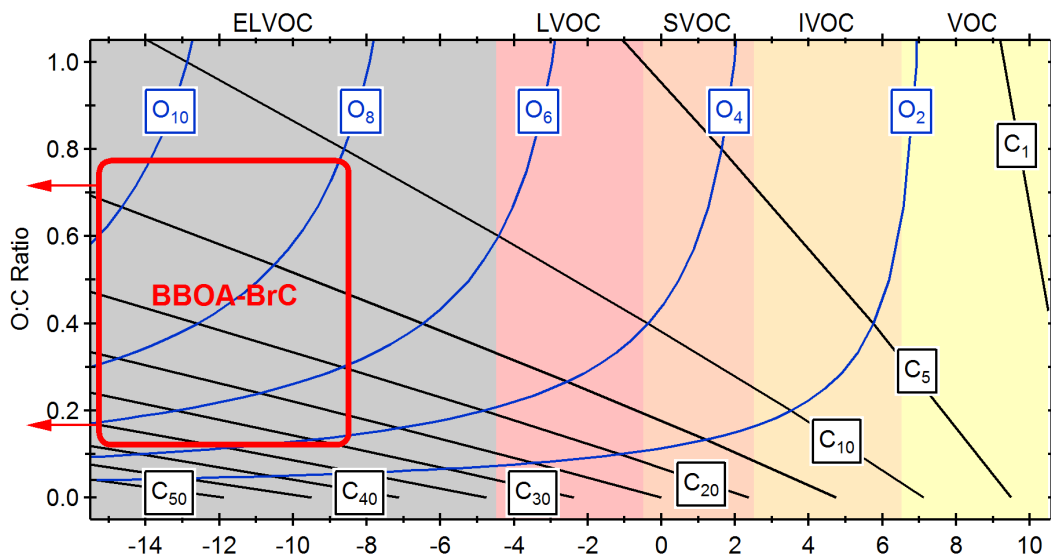


Figure 5-7: 2D Volatility Basis Set space based on Donahue et al.⁴⁹, highlighting in red the region likely occupied by the large molecular weight BrC species characterized in this study based on molecular weight and probable O:C ratios. Red arrows indicate that the lower end $\log_{10}(C^{\circ})$ for the largest molecules is likely lower than -14, based on the molecular weights calculated.

5.6 References

- (1) Myhre, G.; Shindell, D.; Bréon, F.-M.; Collins, W.; Fuglestvedt, J.; Huang, J.; Koch, D.; Lamarque, J.-F.; Lee, D.; Mendoza, B.; et al. Anthropogenic and Natural Radiative Forcing. In *Climate Change 2013: The Physical Science Basis. Contribution of Working Group I to the Fifth Assessment Report of the Intergovernmental Panel on Climate Change*; Stocker, T. F., Qin, D., Plattner, G.-K., Tignor, M., Allen, S. K., Boschung, J., Nauels, A., Xia, Y., Bex, V., Midgley, P. M., Eds.; Cambridge University Press: Cambridge, United Kingdom and New York, NY, USA, **2013**; Vol. AR5.
- (2) Kirchstetter, T. W.; Novakov, T.; Hobbs, P. V. Evidence that the spectral dependence of light absorption by aerosols is affected by organic carbon. *J. Geophys. Res. D Atmos.* **2004**, *109* (21), D21208.
- (3) Andreae, M. O.; Gelencsér, A. Black carbon or brown carbon? The nature of light-absorbing carbonaceous aerosols. *Atmos. Chem. Phys.* **2006**, *6* (10), 3131–3148.
- (4) Saleh, R.; Marks, M.; Heo, J.; Adams, P. J.; Donahue, N. M.; Robinson, A. L. Contribution of brown carbon and lensing to the direct radiative effect of carbonaceous aerosols from biomass and biofuel burning emissions. *J. Geophys. Res. Atmos.* **2015**, *120* (19), 10,285–10,296.
- (5) Kodros, J. K.; Scott, C. E.; Farina, S. C.; Lee, Y. H.; L'Orange, C.; Volckens, J.; Pierce, J. R. Uncertainties in global aerosols and climate effects due to biofuel emissions. *Atmos. Chem. Phys.* **2015**, *15* (15), 8577–8596.
- (6) Laskin, A.; Laskin, J.; Nizkorodov, S. A. Chemistry of atmospheric brown carbon. *Chem. Rev.* **2015**, *115* (10), 4335–4382.

- (7) Slikboer, S.; Grandy, L.; Blair, S. L.; Nizkorodov, S. a.; Smith, R. W.; Al-Abadleh, H. a. Formation of light absorbing soluble secondary organics and insoluble polymeric particles from the dark reaction of catechol and guaiacol with Fe(III). *Environ. Sci. Technol.* **2015**, No. Iii, 150615070810007.
- (8) Shapiro, E. L.; Szprengiel, J.; Sareen, N.; Jen, C. N.; Giordano, M. R.; McNeill, V. F. Light-absorbing secondary organic material formed by glyoxal in aqueous aerosol mimics. *Atmos. Chem. Phys.* **2009**, *9* (7), 2289–2300.
- (9) Lee, A. K. Y.; Zhao, R.; Li, R.; Liggio, J.; Li, S. M.; Abbatt, J. P. D. Formation of light absorbing organo-nitrogen species from evaporation of droplets containing glyoxal and ammonium sulfate. *Environ. Sci. Technol.* **2013**, *47* (22), 12819–12826.
- (10) Lin, P.; Liu, J.; Shilling, J. E.; Kathmann, S. M.; Laskin, J.; Laskin, A. Molecular characterization of brown carbon (BrC) chromophores in secondary organic aerosol generated from photo-oxidation of toluene. *Phys. Chem. Chem. Phys.* **2015**, *17* (36), 23312–23325.
- (11) Iinuma, Y.; Böge, O.; Gräfe, R.; Herrmann, H. Methyl-nitrocatechols: atmospheric tracer compounds for biomass burning secondary organic aerosols. *Environ. Sci. Technol.* **2010**, *44* (22), 8453–8459.
- (12) Bond, T. C.; Bergstrom, R. W. Light Absorption by Carbonaceous Particles: An Investigative Review. *Aerosol Sci. Technol.* **2006**, *40* (1), 27–67.
- (13) Yang, M.; Howell, S. G.; Zhuang, J.; Huebert, B. J. Attribution of aerosol light absorption to black carbon, brown carbon, and dust in China – interpretations of atmospheric measurements during EAST-AIRE. *Atmos. Chem. Phys. Discuss.* **2008**, *8* (3), 10913–10954.

- (14) Favez, O.; Alfaro, S. C.; Sciare, J.; Cachier, H.; Abdelwahab, M. M. Ambient measurements of light-absorption by agricultural waste burning organic aerosols. *J. Aerosol Sci.* **2009**, *40* (7), 613–620.
- (15) Hecobian, A.; Zhang, X.; Zheng, M.; Frank, N.; Edgerton, E. S.; Weber, R. J. Water-Soluble Organic Aerosol material and the light-absorption characteristics of aqueous extracts measured over the Southeastern United States. *Atmos. Chem. Phys.* **2010**, *10* (13), 5965–5977.
- (16) Di Lorenzo, R. A.; Young, C. J. Size separation method for absorption characterization in brown carbon: Application to an aged biomass burning sample. *Geophys. Res. Lett.* **2016**, *43* (1), 458–465.
- (17) Saleh, R.; Robinson, E. S.; Tkacik, D. S.; Ahern, A. T.; Liu, S.; Aiken, A. C.; Sullivan, R. C.; Presto, A. a.; Dubey, M. K.; Yokelson, R. J.; et al. Brownness of organics in aerosols from biomass burning linked to their black carbon content. *Nat. Geosci.* **2014**, *7* (9), 647–650.
- (18) Zhang, X.; Lin, Y. H.; Surratt, J. D.; Zotter, P.; Prévôt, A. S. H.; Weber, R. J. Light-absorbing soluble organic aerosol in Los Angeles and Atlanta: A contrast in secondary organic aerosol. *Geophys. Res. Lett.* **2011**, *38* (21), 2–5.
- (19) Washenfelder, R. A.; Attwood, A. R.; Brock, C. A.; Guo, H.; Xu, L.; Weber, R. J.; Ng, N. L.; Allen, H. M.; Ayres, B. R.; Baumann, K.; et al. Biomass burning dominates brown carbon absorption in the rural southeastern United States. *Geophys. Res. Lett.* **2015**, *42*, 653–664.
- (20) Lack, D. A.; Langridge, J. M.; Bahreini, R.; Cappa, C. D.; Middlebrook, A. M.; Schwarz, J. P. Brown carbon and internal mixing in biomass burning particles. *Proc.*

Natl. Acad. Sci. **2012**, *109* (37), 14802–14807.

- (21) Forrister, H.; Liu, J.; Scheuer, E.; Dibb, J.; Ziemba, L.; Thornhill, K. L.; Anderson, B.; Diskin, G.; Perring, A. E.; Schwarz, J. P.; et al. Evolution of brown carbon in wildfire plumes. *Geophys. Res. Lett.* **2015**, *42* (11), 4623–4630.
- (22) Liu, J.; Scheuer, E.; Dibb, J.; Diskin, G. S.; Ziemba, L. D.; Thornhill, K. L.; Anderson, B. E.; Wisthaler, A.; Mikoviny, T.; Devi, J. J.; et al. Brown carbon aerosol in the North American continental troposphere: Sources, abundance, and radiative forcing. *Atmos. Chem. Phys.* **2015**, *15* (14), 7841–7858.
- (23) Xu, L.; Suresh, S.; Guo, H.; Weber, R. J.; Ng, N. L. Aerosol characterization over the southeastern United States using high-resolution aerosol mass spectrometry: Spatial and seasonal variation of aerosol composition and sources with a focus on organic nitrates. *Atmos. Chem. Phys.* **2015**, *15* (13), 7307–7336.
- (24) Guenther, A. B.; Jiang, X.; Heald, C. L.; Sakulyanontvittaya, T.; Duhl, T.; Emmons, L. K.; Wang, X. The model of emissions of gases and aerosols from nature version 2.1 (MEGAN2.1): An extended and updated framework for modeling biogenic emissions. *Geosci. Model Dev.* **2012**, *5* (6), 1471–1492.
- (25) Washenfelder, R. A.; Flores, J. M.; Brock, C. A.; Brown, S. S.; Rudich, Y. Broadband measurements of aerosol extinction in the ultraviolet spectral region. *Atmos. Meas. Tech.* **2013**, *6* (4), 861–877.
- (26) Timko, M. T.; Yu, Z.; Kroll, J.; Jayne, J. T.; Worsnop, D. R.; Miake-Lye, R. C.; Onasch, T. B.; Liscinsky, D.; Kirchstetter, T. W.; Destailhats, H.; et al. Sampling Artifacts from Conductive Silicone Tubing. *Aerosol Sci. Technol.* **2009**, *43* (9), 855–865.

- (27) Yu, Y.; Liz Alexander, M.; Perraud, V.; Bruns, E. A.; Johnson, S. N.; Ezell, M. J.; Finlayson-Pitts, B. J. Contamination from electrically conductive silicone tubing during aerosol chemical analysis. *Atmos. Environ.* **2009**, *43* (17), 2836–2839.
- (28) Cai, D.; Neyer, A.; Kuckuk, R.; Heise, H. M. Raman, mid-infrared, near-infrared and ultraviolet-visible spectroscopy of PDMS silicone rubber for characterization of polymer optical waveguide materials. *J. Mol. Struct.* **2010**, *976* (1–3), 274–281.
- (29) Rumsey, I. C.; Cowen, K. A.; Walker, J. T.; Kelly, T. J.; Hanft, E. A.; Mishoe, K.; Rogers, C.; Proost, R.; Beachley, G. M.; Lear, G.; et al. An assessment of the performance of the Monitor for AeRosols and GAses in ambient air (MARGA): A semi-continuous method for soluble compounds. *Atmos. Chem. Phys.* **2014**, *14* (11), 5639–5658.
- (30) DeCarlo, P. F.; Kimmel, J. R.; Trimborn, A.; Northway, M. J.; Jayne, J. T.; Aiken, A. C.; Gonin, M.; Fuhrer, K.; Horvath, T.; Docherty, K. S.; et al. Field-deployable, high-resolution, time-of-flight aerosol mass spectrometer. *Anal. Chem.* **2006**, *78* (24), 8281–8289.
- (31) Petzold, A.; Kramer, H.; Schönlinner, M. Continuous Measurement of Atmospheric Black Carbon Using a Multi-angle Absorption Photometer. *Environ. Sci. Pollut. Res. Int.* **2002**, *4* (4), 78–82.
- (32) Stein, A. F.; Draxler, R. R.; Rolph, G. D.; Stunder, B. J. B.; Cohen, M. D.; Ngan, F. NOAA's hysplit atmospheric transport and dispersion modeling system. *Bull. Am. Meteorol. Soc.* **2015**, *96* (12), 2059–2077.
- (33) Hobbs, P. V. Evolution of gases and particles from a savanna fire in South Africa. *J. Geophys. Res.* **2003**, *108* (D13), 8485.

- (34) Zhao, R.; Lee, A. K. Y.; Huang, L.; Li, X.; Yang, F.; Abbatt, J. P. D. Photochemical processing of aqueous atmospheric brown carbon. *Atmos. Chem. Phys.* **2015**, *15* (11), 6087–6100.
- (35) Vakkari, V.; Kerminen, V. M.; Beukes, J. P.; Tiitta, P.; Van Zyl, P. G.; Josipovic, M.; Venter, A. D.; Jaars, K.; Worsnop, D. R.; Kulmala, M.; et al. Rapid changes in biomass burning aerosols by atmospheric oxidation. *Geophys. Res. Lett.* **2014**, *41*, 2644–2651.
- (36) Sullivan, A. P.; Weber, R. J.; Clements, A. L.; Turner, J. R.; Bae, M. S.; Schauer, J. J. A method for on-line measurement of water-soluble organic carbon in ambient aerosol particles: Results from an urban site. *Geophys. Res. Lett.* **2004**, *31* (13), n/a-n/a.
- (37) Chen, Y.; Bond, T. C. Light absorption by organic carbon from wood combustion. *Atmos. Chem. Phys. Discuss.* **2009**, *9* (5), 20471–20513.
- (38) Zhang, X.; Lin, Y. H.; Surratt, J. D.; Weber, R. J. Sources, composition and absorption Ångström exponent of light-absorbing organic components in aerosol extracts from the Los Angeles basin. *Environ. Sci. Technol.* **2013**, *47* (8), 3685–3693.
- (39) Alfarra, M. R.; Prevot, A. S. H.; Szidat, S.; Sandradewi, J.; Lanz, V. a; Schreiber, D.; Mohr, M.; Baltensperger, U. Identification of the Mass Spectral Signature of Organic Aerosols from Wood Burning Emissions Identification of the Mass Spectral Signature of Organic Aerosols from Wood Burning Emissions. *Environ. Sci. Technol.* **2007**, *41* (16), 5770–5777.
- (40) Shrivastava, M. K.; Subramanian, R.; Rogge, W. F.; Robinson, A. L. Sources of

- organic aerosol: Positive matrix factorization of molecular marker data and comparison of results from different source apportionment models. *Atmos. Environ.* **2007**, *41* (40), 9353–9369.
- (41) Xu, L.; Guo, H.; Boyd, C. M.; Klein, M.; Bougiatioti, A.; Cerully, K. M.; Hite, J. R.; Isaacman-VanWertz, G.; Kreisberg, N. M.; Knote, C.; et al. Effects of anthropogenic emissions on aerosol formation from isoprene and monoterpenes in the southeastern United States. *Proc. Natl. Acad. Sci.* **2015**, *112* (1), 37–42.
- (42) Ulbrich, I. M.; Canagaratna, M. R.; Zhang, Q.; Worsnop, D. R.; Jimenez, J. L. Interpretation of Organic Components from Positive Matrix Factorization of Aerosol Mass Spectrometric Data. *Atmos. Chem. Phys.* **2009**, *9*, 2891.
- (43) Xu, L.; Williams, L. R.; Young, D. E.; Allan, J. D.; Coe, H.; Massoli, P.; Fortner, E.; Chhabra, P.; Herndon, S.; Brooks, W. A.; et al. Wintertime aerosol chemical composition, volatility, and spatial variability in the greater London area. *Atmos. Chem. Phys.* **2016**, *16*, 1139–1160.
- (44) Bougiatioti, A.; Stavroulas, I.; Kostenidou, E.; Zarmas, P.; Theodosi, C.; Kouvarakis, G.; Canonaco, F.; Prevot, A. S. H.; Nenes, A.; Mihalopolous, N. Processing of biomass-burning aerosol in the eastern Mediterranean during summertime. *Atmos. Chem. Phys.* **2014**, *14*, 4793–4807.
- (45) Donahue, N. M.; Kroll, J. H.; Pandis, S. N.; Robinson, A. L. A two-dimensional volatility basis set – Part 2: Diagnostics of organic-aerosol evolution. *Atmos. Chem. Phys.* **2012**, *12* (2), 615–634.
- (46) Lin, Y. C.; Lin, C. Y.; Lin, P. H.; Engling, G.; Lin, Y. C.; Lan, Y. Y.; June Chang, C. W.; Kuo, T. H.; Hsu, W. T.; Ting, C. C. Influence of Southeast Asian biomass

burning on ozone and carbon monoxide over subtropical Taiwan. *Atmos. Environ.*

2013, *64* (x), 358–365.

6 Conclusions

This work represents a comprehensive analytical approach to the characterization of brown carbon (BrC). Although the techniques used herein themselves are not novel to the analytical community, in conjunction the work represents a novel approach to the analysis of atmospheric particulate matter. This thesis describes the first combination of size exclusion chromatography (SEC) and UV-vis absorption spectrophotometry as an analytical tool to characterize light-absorbing organic species in atmospheric particles. This method has unambiguously shown that the majority of BrC in atmospheric aerosols to be primarily derived from biomass burning (BB) and is primarily composed of extremely low volatility organic compounds (ELVOCs) of large molecular weight origin. Compounds up to 10 000 Da were identified in using this method, species much larger than previously thought to be contained in this category of atmospheric organics. The use of size exclusion chromatography (SEC) has been shown not only to yield information into the molecular weight of absorbing species, but acts as an orthogonal molecular weight distribution tool to that of mass spectrometry (MS). Coupling these two techniques together has shown that MS greatly underestimates molecular weight distributions of BB aerosol in comparison to SEC analyses; whether this is due to fragmentation or selective ionization is worthy of further study.

This work has also shown that BB derived aerosols contain a highly complex mixture of organic compounds, with thousands of identifiable individual molecular formulae being assigned using ultra-high resolution mass spectrometric (UHRMS) techniques. The prevailing trend in the literature to simply use electrospray ionization (ESI) in negative

mode to characterize the entirety of the sample is shown to be insufficient, particularly when attempting to characterize the light absorbing organic species present in the mixture. Atmospheric pressure photo ionization (APPI) represents a very useful technique for the molecular characterization of BrC, as it selects for compounds that absorb light. Future work using this ionization technique coupled to an UHRMS-capable instrument can potentially yield the identification of BrC species not previously identified in literature. Comparisons between APPI and ESI spectra of a BrC-rich sample could yield information into the types of functionality that cause the absorptivity in these species. Although individual structural identification was beyond the scope of this work, it is expected that the structural motifs of BB-derived organics would be similar to the fuel sources (lignin, cellulose), although with less regular connectivity than the highly ordered biopolymers. Due to the prevalent use of anhydrosugars and methoxyphenols as molecular markers for BB in the literature, it is expected that the BB-derived BrC would contain a large number of aromatic and glycan ring structures, with conjugated unsaturation that enhances light-absorptivity. The inclusion nitrogen is expected in the form of pyrrole-type structures, due to their role producing light-absorbing organics in soil. Further, in depth tandem MS analysis could yield further information into the molecular connectivity and monomeric components of these species, rather than relying on Van Krevelen diagrams for structural identification. It is expected that the tandem MS spectra would be similar to the DIP-EI spectra acquired, and similar in composition to most of the hard ionization sources used in field-deployed aerosol mass spectrometers.

The molecular weight distribution of absorbing species has been shown to be remarkably similar between multiple forest fire samples as well as in regional background

aerosol of suspected BB origin. Size resolved BB samples showed that BrC absorption as measured by SEC with UV-vis spectrophotometry arose entirely in submicron aerosols. The particle size distribution of common BB markers, such as levoglucosan, acetate and potassium, were shown to have different size distributions suggesting that these species are externally mixed with BrC chromophores. For this reason, these markers should not be used to infer BrC concentrations. Ammonium and dialkyl ammonium species size distributions were, however, highly correlated with BrC absorption. Unfortunately, due to the fact that these ammonium species have multiple origins, specifically from agriculture and ocean biology, and that the collected aerosol was transported over the open ocean and potential farmland, it is uncertain whether these species have a role in BrC formation during BB, that they preferentially partition into BrC containing particles, or that they are externally mixed with a remarkably similar size distribution. It is expected that, due to the productive ocean biota at the time of sample collection, that the amine sources are marine-derived. Further characterization of amines contained within additional BB samples which have little or no ocean interaction would yield more conclusive source apportionment of the amines. Interestingly, however, this is the first known observance of high concentrations of diethyl ammonium in particles, greater than both ammonium and dimethyl ammonium. This alone warrants further study of the interaction of amines and BB aerosol, regardless of their source.

Using these newly developed chromatographic techniques, characterization of many more field and laboratory generated samples is necessary. It would be interesting to use this technique on secondary organic aerosol (SOA)-derived BrC to determine whether the species produced during that process are similar to those produced during BB events. The

fact that it is these large molecules that remain after days of atmospheric transport and oxidation, where smaller molecules rapidly oxidize and lose their absorptive properties, gives credit to the fact that ELVOC-BrC are climactically relevant species worthy of further characterization to improve their use in radiative forcing models.

Appendix A Supporting Information for Chapter 2

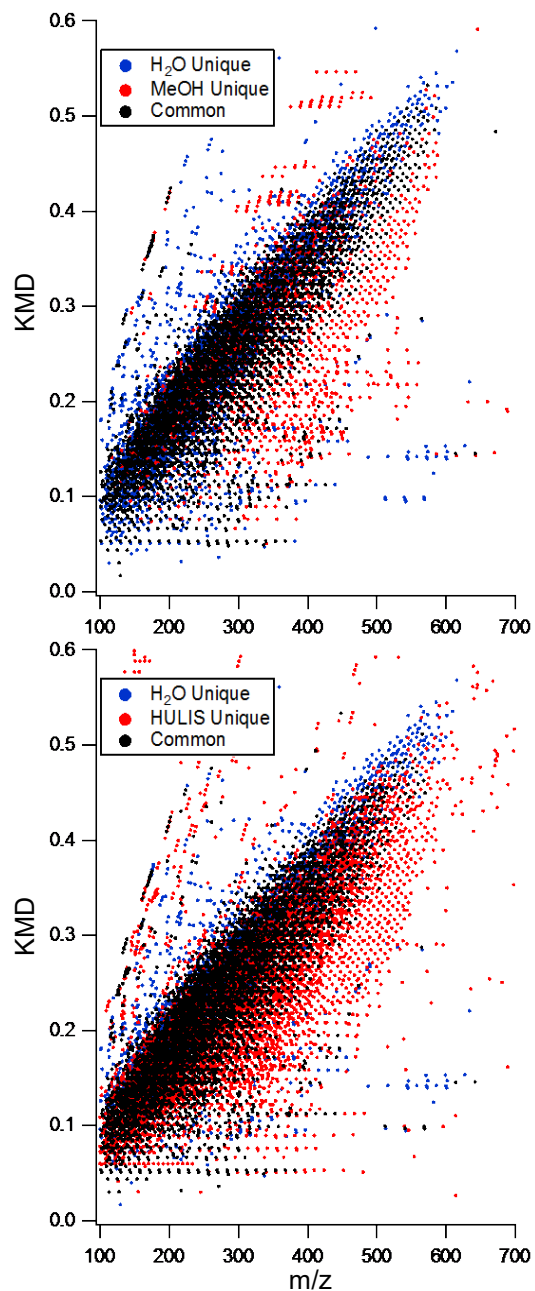


Figure A-1: Kendrick Mass Defect plot comparison between aqueous extracts, in blue dots and (top) methanolic and (bottom) HULIS extracts, in red dots as analyzed using electrospray ionization in negative mode. Common peaks between extracts are represented in black dots.

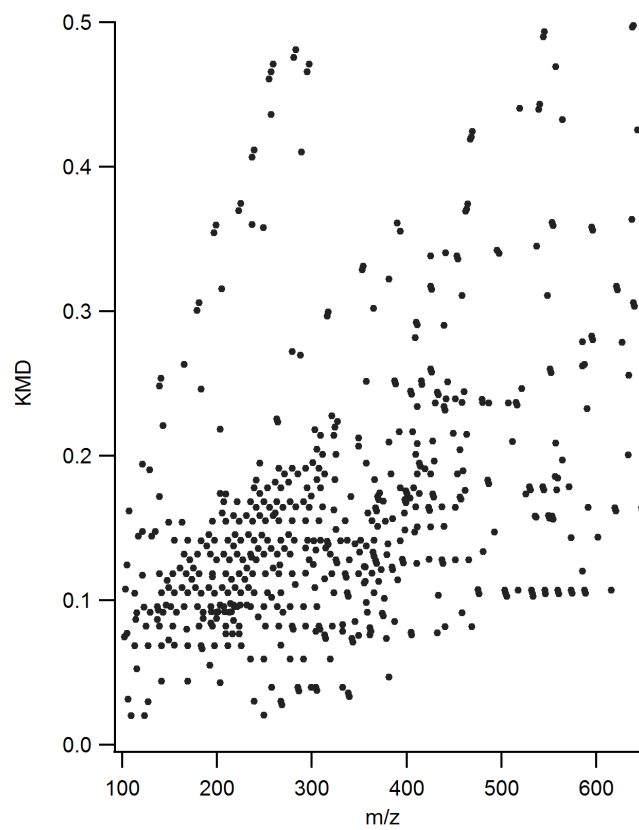


Figure A-2: Kendrick Mass Defect plot of humic acids as analyzed using electrospray ionization in positive mode.

Appendix B Supporting Information for Chapter 3

B.1 Size Exclusion Chromatography Molecular Weight Calibration

In order to estimate the molecular weight distribution of the measured samples, the Polysep GFC P-3000 column was internally calibrated against a Polysep GFC P-2000 column (molecular weight range = 10 000 – 100 Da, Phenomenex, Torrance, Ca, USA), using the known exclusion and void volumes where appropriate.

Figure B-1 shows chromatograms representing the size separation of an aqueous biomass burning aerosol and Suwanee River Humic Acid extracts as measured by the Polysep GFC P-2000 column. The new peak observed in both chromatograms at roughly 5.3 minutes represents the void volume of the column, or where compounds above the maximum molecular weight limit (>10 000 Da on the GFC P-2000 column) will elute together. The peak at 8.2 minutes observed in both chromatograms represents the exclusion volume of the column, or where compounds below the minimum molecular weight limit (<100 Da on the GFC P-2000 column) will elute together. Since SEC columns have a negative log-linear relationship between molecular weight and retention time within their void and exclusion volumes, we can estimate that maxima A, B, and C in the BMB represent 2750 Da, 1900 Da and 900 Da respectively, and maximum A in the SRHA represents approximately 4500 Da. We can then use these molecular weights along with its exclusion volume to internally calibrate the GFC-P3000 column. Our results for the SRHA are consistent with literature values, thus we are confident in the accuracy of this calibration method.

B.2 Total Organic Carbon Analysis

Quartz fiber filters were subsampled with a 10 mm arch punch identically to those for SEC and RP-HPLC analyses. Subsamples (one 3/8" punch) was placed in a pre-muffled 40 mL amber vial where 30.00 mL of NanoUV water (Barnstead Infinity Ultrapure Water System, Thermo Scientific, Waltham, MA, USA) was added. Extraction was performed by sonication for 40 minutes. A 15.00 mL aliquot was placed in a pre-muffled 24 mL glass vial for analysis.

Samples were analyzed using a total carbon analyzer (TOC-VCHS, Shimadzu, Kyoto, Japan). An ASI-V autosampler was used to inject the samples into the TOC interface. A calibration curve was generated through a series of auto dilutions from a 10ppm stock solution of potassium hydrogen phthalate (KHP, Fisher Scientific) using the TOC Control-V software. NanoUV water samples were run to assess the concentrations of dissolved organics in the water and 5ppm check standards of KHP were run every 10 samples to assess the variability in the TOC measurements.

Total organic concentrations were measured to be $0.521 \pm .002$ mg/L in the sample vial. This would correspond to 15.6 μ g of organic carbon per subsample.

B.3 MOUDI Analysis

Size-resolved aerosol samples were also collected with 13-stage cascade impactor (nanoMOUDI II, model 122-R, MSP Corp., Shoreview, MN, USA) on pre-muffled (500 °C, 4 h) aluminum substrates. Substrates were sub-sampled using into 10% "pie slices". Each subsample was placed in a pre-muffled 2 mL glass vial where 750 μ L of NanoUV water (Barnstead Infinity Ultrapure Water System, Thermo Scientific, Waltham, MA,

USA) was added. Vials were sealed with Teflon-lined caps, wrapped in parafilm, and sonicated for 40 min at room temperature. After sonication, extracts were filtered with 0.2 μm PTFE syringe filters (Iso-Disc, Supelco, Bellefonte, PA, USA), transferred to pre-muffled glass sample vials. Samples were stored at 4 $^{\circ}\text{C}$ until analysis.

SEC-UV absorption density measurements were acquired using an HPLC system (1260 Infinity, Agilent Technologies, Santa Clara, CA, USA) coupled to a diode array detector (1260, Agilent Technologies, Santa Clara, CA, USA). Separations were performed using an aqueous gel filtration column (molecular weight range = 75 000 - 250 Da, Polysep GFC P-3000, Phenomenex, Torrance, CA, USA). Isocratic elutions were performed at a flow rate of 1 mL/min using a water with an ammonium acetate concentration of 25 mM.

Figure B-4 below shows an absorption density plot of stage 6 of the MOUDI samples, which corresponds to particles between 0.56 and 1 μm in diameter. Note the similarity in molecular weight distribution to the PM_{2.5} samples described in the main manuscript. This molecular weight distribution was consistent across all MOUDI stages.

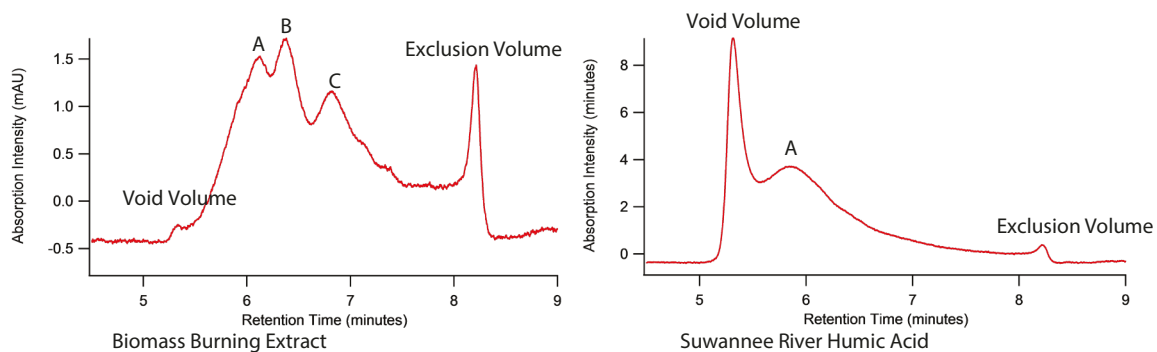


Figure B-1: Calibration of size exclusion chromatography molecular weight distributions using Polysep GFC P-2000 column.

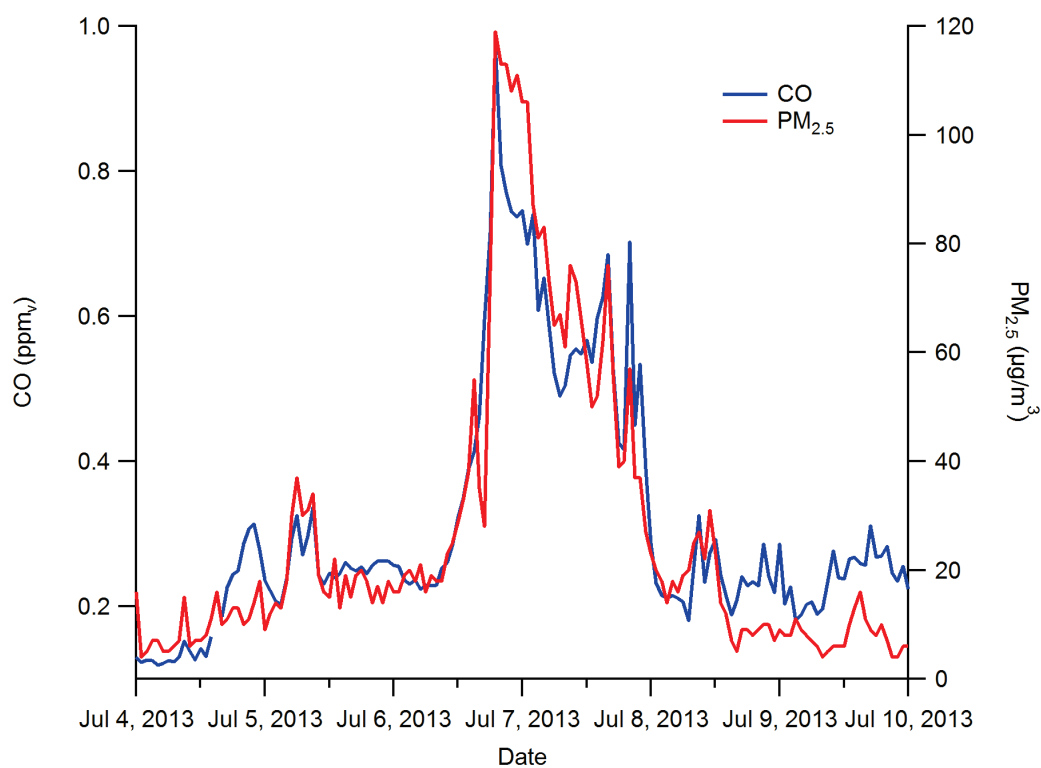


Figure B-2: Real-time PM_{2.5} and CO measurements from St. John's monitoring site. Measurements were averaged to an hourly time base. The average PM_{2.5} concentration during the sampling period was 78.6 µg/m³, where background PM_{2.5} concentrations were 5.7 µg/m³ from June 1 to August 31, 2013.

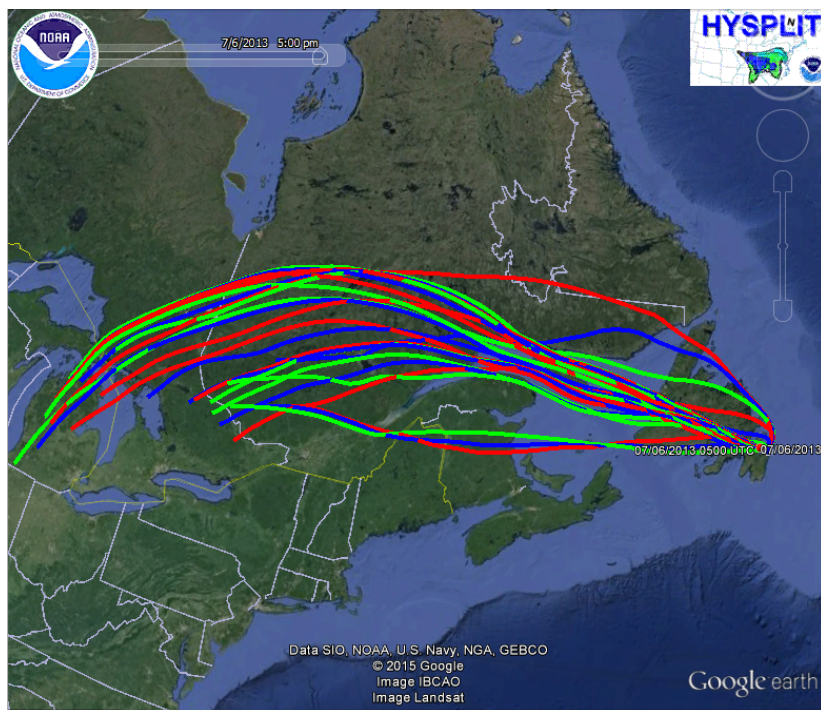


Figure B-3: 48h air mass back-trajectories from July 6, 2013 in St. John's, NL as computed using the Hybrid Single Particle Lagrangian Integrated Trajectory Model (HYSPLIT).

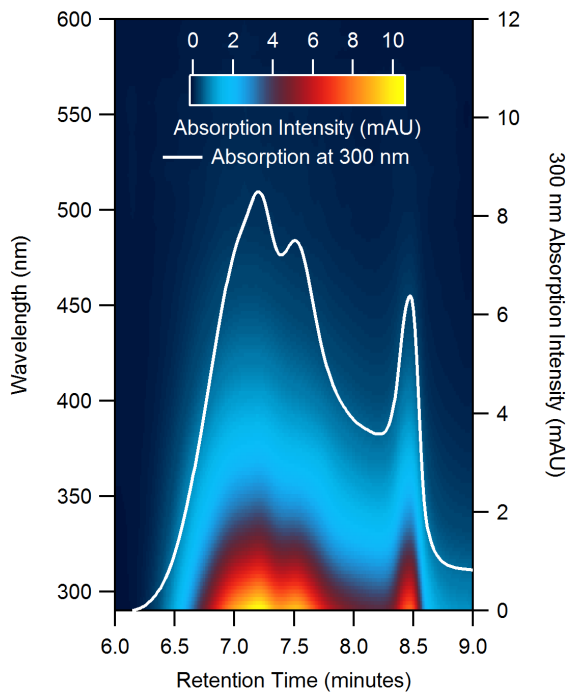


Figure B-4: Absorption density plot of an aqueous extract of BMB aerosols collected on stage 6 ($0.56 < D_p < 1 \mu\text{m}$) of the nanoMOUDI. Overlaid is the absorption at 300 nm to highlight the molecular weight distribution of absorbing species.

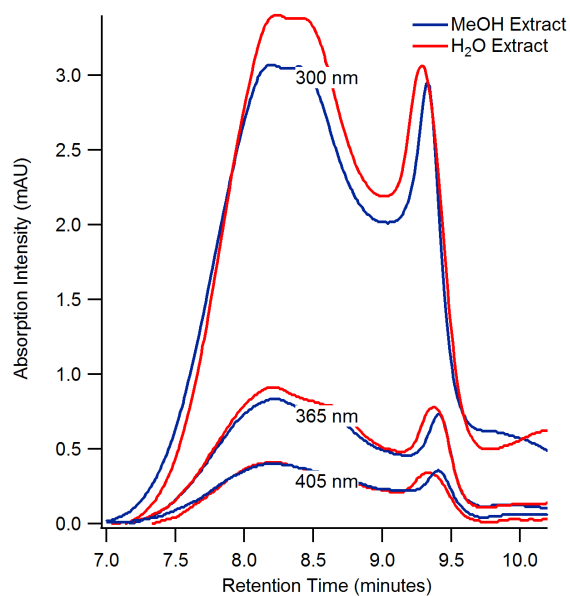


Figure B-5: SEC-UV chromatograms at 300, 365 and 405 nm of water and methanol PM2.5 extracts highlighting their similarity in the quantity of light absorption and molecular weight distribution. No statistical difference in the integrated quantity of light absorption at 300, 365, and 405 nm was found ($P < 0.46$).

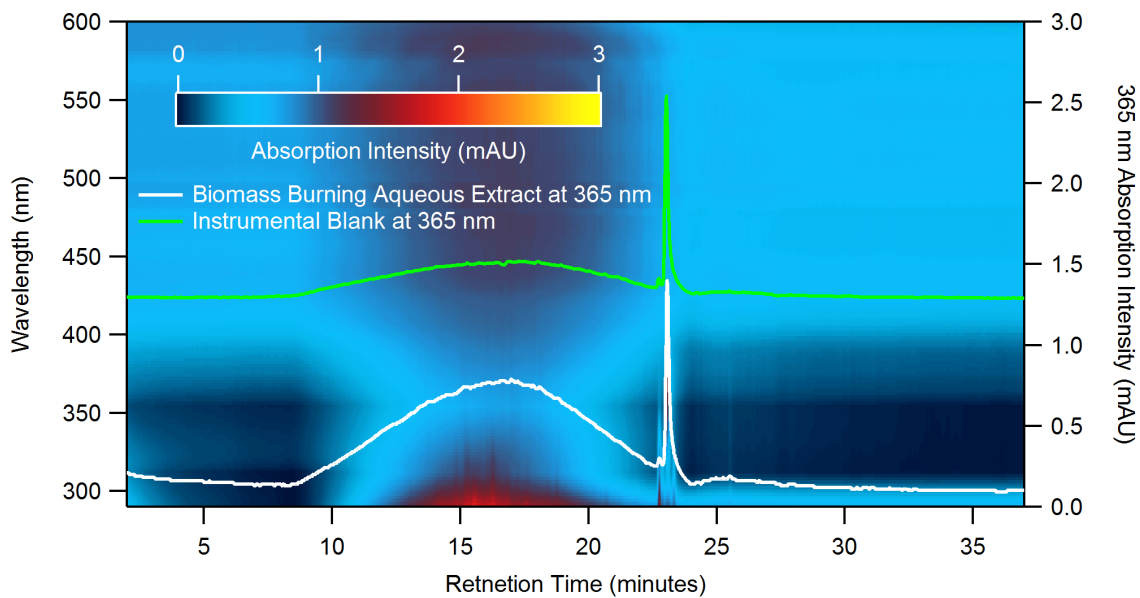


Figure B-6: Absorption density of an aqueous extract of BMB aerosols as measured by RP-HPLC-UV. Overlaid is the absorption at 365 nm to highlight the unresolved absorption feature. The absorption at 23 minutes is an instrumental artifact.

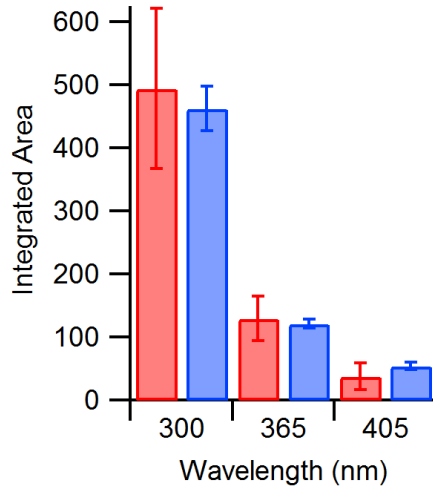


Figure B-7: Total absorption comparison as measured by total integrated area between SEC-UV and RP-HPLC-UV analyses. Error bars indicate the standard deviation of multiple integrations. Red bars represent absorption measured by RP-HPLC. Blue bars represent absorption measured by SEC.

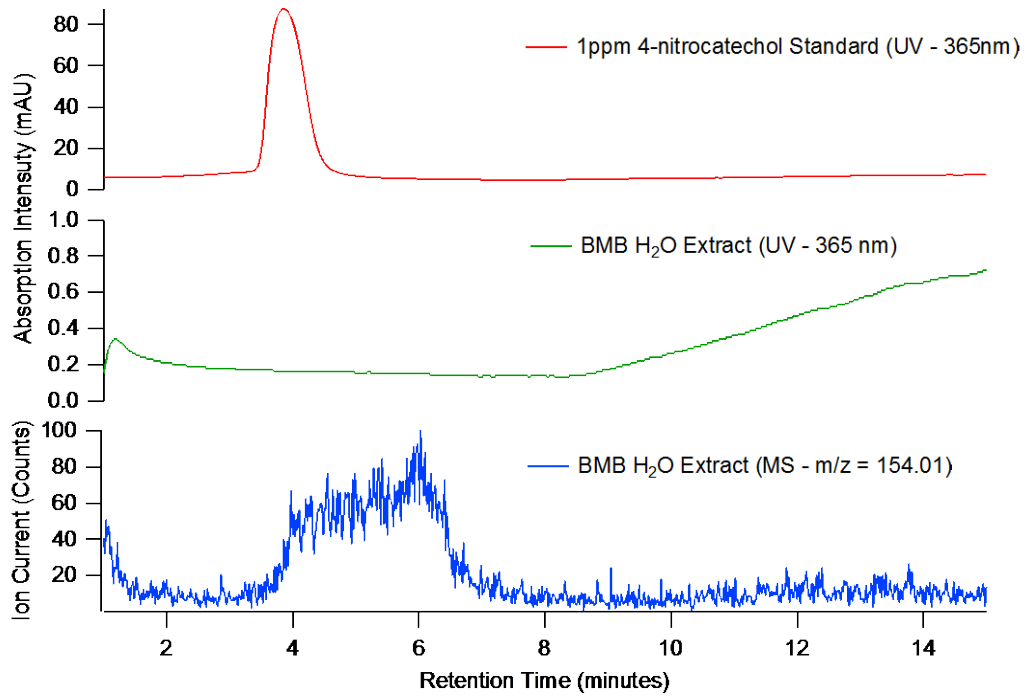


Figure B-8: Top Panel – RP-HPLC chromatogram of a 1ppm 4-nitrocatechol standard measured at 365 nm. Middle Panel – RP-HPLC chromatogram of an aqueous extract of a BMB aerosol sample measured at 365 nm with no evidence of absorption from 4-nitrocatechol. Bottom Panel – Extracted ion chromatogram at $m/z = 154.01$ (representing the $[M-H]^-$ ion for 4-nitrocatechol) as measured by RP-HPLC with ESI- detection. Although there is an increase in signal near the expected elution time of 4-nitrocatechol, the peak shape is not representative and the intensity is very low.

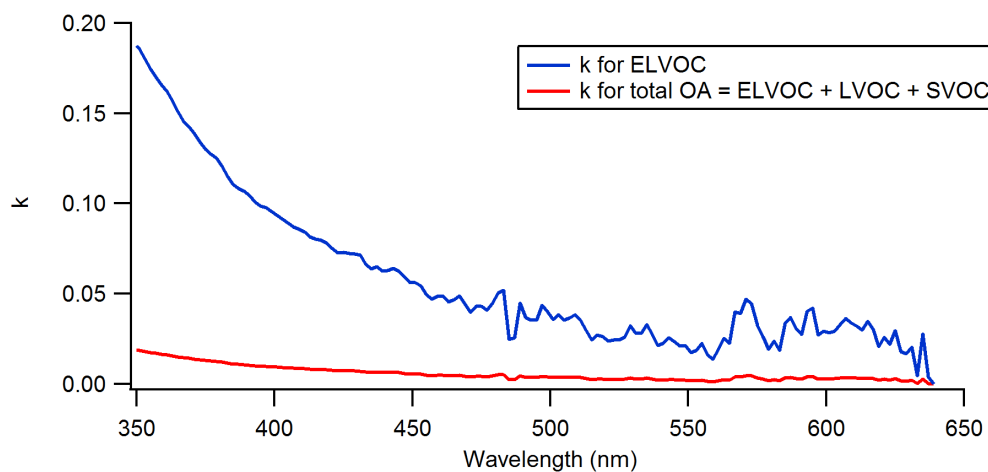


Figure B-9: Range of k values as a function of wavelength for total OA (ELVOCs, LVOCs and SVOCs) and ELVOCs only, assuming ELVOCs are 10% of total particle mass.

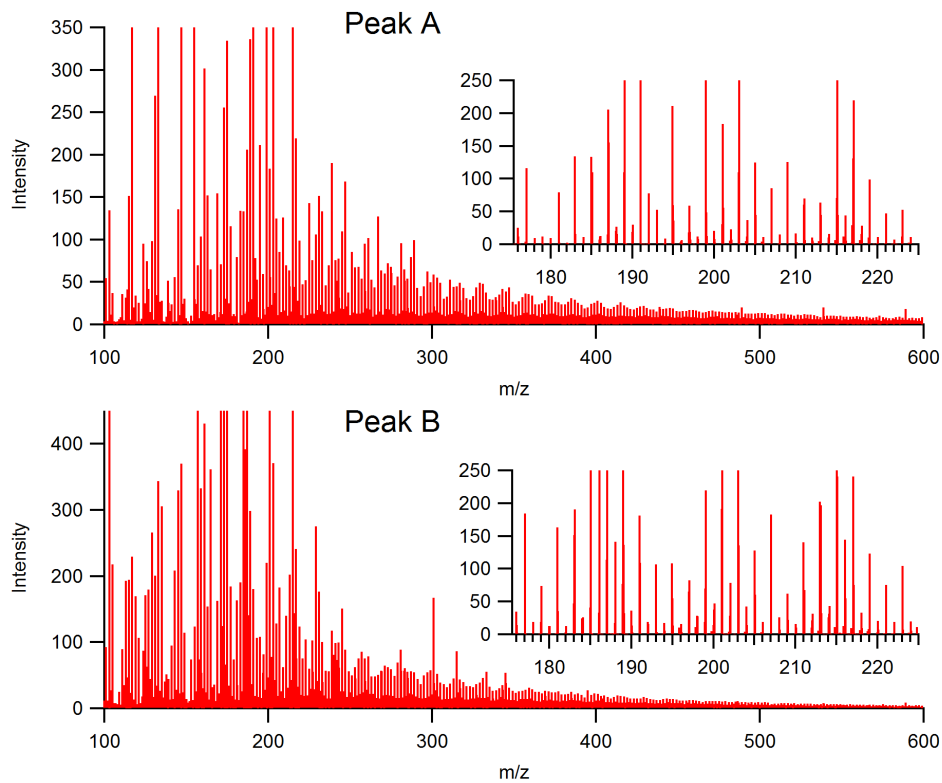


Figure B-10: Summed mass spectra under peaks A and B from SEC-MS TICs. Inset spectra show ion clusters and ^{13}C isotope peaks are separated by 1 m/z , thus it can be assumed that the majority of ions are singly charged.

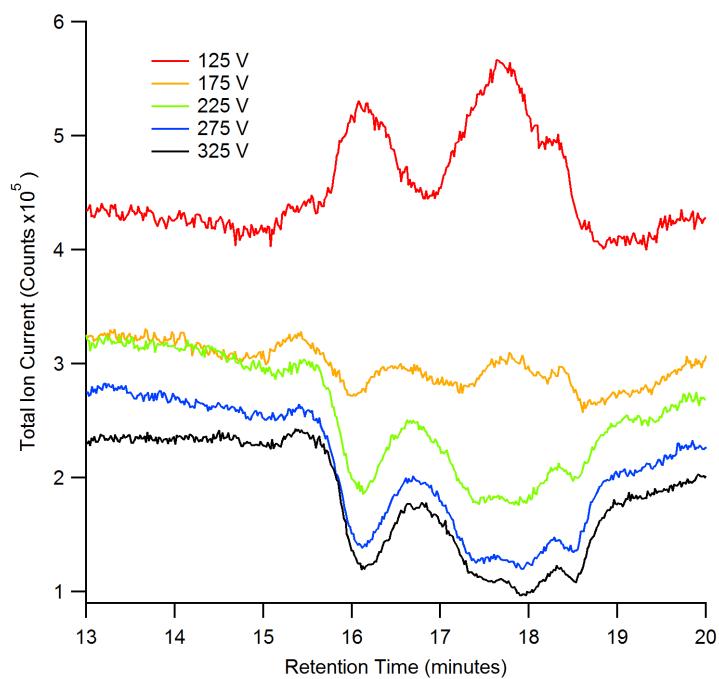


Figure B-11: SEC-MS chromatograms at cone voltages ranging from 125 to 325 V. As cone voltage is increased, the absolute intensity decreases resulting in negative peaks during the elution of absorbing species from the column

Appendix C Supporting Information for Chapter 4

C.1 Conversion of peak areas to absorption coefficients

Chromatographic analysis with a UVvis spectrophotometer gives absorbance A , in a unitless value denoted AU, as a function of time where:

$$A = -\log(I/I_0) \quad (1)$$

Using Beer Lambert Law, one must first account for the effect of dilution of the sample during chromatographic analysis. Where the pathlength and molar absorptivity and the number of moles of the measured species is constant, the relationship between the absorbance of the sample extract, A_{λ_E} , and the average absorbance across a peak, $\overline{A_{\lambda_p}}$, is a function of the injection volume, V_i , and the total volume across the peak, V_p , as follows:

$$\begin{aligned} A_{\lambda} &= \varepsilon_{\lambda} l c \\ A_{\lambda_E} &= \varepsilon_{\lambda} l c_E \quad \overline{A_{\lambda_p}} = \varepsilon_{\lambda} l \overline{c_p} \\ \therefore c &= \frac{n}{V} \\ A_{\lambda_E} &= \varepsilon_{\lambda} l \frac{n}{V_i} \quad \overline{A_{\lambda_p}} = \varepsilon_{\lambda} l \frac{n}{V_p} \\ \boxed{A_{\lambda_E} &= \frac{\overline{A_{\lambda_p}} V_p}{V_i}} \quad (2) \end{aligned}$$

The chromatographic peak area, a_p in units of AU·min, is equivalent to the average absorbance across the peak multiplied by the peak width, w_p in minutes. The peak width can be converted to a peak volume using the mobile phase flow rate, r_f in mL·min⁻¹. In this way, one can directly relate the peak area to the absorbance of the sample extract:

$$\begin{aligned}
&\because a_p = \overline{A_{\lambda_p}} w_p \\
&\because w_p = \frac{V_p}{r_f} \\
&a_p \cdot r_f = \overline{A_{\lambda_p}} V_p \\
&\boxed{A_{\lambda_E} = \frac{a_p \cdot r_f}{V_i}} \quad (3)
\end{aligned}$$

One can then use the equation in Hecobian et al. (2010) to calculate the absorption coefficient, Abs_{λ} , where V_l is the volume of liquid used to extract the sample filter, V_a is the volume of air sampled through the filter and l is the optical pathlength.

$$Abs_{\lambda} = (A_{\lambda_E} - A_{700_E}) \frac{V_l}{V_a \cdot l} \ln(10) \quad (4)$$

Substituting equation (3) into equation (4), noting that $A_{700} = 0$ for all measured samples, and correcting for the fraction of filter analyzed, f , gives the following equation used to calculate the absorption coefficient from the size exclusion chromatographic analysis:

$$Abs_{\lambda} = \frac{1}{f} \left(\frac{a_p \cdot r_f}{V_i} \right) \frac{V_l}{V_a \cdot l} \ln(10) \quad (5)$$

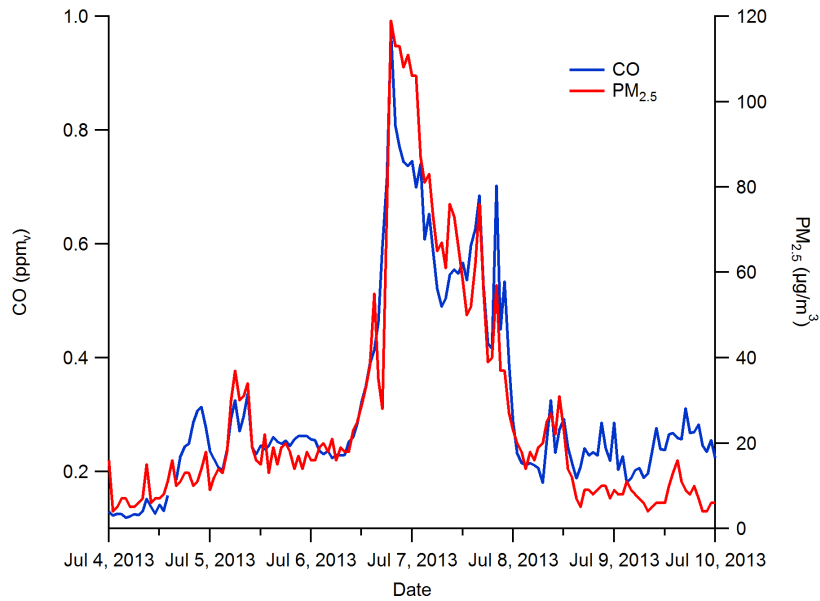


Figure C-1: Real-time PM_{2.5} and CO measurements from St. John's monitoring site. Measurements were averaged to an hourly time base. The average PM_{2.5} concentration during the sampling period was 78.6 µg/m³, where background PM_{2.5} concentrations were 5.7 µg/m³ from June 1 to August 31, 2013.

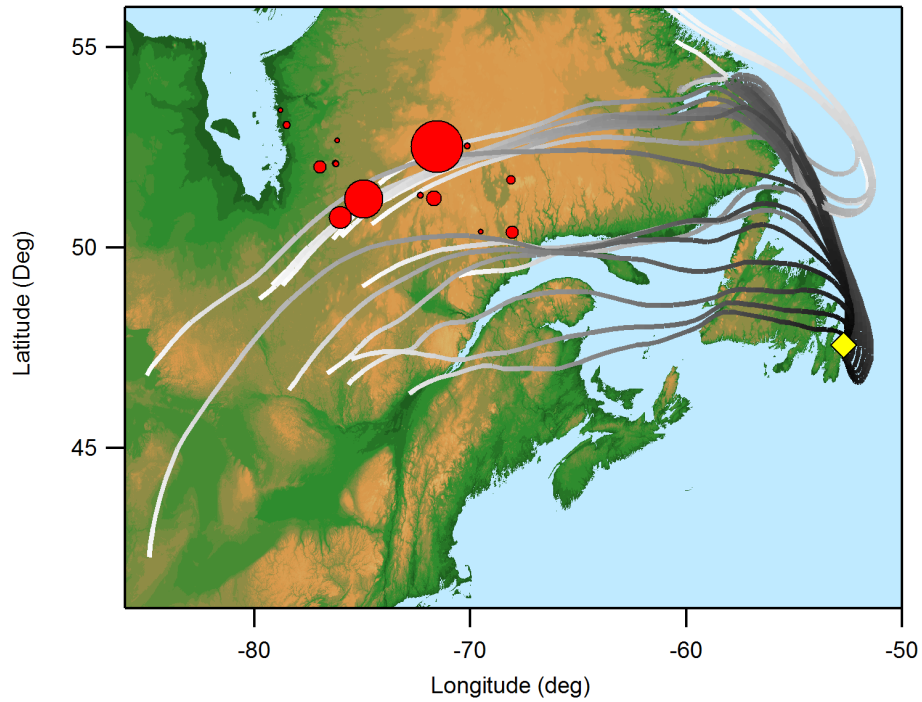


Figure C-2: 72 h airmass back-trajectories from July 6, 2013 in St. John's, NL as computed using the Hybrid Single Particle Lagrangian Integrated Trajectory Model (HYSPLIT).

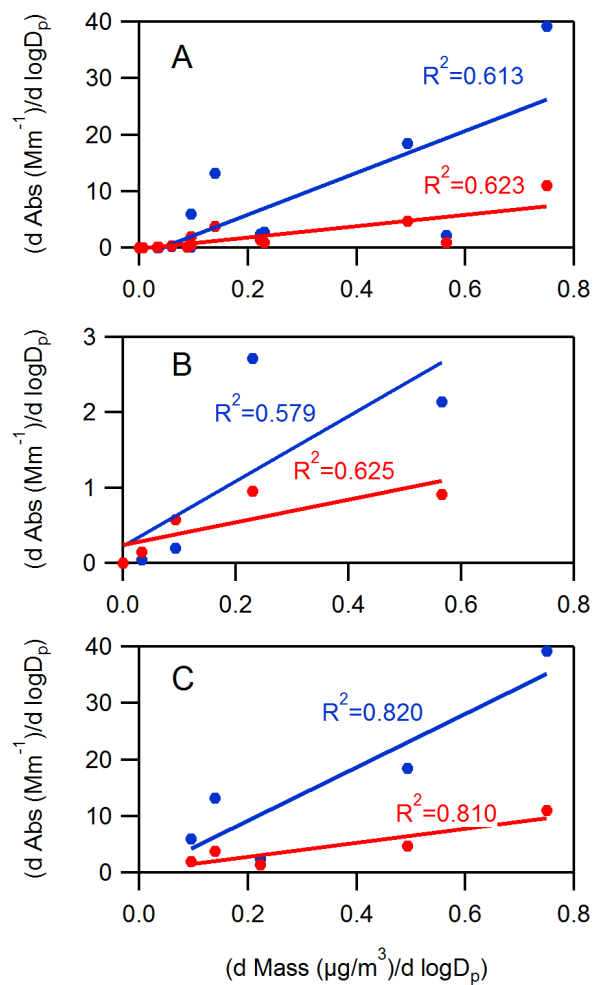


Figure C-3: Correlations between absorbance by (blue) molecules greater than 500 Da and (red) molecules less than 500 Da with potassium in A) all particle diameters, B) ultrafine particles and C) accumulation mode particles

Table C-1: Summary of measured particle-bound species concentrations reported as d mass/d log D_p concentrations in units of µg/m³. MMA – monomethyl ammonium, DMA – dimethyl ammonium, TMA – trimethyl ammonium, MEA – monoethyl ammonium, DEA – diethyl ammonium, TEA – triethyl ammonium.

		MOUDI Stage													
		0	1	2	3	4	5	6	7	8	9	10	11	12	13
Cutoff Diameter (µm)		18	10	5.6	3.2	1.8	1	0.56	0.32	0.18	0.10	0.056	0.032	0.018	0.010
ICP-OES	Al	0.20	0.15	0.33	0.17	0.23	0.45	0.89	0.18	0.18	0.13	4.46	0.22	<LOD	<LOD
	Ca	0.13	0.19	0.19	0.15	0.13	0.17	0.15	0.11	<LOD	<LOD	<LOD	<LOD	<LOD	<LOD
	Fe	0.02	0.02	0.18	0.03	0.05	0.05	0.02	0.03	0.04	0.05	0.05	0.07	<LOD	<LOD
	K	<LOD	<LOD	<LOD	<LOD	<LOD	<LOD	0.45	0.38	0.23	<LOD	<LOD	<LOD	<LOD	<LOD
	Mg	0.05	0.07	0.10	0.12	0.10	0.12	0.05	0.04	0.02	0.01	0.02	0.12	<LOD	<LOD
	Mn	<LOD	<LOD	<LOD	<LOD	<LOD	<LOD	<LOD	<LOD	<LOD	<LOD	<LOD	<LOD	<LOD	<LOD
	Na	0.10	0.19	0.38	0.59	0.47	0.57	0.21	0.21	<LOD	<LOD	0.10	<LOD	<LOD	<LOD
	P	<LOD	0.03	<LOD	<LOD	0.03	<LOD	<LOD	0.03	<LOD	<LOD	0.04	0.03	<LOD	<LOD
	S	<LOD	<LOD	<LOD	<LOD	0.09	0.23	0.71	0.52	0.36	0.12	<LOD	<LOD	<LOD	<LOD
	Si	0.77	1.08	1.17	0.79	0.85	0.91	0.84	0.99	0.72	0.79	0.99	0.98	<LOD	<LOD
Cation IC	Li ⁺	<LOD	<LOD	<LOD	<LOD	<LOD	<LOD	<LOD	<LOD	<LOD	<LOD	<LOD	<LOD	<LOD	<LOD
	Na ⁺	0.11	0.18	0.38	0.62	0.48	0.54	0.21	0.22	<LOD	<LOD	0.10	<LOD	<LOD	<LOD
	NH ₄ ⁺	<LOD	<LOD	<LOD	<LOD	<LOD	<LOD	0.72	0.44	0.24	0.03	0.02	0.04	<LOD	<LOD
	K ⁺	<LOD	0.09	0.04	0.06	0.09	0.22	0.75	0.49	0.14	0.10	0.23	0.09	0.57	0.03
	MMA	<LOD	<LOD	<LOD	<LOD	<LOD	<LOD	<LOD	0.01	<LOD	<LOD	<LOD	<LOD	<LOD	<LOD
	DMA	<LOD	<LOD	<LOD	<LOD	<LOD	<LOD	0.19	0.21	0.08	0.03	<LOD	<LOD	<LOD	<LOD
	TMA	<LOD	<LOD	<LOD	<LOD	<LOD	<LOD	<LOD	<LOD	<LOD	<LOD	<LOD	<LOD	<LOD	<LOD
	MEA	<LOD	<LOD	<LOD	<LOD	<LOD	<LOD	<LOD	<LOD	<LOD	<LOD	<LOD	<LOD	<LOD	<LOD
	DEA	<LOD	<LOD	<LOD	<LOD	<LOD	0.03	1.27	1.27	0.56	0.20	0.06	0.05	<LOD	<LOD
TEA	0.02	<LOD	<LOD	<LOD	<LOD	<LOD	<LOD	<LOD	<LOD	<LOD	<LOD	<LOD	<LOD	<LOD	
Anion IC	F ⁻	<LOD	0.07	0.04	0.05	0.06	0.03	0.08	0.07	<LOD	0.03	0.06	0.06	0.05	0.04
	Cl ⁻	0.15	0.25	0.43	0.53	0.81	1.72	0.14	0.19	0.16	0.12	0.26	0.16	0.25	0.15
	NO ₂ ⁻	<LOD	0.04	0.03	<LOD	0.16	0.08	0.04	0.01	<LOD	0.25	0.01	0.03	0.03	0.04
	NO ₃ ⁻	<LOD	0.10	0.16	0.52	0.63	0.52	0.38	0.21	0.09	0.13	0.08	0.07	0.07	0.07
	SO ₄ ²⁻	0.10	2.43	0.22	0.27	0.37	1.10	1.53	1.34	0.67	0.36	0.46	0.27	0.20	0.14
	Acetate	3.78	2.07	3.42	1.78	1.80	0.31	0.23	1.24	<LOD	0.70	1.28	2.00	1.76	1.44
	Formate	0.04	0.34	0.19	0.34	0.29	0.04	0.16	0.12	0.02	0.04	0.07	0.03	0.01	0.30
	Propionate	0.15	0.17	0.17	0.18	0.19	0.07	0.02	0.15	<LOD	0.13	0.17	0.19	0.23	0.20
	Butyrate	0.10	0.18	0.17	0.21	0.44	4.03	0.19	0.26	0.16	0.10	0.21	0.17	1.22	0.41

Appendix D Supporting Information for Chapter 5

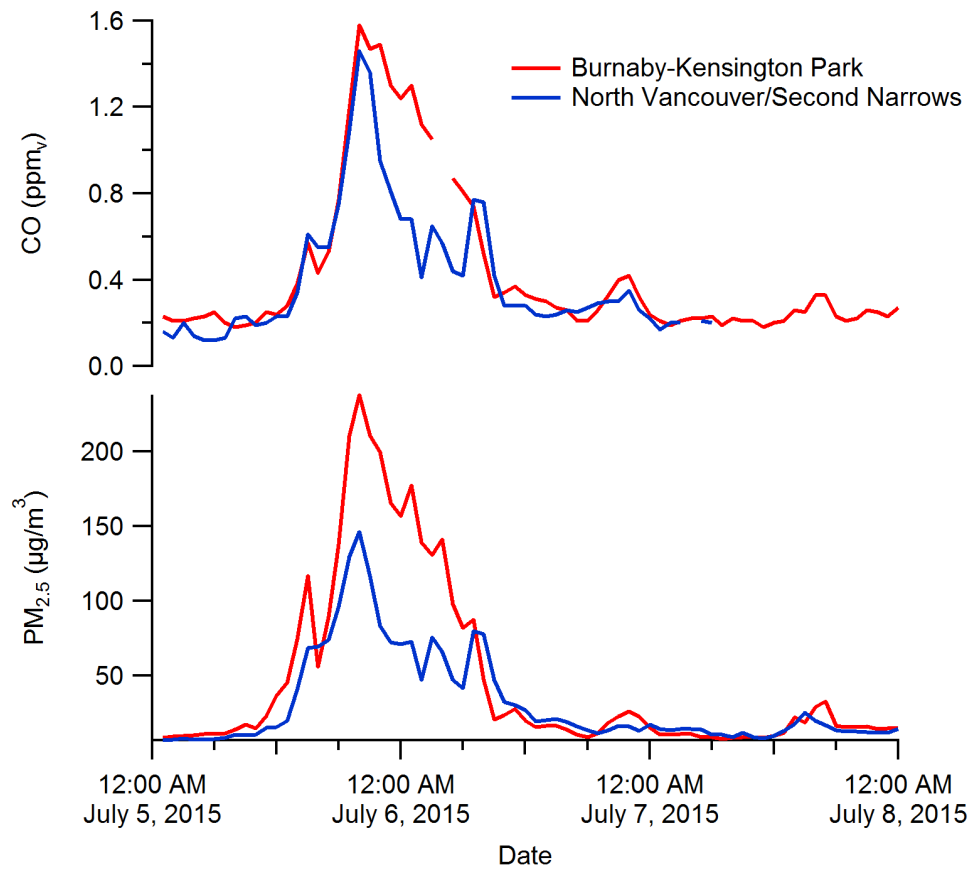


Figure D-1: CO and PM_{2.5} loading in Vancouver during wildfire collection. Data acquired from British Columbia Air Data Archive, as part of the British Columbia Ministry of Environment, available at <http://envistaweb.env.gov.bc.ca/>

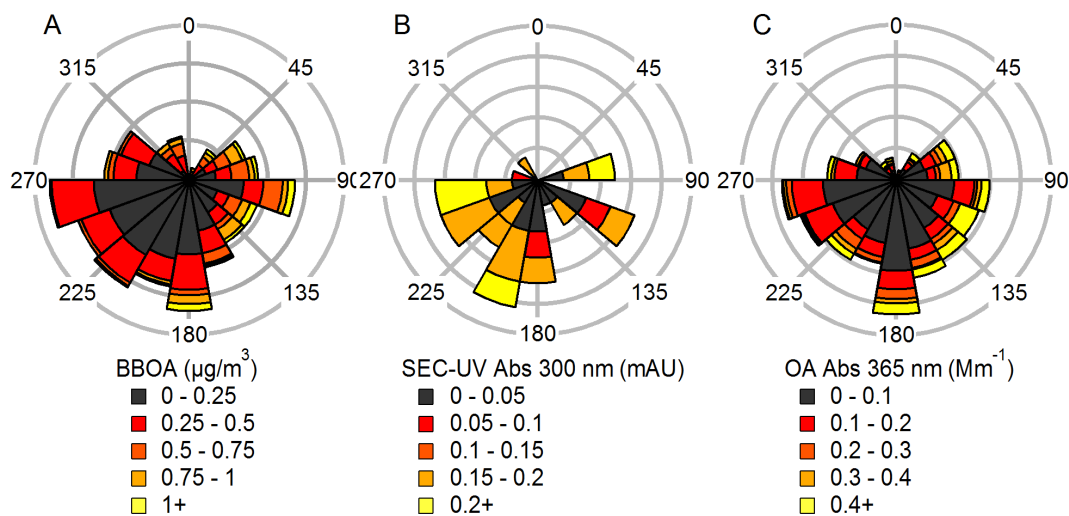


Figure D-2: Directionality of signals arising from A) BBOA from AMS, B) absorbance by SEC-UV, and C) organic aerosol absorption by PiLS-LWCC

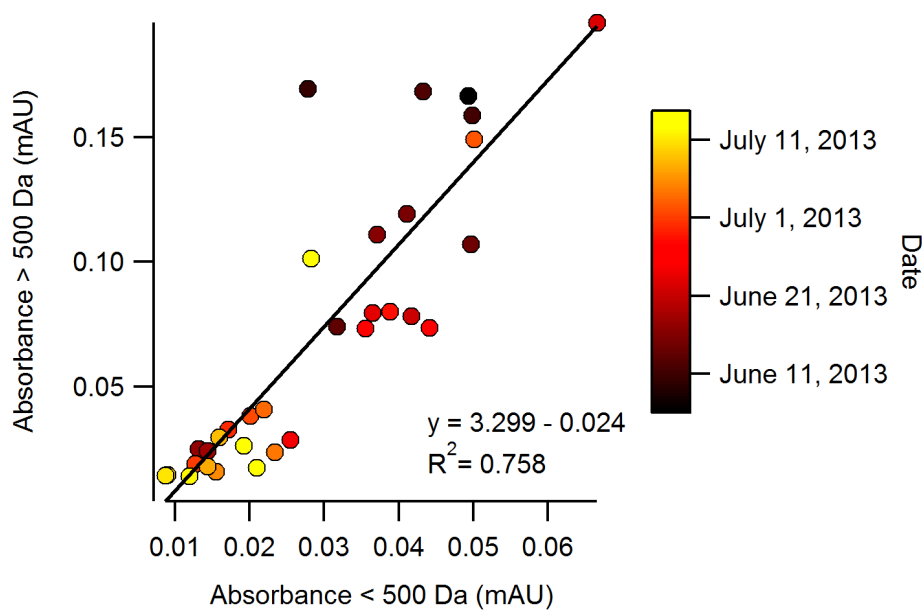


Figure D-3: Ratio of large to small molecular weight absorbers throughout the SOAS campaign. Species greater than 500 Da consistently contributed roughly three times greater absorption than species less than 500 Da.

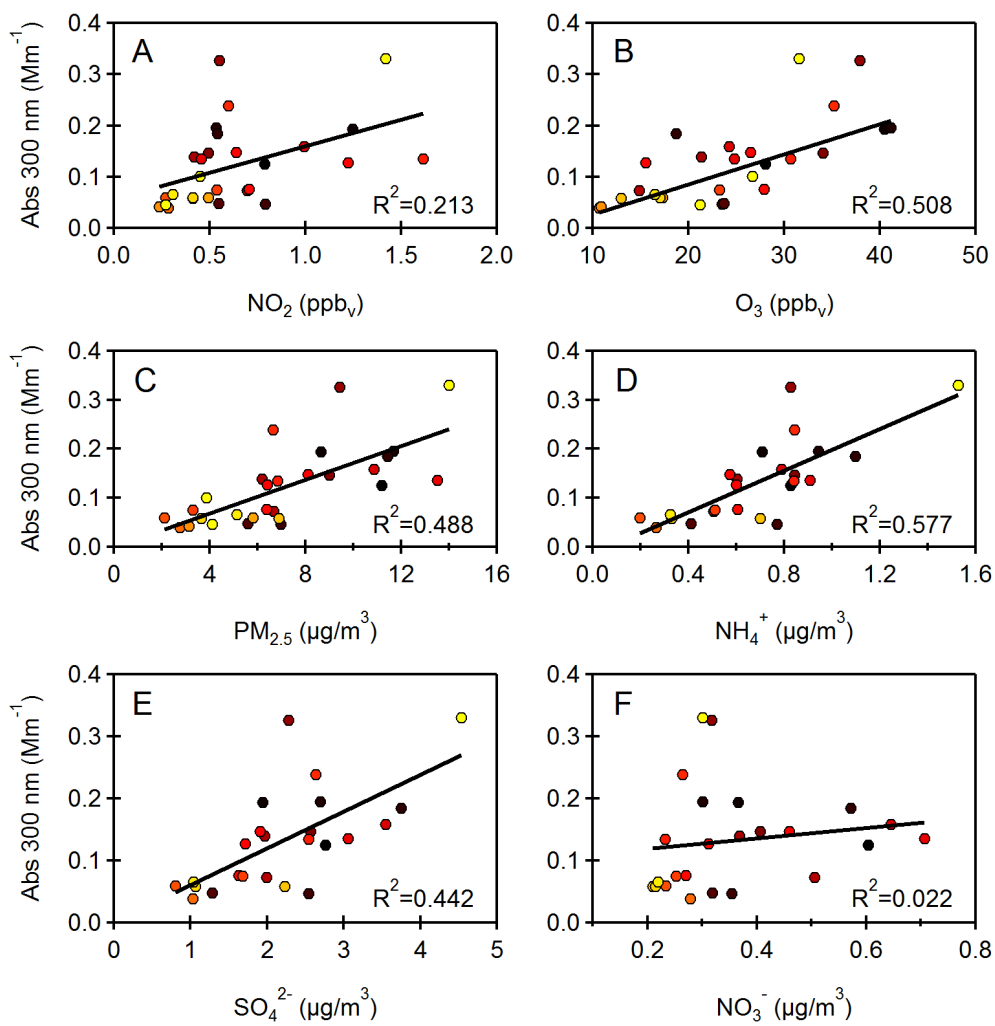


Figure D-4: Correlations between absorbance determined by SEC-UV with (A) NO_2 , (B) O_3 , (C) $\text{PM}_{2.5}$ mass, (D) particulate NH_4^+ , (E) particulate SO_4^{2-} , and (F) particulate NO_3^- .